ENVIRONMENTALLY INDUCED FRACTURE OF NICKEL ALLOYS: A COMPARISON OF HYDROGEN AND MERCURY EMBRITTLEMENT WITH RESPECT TO TEMPERATURE

By

Randall K. King

Bachelor of Science
Oklahoma State University
Stillwater, Oklahoma
1972

Master of Engineering
Oklahoma State University
Stillwater, Oklahoma
1974

Submitted to the Faculty of the Graduate College
of the Oklahoma State University
in partial fulfillment of the requirements
for the Degree of
DOCTOR OF PHILOSOPHY
May, 1985

ENVIRONMENTALLY INDUCED FRACTURE OF NICKEL ALLOYS:

A COMPARISON OF HYDROGEN AND MERCURY

EMBRITTLEMENT WITH RESPECT

TO TEMPERATURE

Thesis Approved:

C E Price
Thesis Adviser

James L. Good

Richard L. Lowery

John C. Lloyd

Norman N. Durham
Dean of the Graduate College

ACKNOWLEDGEMENTS

I would like to express my appreciation to all those who have helped in this study. Special thanks go to Dr. C. E. Price, my major advisor, for his guidance, encouragement, and the many hours of work which he invested in this study. My thanks go also to Dr. R. L. Lowery, Dr. J. K. Good, and Dr. J. Lloyd for serving on my advisory committee.

I would also like to thank Dr. J. K. Good, L. B. Traylor, R. S. Fredell, J. A. Morris, G. R. Peevy, and J. K. Willoughby for their studies which led up to this work. Special thanks go to Dr. G. E. Maroney for the years of example, enthusiasm, and encouragement which have been such a help in my professional life.

The School of Mechanical and Aerospace Engineering is gratefully acknowledged for funding a portion of this research. I thank Halliburton Services and particularly Clinton Cole for all the support and assistance received while finishing this document with special thanks to go to Sibyl Greenwood for her tireless work in typing and retyping this manuscript.

I am very grateful to my wife, Deborah, and daughter, Kristi, for all their encouragement, understanding and patience during my graduate study.

TABLE OF CONTENTS

LIST OF TABLES

LIST OF FIGURES

Figure Page

CHAPTER I

INTRODUCTION

Environmentally induced embrittlement of engineering materials is a substantial problem affecting the cost, reliability, and safety of many products and processes. Embrittlement refers to loss of ductility by a material, often accompanied by a decrease in tensile strength. Embrittlement results from several different types of environments or conditions and has historically been studied segregated into compartments, for example:

Hydrogen Embrittlement	Stress Corrosion Cracking	Temper Embrittlement	Liquid & Solid Metal Embrittlement

It has been suggested that these different embrittlement systems are variations on a theme; that controlling mechanisms or kinetic factors in one embrittlement system are the same or closely related to those in the other systems (1). In fact, a recent conference was dedicated to bringing together specialists in the fields of materials science, mechanics, physical chemistry, surface chemistry and physics, and atomic modeling, to share knowledge of all types of environmentally induced fracture, with the aim of gaining enhanced understanding of the fracture process (2).

Similarities between different modes of environmentally induced fracture were noted long ago. As far back as 1874, Johnson (3) noted similarities between hydrogen embrittlement (HE) and liquid metal embrittlement (LME) by molten tin of steel. More recently, Lynch (4) and other investigators [5-11] have observed many similarities between the fractographies and effect of test variables for LME and HE, and Lynch has theorized that both occur by the same mechanism. Others have noted these and other similarities and have theorized a connection between stress corrosion cracking (SCC) and HE (12,13,14). Similarly, the reduction of surface energy due to adsorption has been proposed as a mechanism for HE (15), SCC (16), and LME (17). Also, crack growth versus time curves have the same shape for SCC, HE, and LME (1). Moreover, the same segregated impurities, tin and antimony, are responsible in steels for temper embrittlement (TE) (18), HE (19,20), and LME (21); and segregated sulphur has been shown to promote both TE (22) and HE (20) in nickel.

This study extends and consolidates previous work at Oklahoma State University comparing HE and LME of nickel alloys (5-10). Comparative studies are valuable in that the similarities between HE and LME in nickel alloys allow observations on the mechanisms and controlling kinetics of the processes. Similarities observed in these and other systems include: similar fractographies (4-11), similar effect of changing strain rate, cold work, and grain size

(5-10), the existence of a "temperature window" for embrittlement (23,24), and similar requirements for embrittlement (tensile stress, existence of the environment at the crack tip, preexisting cracks or obstacles to slip)(1).

This investigation directly compares the effect of temperature on HE and LME of nickel alloys. The main focus of study is on Monel 400, building upon Fredell's (8) work, with comparisons made to the behavior of Nickel 200, Inconel 600, and Incoloy 800. The major objectives are to examine the validity of existing embrittlement theories, and to further characterize the embrittled behavior of nickel alloys.

CHAPTER II

REVIEW OF THE LITERATURE

Hydrogen Embrittlement

A wide range of engineering alloys can be embrittled by hydrogen, including steels, superalloys, and aluminum alloys. Because of its great commercial significance, the subject has been studied for over one hundred years (3). It is not fully understood because of the large number of variables involved. For example, HE is more common in high strength alloys, but single crystals can also be embrittled, and embrittlement is typically encountered only over a limited temperature range (usually near room temperature in steels). HE induced fractures can be either transgranular or intergranular. Some metals form hydrides. Some diffuse hydrogen readily, while others have very low solubilities. Some metals have many internal traps of varied effectiveness including: carbide particles, grain boundaries, dislocations, and inclusions. Hydrogen has been reported to cause hardening, softening, serrated yielding, delayed failures, decreased fatigue life, and increased fatigue life. The form in which the hydrogen is encountered makes a difference; whether it is internal HE (dissolved in the metal matrix), gaseous HE (hydrogen gas on the metal's

surface), or electrolytic HE (hydrogen produced on the metal's surface by an electrochemical reaction). Common sources of hydrogen include: pickup of hydrogen while the metal is still in the molten state, exposure to gaseous hydrogen or H_2S, moisture during welding, electroplating and acid pickling operations, and hydrogen reduction reactions accompanying cathodic protection or corrosion processes.

The nickel alloys considered in this study are all one-phase, face-centered-cubic (FCC) alloys that are normally ductile. The close-packed FCC structure allows very little diffusion and solubility of hydrogen. The diffusion coefficient of hydrogen in nickel is 10^{-14} m^2 s^{-1} at room temperature, as opposed to 10^{-10} m^2 s^{-1} in ferritic steels (25).

The subject of HE is so widely investigated that major conferences are held every few years, and review articles are frequently published, e.g., by Hirth (26) and Birnbaum (27). The major theories of HE are summarized here, with their likely reference to nickel alloys assessed. Models having limited applicability to nickel alloys are considered only briefly.

Formation of Hydrides

Many metals form hydrides which are thermodynamically stable or can be stabilized by applied stresses. These include the group IVb and Vb metals. Embrittlement occurs due to the fracture of a brittle hydride phase which forms

at stress concentrations. Direct evidence for embrittlement due to stress induced hydrides has been obtained for niobium, vanadium, titanium, zirconium, and magnesium based systems (27). Formation of nickel hydrides can occur at very high hydrogen fugacities (28) but is not generally regarded to be an embrittlement mechanism at conditions where embrittlement is normally observed (27).

Internal Pressure

This theory, first proposed by Zapffe (29) proposed that HE is caused by monotonic hydrogen diffusing through the metal matrix and recombining at internal defects or voids where it becomes trapped. Such a process is known to produce hydrogen blistering and internal cracking of unstressed parts. It is now generally accepted that internal pressurization causes HE under certain conditions, but must not be the major cause of HE, since embrittlement can occur in low pressure hydrogen gas, and blisters are not observed in most cases of HE. This form of HE is much less common nowadays with vacuum degassing. Recently, theoretical analyses have been put forth which show that voids ahead of crack tips can become pressurized if hydrogen is transported by dislocations into voids faster than it can escape from voids (30). However, there is not known evidence that such an effect occurs (11). Pressure theories, by themselves do not explain the quite large difference in the amount of

ductility reduction between similar alloys. They also have difficulty explaining HE in nickel alloys where the amount of hydrogen diffusion is so small.

Decohesion

Originally proposed by Troiano (31) and extended by Oriani and Josephic (32), the decohesion theory proposes that the tensile stress required for decohesion of the metal matrix is reduced by increased concentrations of hydrogen that accumulate in regions of "high non-Hookean elastic stress" within a few atomic layers of the crack tip. After fractographic evidence was observed that some plastic flow occurs even in HE of very high-strength steels, the theory was modified to say that brittle decohesion occurs leaving enclaves of unbroken material which then fail by plastic tearing.

According to Kelly, Tyson, and Cottrell (33), brittle crack propagation occurs if the ratio of the largest tensile stress to the largest shear stress at the crack tip exceeds the ratio of the ideal cleavage stress to the ideal shear stress. Rice and Thompson (34) used this theory to propose that a barrier to dislocation emission at the crack tip would promote brittle behavior by raising the shear/tensile stress ratio. The presence of hydrogen could therefore promote brittle fracture by either inhibiting dislocation nucleation or reducing decohesion stress at the crack tip (13). The decohesion theory is probably the most widely

accepted explanation for HE, but "no evidence exists to support the assumption that hydrogen in solid solution decreases the strength of the atomic bonding" (27). Birnbaum (27) summaries results of some very basic work which has measured the effect of dissolved hydrogen on phonon frequencies, but concludes that "these measurements do not directly address the effect of hydrogen on lattice potential at the large displacements which are of interest in fracture." Thus, for the decohesion theory, as for other embrittlement theories, evidence from macroscopic tests must be used to deduce whether the proposed effects occur or not.

The decohesion theory implies that fractography of HE should contain at least some areas of microscopically brittle fracture. However, embrittled fractures consisting of 100% microvoid coalescence have been observed, even in very high strength steel (35). Lynch (36) has reported that even flat "cleavage" embrittled fracture surfaces are actually covered by very small, shallow dimples which are apparent only at magnifications greater than 5000X using transmission electron microscopy of replicas. (See further discussion below.) However, in other cases of intergranular fracture, no evidence of microvoids could be found, even when samples were sent to Lynch for his analysis (37).

Reduction in Surface Energy by Adsorption

If HE fractures are considered to be brittle then it is logical to consider Griffith's criterion for fracture of

ideally brittle (elastic) solids. Griffith demonstrated that a crack in a stressed brittle material (he used silica glass) will propagate unstably when the decrease in potential energy resulting from the introduction of the crack is greater than the increase in surface energy resulting from the presence of the crack (38). Petch and Stables (15) proposed that hydrogen adsorbed on the crack tip reduces the surface energy of the fracture surface, allowing brittle fracture. This approach was widely discounted after it was determined that the energy associated with plastic deformation during fracture is much larger than the change in surface energy. However, the total energy for crack propagation can be expressed as:

$$\emptyset_T = \emptyset_b + \emptyset_P \qquad (1.1)$$

where $\emptyset_b$ is the energy to produce an ideally brittle fracture, and $\emptyset_P$ is the energy expanded by dislocation motion (plasticity) (39). It can be shown that $\emptyset_p$ depends on the stress field about the crack tip which in turn depends on $\emptyset_b$. Hirth (35) proposed that the resulting fractures are intergranular due to segregation of hydrogen at the grain boundaries. Recent experiments have provided direct evidence of hydrogen segregation at grain boundaries in niobium and nickel using the Secondary Ion Microprobe Spectroscopy (SIMS) method with deuterium (27,40). Clark (41) has shown that while the surface free energy of a Ni-300 ppm hydrogen solution is nearly equal to that of pure nickel, the dissolved hydrogen decreases the grain

boundary energy by about 20%. He concluded that hydrogen can decrease the work for intergranular or transgranular fracture due solely to adsorption effects and not by significantly altering the lattice potential between the solvent atoms (41).

A difficulty with this approach is that hydrogen is unique among the strong surface adsorbers in causing embrittlement. Many gases (O_2, H_2O, SO_2, etc.) have larger enthalpies of adsorption on clean surfaces than hydrogen but do not cause embrittlement (and will even stop crack propagation due to the presence of hydrogen) (27). Only fugacities of hydrogen in the gas phase (H_2, H_2S, etc.) produce embrittlement, while many segregated species in the solid phase lead to low energy intergranular fracture (18).

Vehoff and Rothe (37) have also suggested a further difficulty with the reduction in surface energy theory. They observed that embrittlement of Fe-3% Si single crystals saturates with increasing gaseous hydrogen pressure. Increasing the hydrogen pressure by three orders of magnitude does not change the degree of embrittlement, but it can be shown that the surface energy decreases continuously with increasing hydrogen pressure.

Hydrogen Enhanced Plasticity

Beachem (35) observed that in many instances fracture surfaces of 4140 steel broken in gaseous and electrolytic hydrogen consist largely of dimpled rupture. He concluded

that "embrittled" fracture (he used the term hydrogen assisted cracking) occurs because dissolved hydrogen increases the plastic deformation around the crack tip. The reason that the fracture mode becomes more brittle and not more ductile on a macroscopic basis is attributed to hydrogen diffusing into the lattice just ahead of the crack tip and aiding "whatever deformation processes the matrix will allow" on a very localized basis only. Transport of hydrogen by dislocations to regions ahead of the crack tip was later incorporated into his model (42). Macroscopic observations of the effect of hydrogen on the flow stress of iron and nickel are inconclusive in that the matrix can be either hardened or softened, depending on variables such as temperature and the presence of impurities such as carbon (43,44). Recent in-situ fracture studies have provided dramatic evidence that hydrogen can facilitate plastic deformation in nickel (45). Nickel specimens were strained plastically in vacuum under the HVEM (X20,000 magnification). The specimen displacement was held constant and H_2 was admitted to the environmental chamber. At about 10^3Pa of H_2, dislocations were observed to move, and at 10^4Pa rapid dislocation movement and generation was observed. Reference (45) also has HVEM micrographs of cracks propagating in H_2 which show a region of intense slip directly ahead of the crack tip.

Beachem (35) also observed a sequence of fracture modes in 4140 sheet, which he correlated with the stress intensity

factor, K. His fracture surfaces progressed from "clean" intergranular to intergranular with plastic tearing to transgranular (referred to a quasicleavage) to microvoid coalescence (35). His interpretation was that the intergranular and transgranular fractures are lower energy processes which can proceed at low K values, while the microvoid coalescence mechanism is faster kinetically and takes over when the stress intensity is high enough.

Hydrogen Enhanced Dislocation Nucleation

Lynch observed marked similarities between HE and LME fracture surfaces and concluded that they probably occur by the same mechanism (4). Since liquid metal atoms are too large to diffuse readily into the embrittled metal matrix, this would indicate that HE occurs due to adsorption of hydrogen onto the surface of the material. He also noted other evidence that HE is due to a surface effect. For example, crack growth rates in gaseous hydrogen respond to changes in the gas pressure almost immediately, and stationary cracks (at stress intensity factors and hydrogen pressures just below threshold values for crack growth) can be restarted by slightly increasing hydrogen pressure (46,47). He also conducted fractographic studies at high resolution using the TEM and observed that many fracture surfaces from both HE and LME that would be considered "flat" under the SEM were actually covered with small, shallow dimples.

From a study of crack propagation in nickel single crystals, he developed a model which he applied to both HE and LME (4). He also observed similar fractographies in an aluminum alloy which he described with the same model (48). Crack propagation occurs along [100] planes by an alternate slip process (see figure 3). The crack extends by emitting dislocations and shearing on slip planes which exactly intersect the crack tip. The crack propagates on the plane bisecting the angle between two slip planes, by alternately slipping on first one slip plane, then the other as shown in Figure 1. This causes small voids to form ahead of the crack tip, and the crack extends further by linking up with them. Weakly adsorbed hydrogen at the crack tip is assumed to facilitate dislocation nucleation by reducing the strong interatomic bonds resulting from the contraction of the surface lattice. In a recent study of HE and LME of quenched and tempered D6-AC steel he concluded that "fracture possibly occurs by decohesion in some areas and by localized plasticity in other areas. An adsorption induced reduction in the strength of interatomic bonds at crack tips is probably the underlying cause for both processes" (49).

Plastically Blunted Decohesion

Vehoff and Rothe (37) studied stable crack propagation as a function of hydrogen pressure, temperature, and crack growth rate in Fe-3% Si and nickel single crystals. They observed crack propagation on the [100] plane, but no

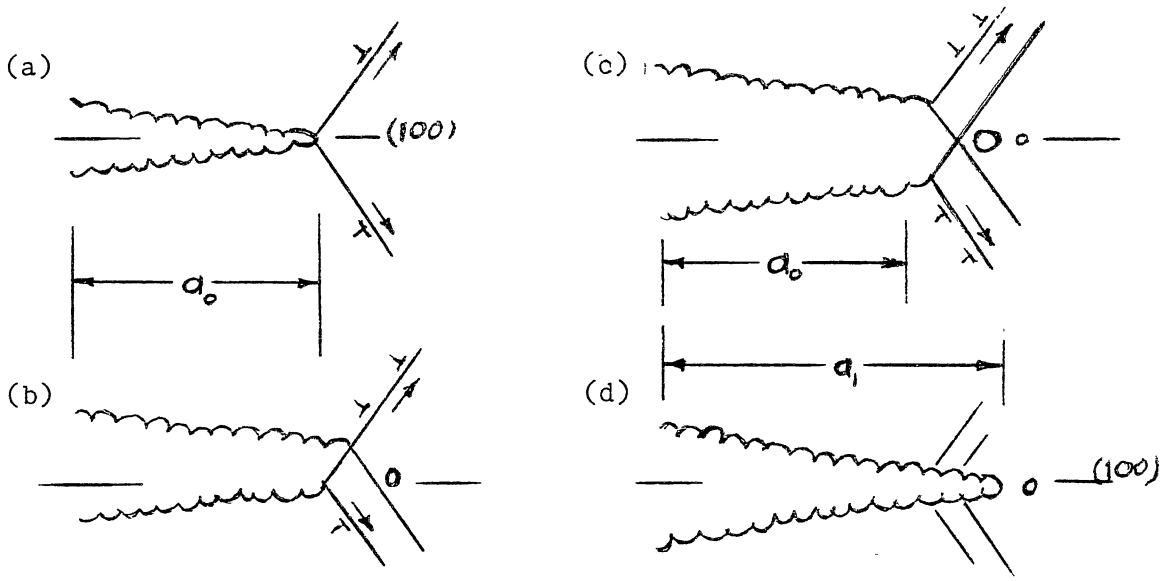

Figure 1. Mechanism of hydrogen enhanced dislocation nucleation model for transgranular propagation in nickel single crystal. After (36)

evidence of dimples on the fracture surface. They used the crack tip angle as a measure of embrittlement, as McClintock (50) had shown that crack tip angles smaller than the angle between the two slip planes involved can only be obtained if another fracture mechanism, yielding zero crack tip angle (such as micro-cleavage or void formation), is superimposed.

They proposed a mechanism whereby the crack propagates in increments as shown by Figure 2, first in a brittle manner by decohesion, but subsequently blunted through dislocation emission. Hydrogen is assumed to lower the cohesive forces in the crystal [per Oriani and Josephic (47)], and is always present in high local concentrations at the crack tip due to efficient supply from the fracture surfaces. In the presence of hydrogen, "the probability of bond breaking versus dislocation emission is shifted towards bond breaking" (37). They were able to induce HE at hydrogen pressures which were low enough to allow in situ observation in the SEM of the propagating crack. They thus directly observed that microcracks initiated along the crack front and encircled enclaves of uncracked material. These enclaves necked down to a point while the crack front continued to propagate far ahead. From this observation and from their examination of the roughness of the fracture surface at high resolution, they concluded that any incremental steps of decohesion and blunting occur at a spacing of less than 0.1 μm.

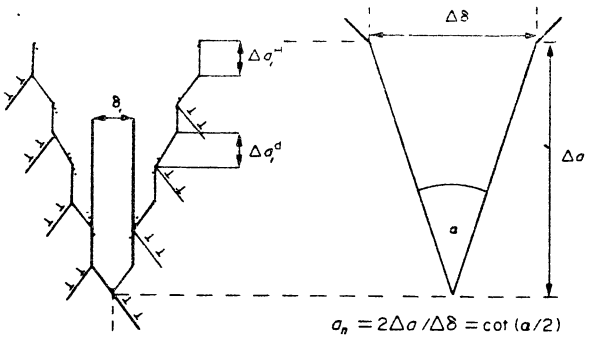

Figure 2. Mechanism of plasticially blunted cleavage. Discontinuous steps are reported to be less than 0.1 μm apart. From (37)

The crack tip angle correlates nicely with gaseous hydrogen pressure, temperature, and crack growth rate for both nickel and Fe-3% Si crystals. Increasing pressure decreased the angle (increasing embrittlement). Below room temperature, the angle increased with increasing crack rate, indicating embrittlement limited by hydrogen transport, and at higher temperatures the angle was independent of crack propagation rate, for both alloys. For the Fe-3% Si crystals tested at 373°K, the crack became more ductile as the crack velocity decreased. This was attributed to the decrease in the yield strength accompanying the higher temperature and slow strain rate.

When partial pressures of oxygen were admitted to a crack undergoing stable propagation at $150 nms^{-1}$ in gaseous hydrogen, the crack blunted within one second; long before the changed environment could have any affect on the bulk material. They concluded that the coverage of adsorbed hydrogen and not the presence of hydrogen in the bulk is necessary for HE, and that the fracture process zone lies within 100 nm of the crack tip.

Liquid Metal Embrittlement

LME is less widespread in industry than HE, but is significant enough for there to have been many studies of LME in diverse systems. Examples of LME in practice include the use of liquid sodium as a heat transfer medium in nuclear reactors (51), brazing and soldering applications

(52), and the embrittlement of vessels containing liquid metals for production processes. For instance, Friehe [52] reports cases of a "gaping crack of several meters length" occurring suddenly in steel galvanizing vessels commonly containing up to $5X10^5$ kg (500 metric tons) of molten zinc. LME has also been experienced in leaded "free machining" alloy at temperatures above the melting point of the lead inclusions (53), and in Monel 400 when low melting point alloys were used as tooling during manufacture (54). A recent text (55) also warns that "if stainless steel is welded in the presence of any amount of zinc, lead, cadmium, aluminum, or copper, wetting and intergranular penetration occurs, resulting in severe cracking." Interestingly, LME has been put to use in a beneficial way. Stoloff (24) reports on the use of liquid metals, such as Pb-Sn eutectics, in the Soviet Union (56,57) to facilitate the drilling of steels, Ni-Cr heat resistant alloys, titanium alloys, and others. This technique reportedly results in increased drill life and improvement in surface finish.

LME has been studied in its own right and for comparison and contrast with other embrittlement modes. It is the similarities between LME and HE that were emphasized by Lynch that stimulated the present investigation (4). Similarities include: fractography, grain size effects, temperature sensitivity, and the observation that elements which form stable compounds with the solid, when added to the liquid, inhibit LME, just as oxygen inhibits HE

(1,3-12,39,36). Recent reviews of LME have been published by Stoloff (1,24), Kamdar (12), and Nicholas and Old (58), and a conference on LME was held in 1982 (59).

Necessary Conditions

The following conditions are generally believed to be necessary for LME to occur (24):

1. A tensile stress in the material.
2. Pre-existing cracks or obstacles to dislocation motion.
3. Presence of the liquid metal, wetting the solid metal surface, and a transport mechanism to keep the liquid metal in contact with the advancing crack tip.
4. A specific solid metal-liquid metal couple.
5. A specific combination of test conditions (such as temperature and strain rate) and metallurgical conditions (such as grain size, amount of cold work, and the presence or absence of impurities).

It has been widely accepted that only specific solid-liquid metal couples will experience LME; those which have low mutual solubilities, little tendency to form compounds, and strong binding energies (1). Tables of specific liquid/solid metal couples which exhibit LME have been published, for instance by Kamdar (12) who lists nickel as being embrittled by Li (with no mention of Hg) and by Rostoker, McCaughey, & Markins (60) and Stoloff (61) who

do not mention nickel alloys at all. However, for every general statement which has been made as to which couples are embrittled, there seem to be exceptions. Many techniques have been developed to predict susceptibility of specific materials to embrittling environments [see (24) for discussion]. Many approaches have been taken, including: a solubility parameter used in conjunction with a fracture surface energy calculated from thermodynamic data (62), reduction in surface energy calculated from thermodynamic data (63), wetting angles (58), or heats of mixing (64), and interatomic bond reduction estimated from heats of fusion (65). Each method has achieved limited success, but none is completely satisfactory for predicting all known couples, and none offer any insight into the mechanisms of LME (24).

As more and more LME data are compiled, applicability of the whole idea of specificity has come into question. Shunk and Warke (66) compiled a large table of reported embrittlement couples and examined reported effects of changing test and metallurgical conditions. They pointed out that LME normally is reported to occur only within a certain temperature range (a temperature "window") which can be changed to a large degree by varying metallurgical and test conditions. Figure 3 shows that the effect of decreasing the strain rate of a tensile test can be to widen the "temperature window" of embrittlement and to move the curve. Decreasing the grain size can also change the location and extent of the "temperature window" (66), and

increasing the amount of cold work can substantially affect the degree of embrittlement (5,8,67). From these considerations it can be readily seen that if a couple is tested for LME, it would be very easy to report no embrittlement, when in fact embrittlement would have been experienced if the test had been conducted at a different temperature, strain rate, or grain size. For instance, fine-grained Cu tested in Hg at room temperature at slow strain rates is not appreciably embrittled, while coarse-grained Cu does show a significant loss in ductility (1). These factors and the lack of any theory of an LME mechanism which directly addresses specificity make such criteria for questionable value (24,66).

Proposed Mechanisms of LME

Most of the mechanisms which have been proposed for LME are very similar to their counterparts proposed for HE, as discussed previously. Stoloff (24) has recently reviewed proposed LME mechanisms, which include:

Decohesion. The most widely accepted view is that the cohesive strength of the matrix at the crack tip is reduced by adsorption of the liquid metal, essentially the same as the mechanism previously described for HE (12,68,69). The most serious criticism of the decohesion mechanism is that while it predicts fracture by cleavage, fractography of many LME fracture surfaces is dominated by small, shallow voids, when viewed at high enough magnification, just as for HE.

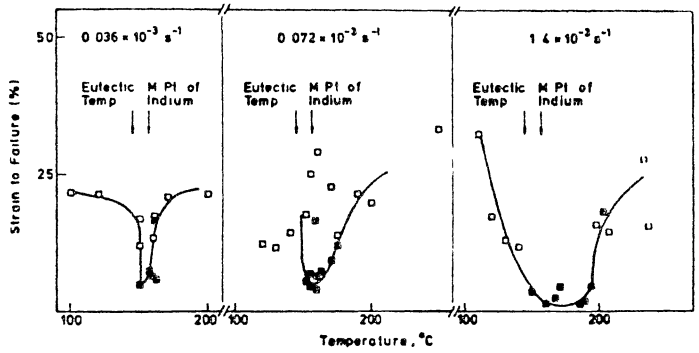

Figure 3. "Temperature window" for zinc tested in liquid indium at various strain rates (24)

Another apparent shortcoming is that it is apparent that the theory has no provision for predicting delayed fracture (following an incubation period) which has been reported by Gordon and An (70) and others (71). A surface-induced decohesion fracture would be expected to occur instantaneously upon contact of the embrittler atoms with a crack nucleus.

Enhanced Dislocation Nucleation. One of the factors which led Lynch to formulate his alternate slip model for embrittled crack propagation was his assumption that HE and LME share a common mechanism (4). His proposed mechanism for LME is the same as that described previously for HE, and is identical to that proposed by Clum (72). The model does not directly predict the occurrence of delayed failures, but Lynch has speculated in a comment to Stoloff's paper (24) that a notch of a certain depth and acuity is necessary to nucleate rapid crack growth, and that enhanced slip would allow such a notch to develop gradually (analogously to fatigue crack propagation).

Stress Aided Dissolution. Robertson (73) proposed that LME cracks propagate by rapid localized dissolution of highly stressed atoms at the crack tip. The dissolved material is then removed by diffusing through the liquid metal. This approach suffers from several problems, including: (1) Cracks are observed to propagate at velocities which are too fast to be caused by the assumed dissolution and diffusion [e.g. $10 mm\, s^{-1}$ for Ni single

crystals in Hg reported by Lynch (4)]. (2) Embrittlement should increase with increasing temperature and mutual solubility, both predictions contrary to observed trends. (3) The mechanism predicts no solid metal embrittlement (SME), or at least a discontinuity at the embrittler melting temperature.

Grain Boundary Diffusion. Gordon and An (70) adapted a theory originally proposed by Krishtal (74) to explain LME as a two step process whereby embrittler atoms initially change from the adsorbed to the dissolved (in the surface) state and then diffuse along grain boundaries or other preferred paths aided by the stress. Crack nucleation occurs when a critical concentration of the embrittler atom is reached after an incubation period. The crack then grows until a visible crack is produced, or until the transport process becomes rate controlling. This model accounts for delayed fracture, but does not predict the existence of transgranular fracture. It also predicts that metals will undergo embrittlement when tested in an inert medium after being exposed to an embrittling liquid metal. Such behavior is rarely observed, except for the Al-Ga system which experiences very rapid grain boundary diffusion (75) and for Zn single crystals which are embrittled by the formation of a brittle alloy layer with Hg or Ga.

Previous Observations

Table I summarizes results of some relevant investigations of the embrittlement of nickel alloys. Many studies of HE of nickel have been done by Smith and his co-workers (76-82). HE studies have been done with internal (dissolved) hydrogen, and with external (gaseous or electrolytic) hydrogen. While solute hydrogen is a common occurrence in ferritic steel, due to the ready diffusion of hydrogen, nickel alloys require precharging at temperatures up to 1000°C in H_2 or electrolytic charging at high currents for long times to get the desired quantity of hydrogen to diffuse into the close packed FCC crystal structure. Most of the Smith studies have used precharged specimens. For nickel single crystals, no HE was observed for small cylindrical samples (79), but transgranular fracture was reported when precracked samples were tested (4,37,45). Vehoff and Rothe (37) reported the necessity to cyclically harden nickel single crystals to raise the yield strength before brittle crack propagation could be induced. The fracture of the single crystals has been variously reported to occur on the [100] plane (4,37,64) and on the [111] plane (45). Usually, no reduction in tensile strength is reported, just a reduction in ductility. The HE exhibits a ductility minimum with temperature, or "temperature window," (76,80-82,37) with minimum ductility reported to occur at about -50°C for precharged polycrystalline samples and about

TABLE I

OVERVIEW OF SELECTED PREVIOUS INVESTIGATIONS

OF EMBRITTLEMENT OF NICKEL ALLOYS

Source	Metal	Crystals	Specimens	Envir.	Charging	Fractog	EFFECT OF $\dot{\varepsilon}$	g.s.	Temp.	C.W.	Remarks
Boniszewski & Smith, 28	Ni	poly	60μm sheet	elect. H	precharge	-	-	-	-	-	
Boniszewski & Smith , 76	Ni	poly	250μm strip	elect. H	precharge	IG	↑%elong @RT	-	window-max embr @-50C	-	
Wilcox & Smith, 78	Ni	poly	1/8" cyl	solute H	precharge 500-1000C	IG	↑%elong & %RA	↓%RA @-80C	-	-	
Windle & Smith, 79	Ni	single	5/16" cyl	solute H	precharge 1000°C	Ductile/ Necking	-	-	-	-	P-L effect
Windle & Smith, 80	Ni	poly	3.2mm cyl	solute H	precharge 1000°C	IG	↑%RA above -150°C	-	window, max embr @ -50°C	-	% Fe embrittlement
Wayman & Smith, 81	Ni/Fe	poly	3.2mm cyl	solute H	precharge 1000°C	IG	-	-	window-max embr. T depends on %Fe	-	
Lynch, 4	Ni	single	2.5mm sheet precracked	H_2 gas	-	TG-[100] plane	-	-	-	-	Fractography same as Hg
Latanision et.al, 83	Ni	poly	2mm cyl	elect. H	dynamic no prechg	IG	-	↓%elong (R.T.)	-	-	IG promoted by seg. of Sb & Sn to g.b.s.
Vehoff & Rothe, 37	Ni	single	6mm bar precracked	H_2 gas	-	TG-[100] plane	↑da/dt →↓embr.	-	window-max embr 300°K	-	Embr. depends on H_2 pressure, see fig. 21
Eastman et.al, 45	Ni	single & poly	"various"	solute & H_2 gas	prechg. 1300°C & no prech.	IG/TG [111] plane	-	-	-	-	Solute H or S seg^n @ g b's required for IG
Traylor, 5	Ni	poly	0.25" cyl	elect. H	no prech.	IG/TG MVC	↑%RA @ RT	-	-	-	Fractography same as Hg

TABLE I

(CONTINUED)

Source	Metal	Crystals	Specimens	Envir.	Charging	Fractog	↓ $\dot{\epsilon}$	↓g.s.	↑Temp.	↑C.W.	Remarks
Fredell, 8	Monel 400	poly	0.25" cyl	elect H	no prech	IG/TG/ MVC	↑%RA @RT	↑%RA @RT	-	↓chng. in %RA & TS	Fractography as Hg
Morris, 10	Ni Monel Inconel Incolloy	poly	0.25" cyl	elect H	no prech	IG/TG/ MVC	-	↓chng. in fatigue life	-	-	Fractography same as Hg
Lynch, 4	Ni	single	2.5mm sheet precracked	Hg	-	TG [100] plane	-	-	-	-	Fractography same as HE
Costas, 84	Monel	poly	1.27mm sheet	Hg	-	IG/TG	-	-	-	-	P seg. to g b's, reduces embrittlement
Funkenbusch et.al, 39	Monel	poly	1.3mm sheet	Hg	-	IG/TG	-	-	-	-	P seg. to g b's reduces embrittlement
Good, 67	Ni Monel Inconel Incolloy	poly	0.25" cyl	Hg	-	IG/TG/ MVC	-	-	-	↓chng. in fatigue life	Fractography same as HE
Fredell, 8	Monel	poly	0.25" cyl	Hg	-	IG/TG/ MVC	↑%RA & TS @ RT	-	-	-	Very large grains embrittled very little
Morris, 10	Ni Monel Inconel Incolloy	poly	0.25" cyl	Hg	-	IG/TG/ MVC	-	↓chng. in fatigue life @RT	-	↓chng. in fatigue life	

room temperature for dynamically charged single crystals.

Lynch (4) compared embrittlement of precracked nickel single crystals by gaseous hydrogen and by liquid mercury. He observed that the fractography produced by each environment was almost identical, and concluded that both types of embrittlement are produced by the same mechanism. Costas (84) and later Funkenbusch, Heldt, and Stein (39) studied the effect of phosphorus segregated at grain boundaries on the embrittlement of Monel 400 (and other Cu-Ni alloys) by mercury and hydrogen at room temperature. They concluded that the segregation of phosphorus to grain boundaries (aided by slow furnace cooling annealed samples) reduced both LME and HE to a large degree. Funkenbusch, et.al. attributed this to an improvement in the packing efficiency of grain boundaries as the segregated phosphorus replaced copper atoms, thus reducing mercury and hydrogen adsorption at the grain boundaries. They interpreted the uniformity of the effect of grain boundary phosphorus on LME and HE as an indication that both processes share a common mechanism. Their tests were conducted on thin (0.35 cm) sheets of 60 μm grain size at a strain rate of 2.2×10^{-1} s^{-1} (considerably faster than the present study). In mercury, intergranular fractures were produced with isolated transgranular areas. When precharged with hydrogen (cathodically charged for 100 hrs. at 90°C at various current densities) intergranular fractures were also noted, but transgranular areas were more common, the extent of

transgranular fracture increasing with increasing sample elongation. In LME samples, a single crack propagated to failure, while all hydrogen charged samples contained cracks which were not involved in sample fracture (referred to subsequently as side cracks).

OSU STUDIES

The recent studies at OSU have compared HE and LME of nickel and nickel alloys. Various alloys have been studied, using slow strain rate tensile tests (under stroke control) and fatigue tests in electrolyticly charged hydrogen and liquid mercury environments. Good (67,85) tested ten nickel alloys in liquid mercury and found that all were embrittled to some degree at room temperature. The alloys Monel 400, Monel 405, and Monel K500, Inconel 625, Inconel 718, and Inconel 750 displayed different degrees of intergranular embrittlement under slow strain rate tensile testing, while Nickel 200 and Inconel 600 fractured transgranularly. Incoloy 800 and Incoloy 825 were not embrittled under tension testing, but all ten alloys exhibited intergranular fractures on their fracture surfaces under fatigue testing. A generalized fracture mode sequence was observed beginning with intergranular (IG) cracking, changing to crystallographic transgranular (TG), then noncrystallographic transgranular fracture, and finally to microvoid coalescence (MVC), as shown in Figure 4. The fracture mode was governed by the strain, with lower strains favoring IG fracture. No

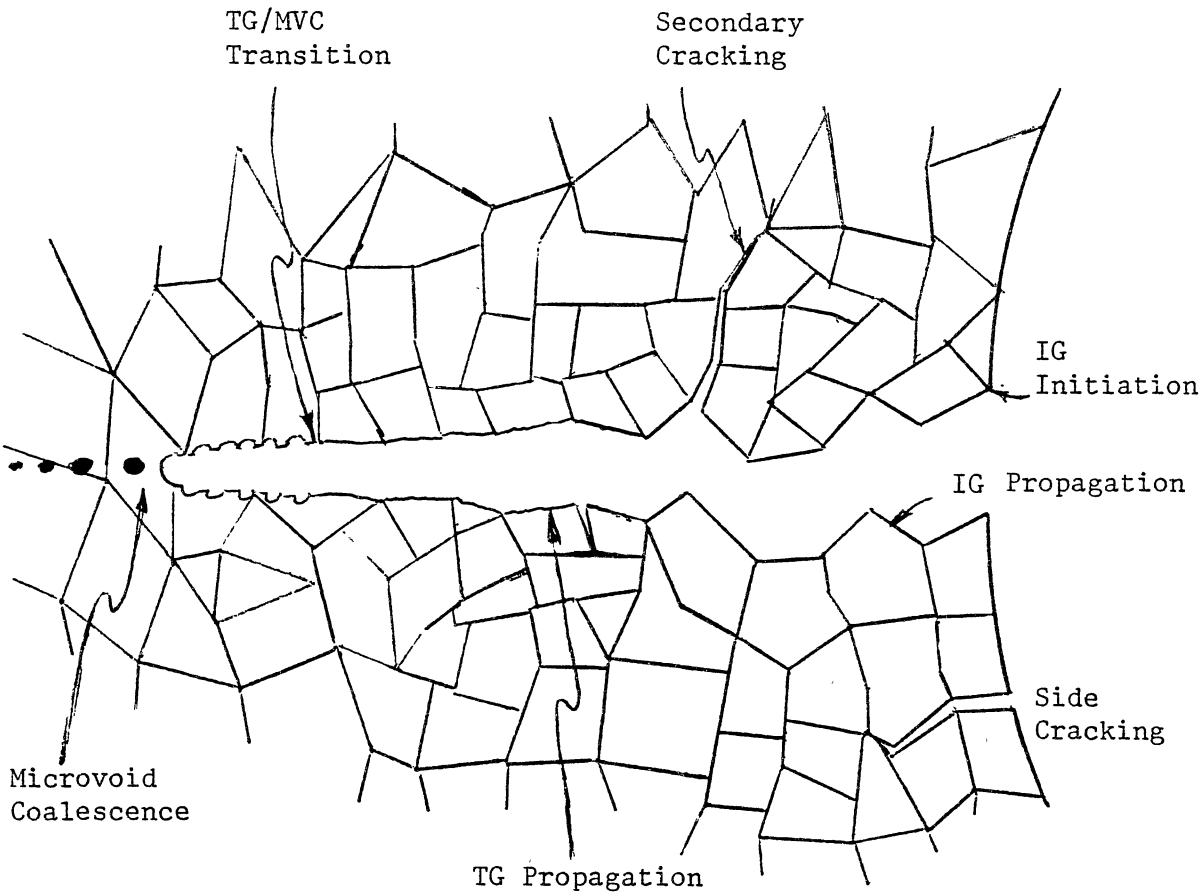

Figure 4. Fracture sequence observed in previous studies at OSU

correlations were apparent with mechanical properties, but less embrittlement was noted with increasing iron content. The same trend was noted by Windle and Smith (80) for HE of nickel alloys. Good (67) found that Monel 400 was the most embrittled alloy having a completely intergranular fracture surface while its free-machining version, R405, (containing 0.04% sulphur) exhibited less embrittlement. Good's study, encompassing nickel and Ni-Cu, Ni-Cr, and Ni-Cr-Fe alloys, strongly suggests that any nickel alloy can be embrittled by mercury under appropriate conditions. Ni-Co alloys would also be expected to exhibit embrittlement by mercury, as Kane and Berkowitz (86) report hydrogen embrittlement of MP35N.

Traylor (5,6,7) investigated most of the same alloys for HE under similar conditions. He determined that all the alloys were embrittled by hydrogen to some degree. As determined by the degradation in the percent reduction in area, hydrogen was the more aggressive environment for Nickel 200 and mercury was more aggressive for Monel 400 and Inconel 625. As in the LME tests, Incoloy 825 was not embrittled by tensile testing, but was embrittled by fatigue tests. Monel 400 again exhibited the most embrittlement of alloys tested, with R405 being less embrittled. The same fracture sequence was observed, and fractography was very similar between the samples fractured in hydrogen and those fractured in mercury. He concluded that both HE and LME are surface phenomena. He also determined that the severity of

HE increased with charging current, up to 200 amps/m^2, where it saturated, and that the amount of precharge time (at room temperature) had no significant effect on HE of dynamically charged Ni 200.

Fredell (8,9) investigated in more detail Monel 400, the most severely embrittled alloy in previous studies. He studied grain size and strain rate effects in both HE and LME. Embrittlement from both hydrogen and mercury decreased with increasing strain rate as shown by Table II. Embrittlement by mercury increased with increasing grain size except for a very coarse grain size (500μm) where embrittlement decreased, see Table III. This decrease was presumed to be due to a lack of plastic constraint. In hydrogen, increasing the grain size led to decreased embrittlement, in disagreement with the trend reported by Wilcox and Smith (78) and Latanision and Opperhauser (83) for nickel. Plastic deformation was reported to be a necessary prerequisite for intergranular fractures, but excess plasticity was reported to prevent such fractures by eliminating stress concentrations. The fracture sequence observed in earlier studies was confirmed, as was the strong similarity between fractography produced by HE and LME. Widespread secondary longitudinal cracking was reported for both HE and LME.

Fredell also conducted tests in which a sample was loaded quickly in mercury, held at a static load for a considerable length of time, and then pulled to failure at

TABLE IIa

TENSILE STRENGTH AND REDUCTION IN AREA
OF MONEL 400 TESTED IN MERCURY
AT ROOM TEMPERATURE [8]

Strain Rate, s^{-1}	Tensile Strength MPa	(ksi)	Reduction in Area, %
1.6×10^{-2}	655	95	64
1.6×10^{-3}	641	93	33
1.6×10^{-4}	475	69	14
1.6×10^{-5}	434	63	11
1.6×10^{-6}	400	58	9

TABLE IIb

TENSILE STRENGTH AND REDUCTION IN AREA
OF MONEL 400 TESTED IN HYDROGEN AT
ROOM TEMPERATURE [8]

Strain Rate, s^{-1}	Tensile Strength MPa	(ksi)	Reduction in Area, %
1.6×10^{-4}	627	91	56
1.6×10^{-5}	572	83	32
1.6×10^{-6}	565	82	30

TABLE IIIa

VARIATION OF TENSILE STRENGTH AND REDUCTION IN AREA WITH GRAIN SIZE OF MONEL 400 TESTED IN MERCURY AT ROOM TEMPERATURE [8]

Grain Diameter, μm	Hardness R_B	Tensile Strength MPa	ksi	Reduction in Area, %
35	70	503	73	12
80	64	531	77	13
150	59	434	63	12
250	57	434	63	11
500	54	579	84	31

TABLE IIIb

VARIATION OF TENSILE STRENGTH AND REDUCTION IN AREA WITH GRAIN SIZE OF MONEL 400 TESTED IN HDYROGEN AT ROOM TEMPERATURE [8]

Grain Diameter, μm	Hardness R_B	Tensile Strength MPa	(ksi)	Reduction in Area, %
35	70	552	80	12
80	64	558	81	19
150	59	593	86	43
250	57	572	83	32
500	54	586	85	45

the standard slow strain rate. The first test was on a 250 μm grain size sample at $1.6x10^{-5}s^{-1}$ strain rate. The standard slow strain rate tensile test had produced a tensile strength of 434 MPa (63 ksi) with 11% reduction in area and clean intergranular fractography. The sample was run up quickly to a load of 434 MPa (63 ksi) and held for 21.5 hours. After the loading was resumed, the sample did not break immediately, but exhibited a tensile strength of 522 MPa (75.8 ksi) with a 16% reduction in area. The fractography was more ductile than the straight tensile test, with the outer two to four grains showing mixed intergranular and tearing and the rest of the fracture surface being relatively pure intergranular. The strain required to produce fracture after commencement of the slow strain rate was estimated from the stress strain curve to be about 5%.

His second test was done at a strain rate of $1.6x10^{-6}s^{-1}$, where a standard tensile test in mercury at the slow strain rate produced 400 MPa (58.0 ksi) tensile strength and 9% reduction in area with clean intergranular fractography. The sample was loaded rapidly to 345 MPa (50 ksi) and held for 153 hours; then strained to failure at the very slow strain rate. It had a tensile strength of 475 MPa (68.9 ksi) and 16% reduction in area. The test was interrupted at 6, 25, 93, 11, and 133 hours and the surface was examined under the SZM for evidence of the beginning of cracks. No cracks were found. However, slip marks were

visible on individual grains, and an intense band of plastic deformation circled the center of the sample beginning at 25 hours. The strain necessary to cause fracture after commencing the slow strain rate was estimated to be 4.5%. In both of these samples, time at load alone was not enough to cause fracture in the mercury environment.

Morris (10) sought possible correlations between the degree of embrittlement and various mechanical properties for HE and LME of Nickel 200, Monel 400, Inconel 600, and Incoloy 800. He could identify no reliable correlation between embrittlement susceptibility and strain hardening exponent, stacking fault energy, and slip character. The fracture mode sequence observed in earlier studies was again confirmed, as was the similarity between HE and LME fractography. Fatigue life was reduced by mercury, as in the other studies, but hydrogen produced enhanced fatigue lives for all of the alloys except Monel 400. He also ran interrupted tests where the sample was removed and inspected for damage before fracture. At 80% of the tensile load in air, most of the alloys tested in mercury and hydrogen showed extensive rumpling and slip marks on the surface, but none except for Inconel 600 exhibited any cracking. At this stress level, Monel 400 was extensively rumpled, but showed no visible cracks. The behavior of Inconel 600 in hydrogen was anomalous. At 80% of the tensile strength, it contained extensive IG cracks on the surface, which widened as the tensile strength was reached. However, fracture was not

experienced until after necking had started, at 96% of the tensile strength in air. Fatigue behavior of the Inconel 600 and Incolloy 800 was unexpected, in that while mercury reduced fatigue lives of both alloys, the hydrogen enhanced fatigue lives of both alloys relative to lives obtained in air. Morris concluded that the fatigue cracks and blunt side cracks in the tensile tests were blunted by enhanced nucleation of dislocations by the hydrogen.

Peevy's (87) investigation, while mainly concerned with copper, also studied the effect of prestrain before the mercury was added to LME of Monel 400. He found that prestrain below the yield point had no noticeable effect on the strength or ductility of the Monel, but as the sample was prestrained in the plastic region, the tensile strength and to a lesser extent, the ductility increased. For instance, samples with no plastic prestrain failed at about 410 MPa (60 ksi), but a sample loaded to 410 MPa before the mercury was added went to 550 MPa (80 ksi) before fracturing. A sample then loaded to 550 MPa before adding mercury went to 640 MPa (93 ksi), the tensile strength in air, before fracture. As the level of plastic prestrain was increased the fractography became less and less embrittled, that is, it exhibited less IG and more TG fracture and tearing. By plotting Peevy's stress levels on Morris' Monel 400 stress-strain curve, it can be estimated that from 7 to 11% strain was required after the mercury was added before fracture occurred.

There are some general features which have been common to all of the OSU studies. All of the investigations have reported side cracking. Good (67) observed side cracks in mercury for all alloys that exhibited some necking, both transgranular crack oriented at 45° to the tensile axis or intergranular cracks oriented 90° to the tensile axis. Traylor (5) reported side cracks for every alloy in hydrogen. In nickel 200, increasing the strain rate produced a larger proportion of 45° cracks, and decreasing it fewer cracks that extended deeper into the surface. Fredell reported side cracking for Monel 400 in both environments. In mercury, the proportion of 45° cracks increased with strain rate, while 90° cracks were predominate in hydrogen. As grain size was incrassed, cracks were observed farther from the fracture. Morris (10) reported some slip band side cracks in air, for all alloys with Monel 400 having the most. He also reported side cracking in all alloys, with Inconel 600 having almost every grain separated on the surface around the fracture by blunt cracks.

The previous OSU studies reported extensive secondary (longitudial) cracking, particularly in the mercury environment. The cracks were typically intergranular and often extended radially from the fracture origin. Sometimes fracture surfaces that were predominately intergranular exhibited transgranular fractography for the first few grains in from the surface.

Russian Work

LME has been the subject of sustained study in the USSR for many years. Russian study has traditionally discussed LME in terms of the Rebinder Effect, which attributes changes in mechanical properties of a material to adsorption of substances on the surface (88). Pickens and Westwood (89) have recently reviewed Russian studies of LME. Shchukin and Yuschenko (90) have developed a computer simulation of the "molecular dynamics" of LME, based on an assumed decrease in the surface free-energy of the solid by the adsorbed embrittler. The methods produces computer-generated "movies" of LME induced cracks and gives predictions of the effects of changing test conditions. A limitation of the technique is that as modeled, crack propagation cannot be accounted for by a reduction in cohesion, but by mechanical pressure on the crack walls by the embrittler. Popovich (91) and coworkers have recently proposed a mechanism for LME, based on adsorption induced changes in material behavior. They go far beyond Lynch's (4) suggesions that adsorbed embrittlers enhance dislocation nucleation, by proposing that adsorption facilitates dislocation outlet to the surface, dislocation nucleation and propagation, the operation of new slip systems, and work hardening. However, this mechanism is not supported by fractographic or microstructural observations.

The most important recent Soviet work is with liquid metal facilitated machining (LMFM). The major advantages

are greatly incrassed machining rates (for example an eightfold increase for a stainless steel drilled under Sn-Zn eutectic) and acceptable machining rates in previously very difficult to machine alloys. Residues of the liquid metal are generally removable by chemical or mechanical polishing. In some cases, the finished part is heated to a temperature where the liquid metal is absorbed into the metal matrix, increasing near surface hardness.

CHAPTER III

The Experiment

Monel 400 was chosen for the experimental portion of this study for a number of reasons. It was the most embrittled nickel alloy investigated by Good (67) and Traylor (5), and Fredell (8) has provided background information at room temperature. Its FCC structure allows for straightforward interpretation of results, without considering interactions with second phases or precipitates.

Monel 400 is a single-phase, solid solution strengthened alloy of approximately two-thirds nickel and one-third copper. It has an important commercial niche because of its excellent corrosion resistance, as it resists reducing environments better than nickel and oxidizing environments better than copper. It is generally not susceptible to stress corrosion cracking (92,93). The composition and typical mechanical properties of the test heat are given in Table IV.

Test equipment, specimens, and conditions were maintained as closely as possible to those reported for previous studies at OSU (5-10,67,85). Slow-strain-rate tensile tests were done under stroke control on an MTS machine. Strain rates of $1.6 \times 10^{-5} s^{-1}$ and $1.6 \times 10^{-3} s^{-1}$, subsequently referred to as the slow strain rate and fast

TABLE IV

COMPOSITION AND MECHANICAL PROPERTIES OF THE COLD DRAWN MONEL 400 ROD IN THE AS-RECEIVED CONDITION. FREDELL'S MATERIAL ALSO SHOWN FOR COMPARISON

	This Study	Fredell (8)
Heat	M0396B	M9631B
Nickel	65.42%	66.71%
Copper	31.66	31.15
Iron	1.50	1.60
Manganese	1.00	1.13
Silicon	0.24	0.23
Carbon	0.14	0.16
Aluminum	0.041	0.013
Sulfur	0.003	0.009
Yield Strength	676 MPa	672 MPa
Tensile Strength	778 MPa	812 MPa
Hardness	R_B 95	R_B 99
% Elongation	25%	25%
% Reduction in Area	70%	64%

strain rate, were chosen. This was because Fredell's results (Table II) indicated that $1.6x10^{-3}s^{-1}$ was the fastest strain rate at which significant embrittlement occurred, and that embrittlement seemed to saturate with decreasing strain rate, such that the $1.6x10^{-5}s^{-1}$ data were approximately equal to that observed at $1.6x10^{-6}s^{-1}$ (8). These strain rates were verified by Good (67) and Fredell (8) for the appropriate crosshead velocities. Slow strain rate tensile tests typically lasted about five hours, and fast strain rate tests about three minutes.

Test specimens were machined from cold drawn bar to a waisted geometry of minimum diameter 6.35mm (0.25 in), as illustrated in Figure 5. Specimens received a 600 grit polish and were vacuum annealed as shown in Table V to produce the indicated grain sizes. Grain sizes of 35 and 250 μm were chosen to effectively "bracket" the range investigated by Fredell (8). Also, the 35 μm size produced maximum HE and the 250 μm size produced maximum LME in his study (see Table I). All of the samples were furnace cooled to less than 50°C to produce the maximum segregation of impurities to the grain boundaries. Grain boundary segregation has been shown to have a significant effect on the magnitude of embrittlement of Monel (39,84). Samples were chemically polished after annealing to provide a good surface for observing side cracks, and to remove scratches from polishing (94).

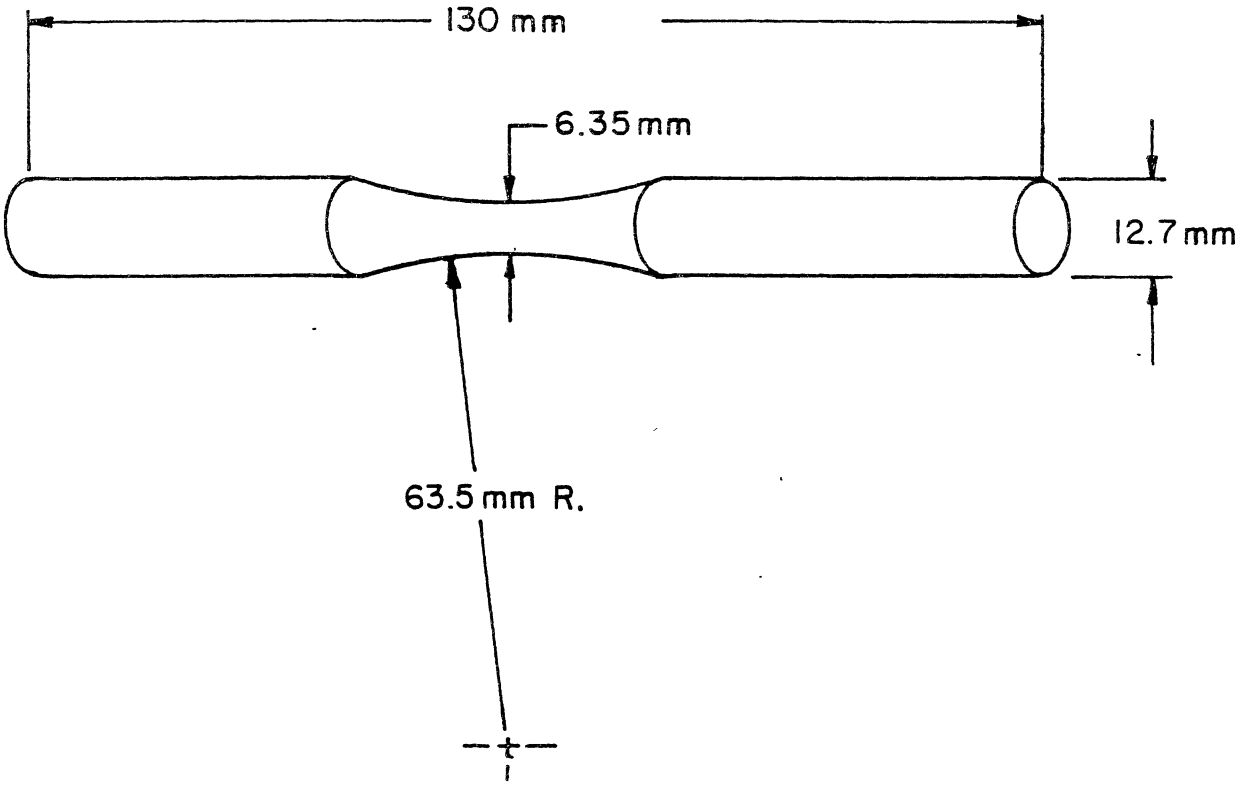

Figure 5. Sample geometry

TABLE V

ANNEALING CYCLES FOR MONEL 400 TEST SAMPLES

Time (hr.)	Temperature (°C)	Grain Size (μm)
3.75	700	35
3	1075	250
4	1090	350

The embrittling environments were contained in environmental cells mounted on the test specimens, as in previous work. Tests were conducted in liquid mercury and under cathodic charging in an electrolytic cell at temperatures of -30, -20, 0, 22, 50, and 80°C. This was the widest temperature range that was readily obtainable in liquid mercury. The mercury freezes at -38°C, and higher temperatures were avoided because of the toxic nature of mercury vapors. For the LME tests, the low temperatures were maintained by passing methanol and dry ice through a cooling coil in a bath of methanol and water, with the composition adjusted to freeze at the desired test temperatures. The mercury was contained in a chamber which was surrounded by the temperature bath, as shown in Figure 6. The temperature was monitored with a copper-constantan thermocouple, as shown in the figure. The methanol and dry ice, at about -80°C, were circulated through the cooling coil until a layer of ice was formed around the coil. The temperature for the hydrogen tests was controlled in the same manner, except that the electrolyte for cathodic charging was also the cooling bath. The electrolyte was the water/methanol mixture of the correct freezing temperature, with one drop per liter of sulfuric acid (approximate pH of 3.2) and 0.25 g/l of sodium arsenite added to inhibit hydrogen recombination. The hydrogen test chamber is shown in Figure 7. The specimens were cathodically charged at a rate of 200 A/m^2 with a galvanostat (Princeton Applied

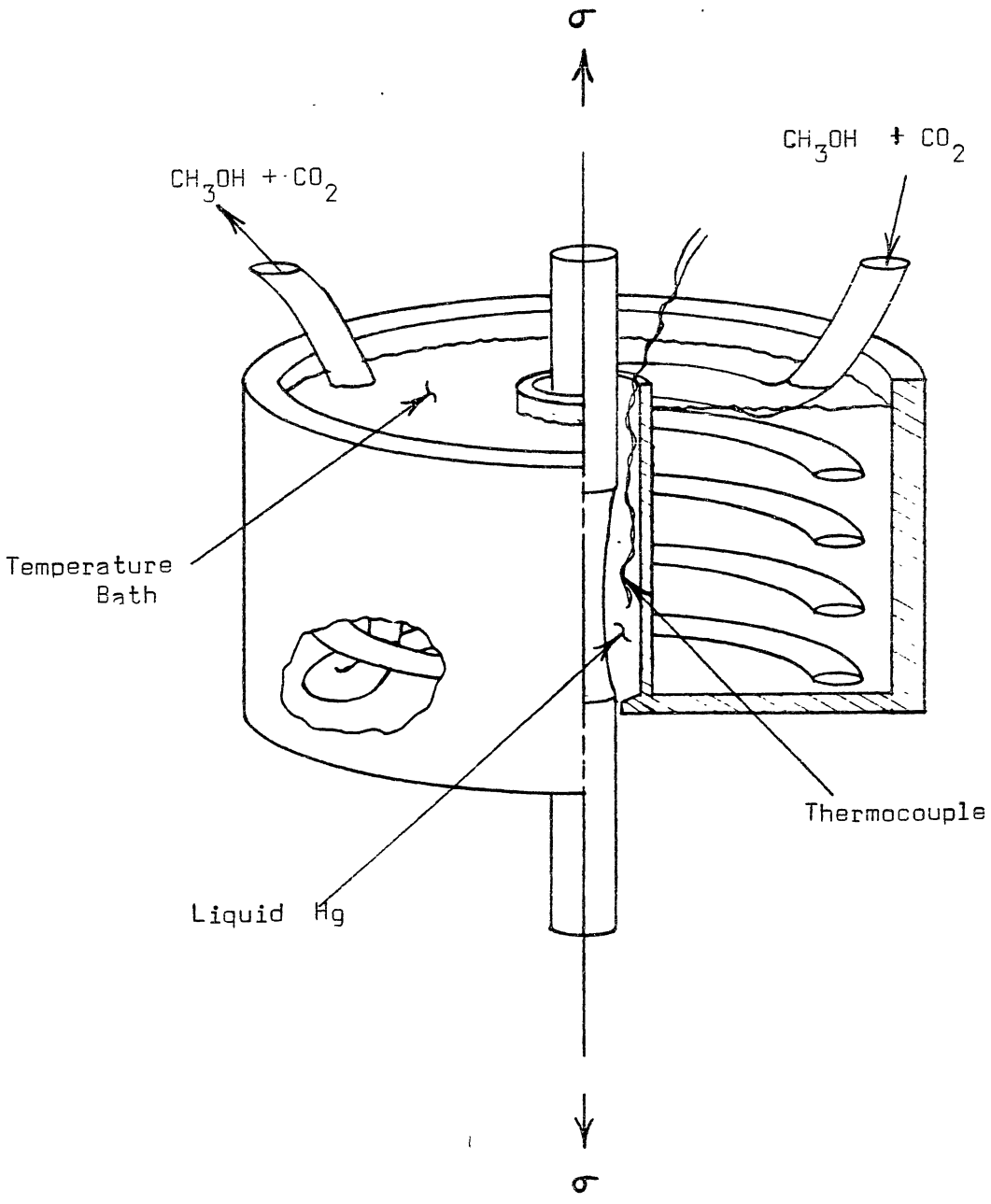

Figure 6. LME low temperature test cell

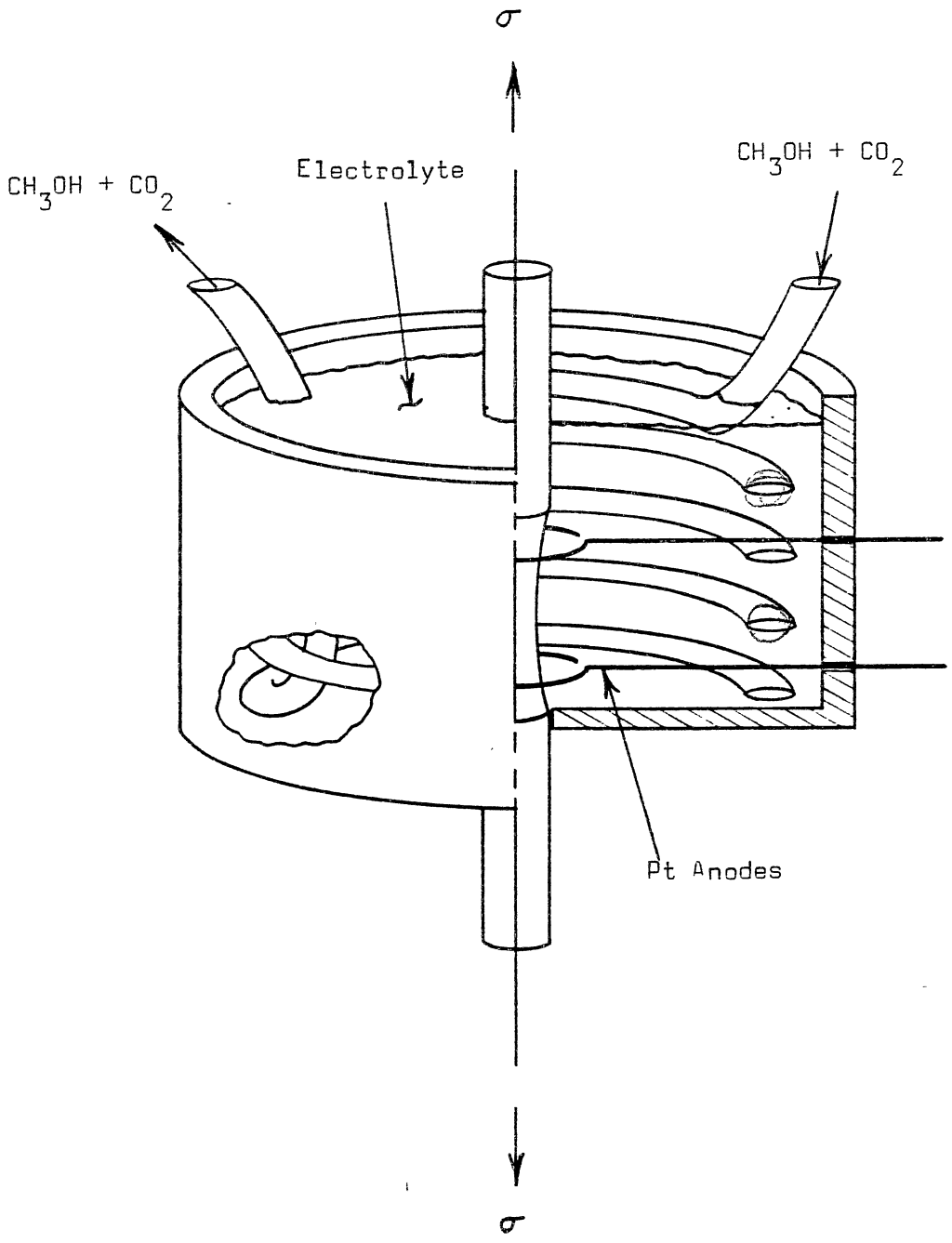

Figure 7. HE low temperature test cell

Research Model 1173). Traylor (5) demonstrated that HE of nickel is saturated and thus insensitive to charging rate at this rate. Platinum wires served as the anode of the electrolytic cell. The temperature for the hydrogen tests was monitored by a spirit thermometer, as the charging current affected the thermocouple readings.

The high-temperature tests were conducted in the same environmental chambers, except that the cooling coil was replaced by a 110VAC electrical resistance heating element, regulated by a variable transformer. Since mercury vapors are hazardous, precautions were taken to insure that all vapors were contained. The top of the mercury chamber was sealed by a rubber bellows, then the entire test chamber and temperature bath was enclosed in a high-temperature plastic bag, sealed with RTV silicone.

Continuous plots of load vs crosshead displacement were recorded during each tensile test.

Some fatigue tests were also conducted on the MTS machine, using axial loading under load control. The test frequency was 30 hz. The load cycle was sinusoidal, varying from a minimum load of 0-40 N to the maximum load. After failure, the samples were removed and cleaned ultrasonically in trichloroethylene, acetone, and ethyl ether. Any excess mercury remaining on the LME samples was vaporized by heating at 100°C for one hour in a mild vacuum. The samples were examined using a 10-70x stereo zoom microscope (SZM), and a JEOL scanning electron microscope.

CHAPTER IV

RESULTS AND DISCUSSION

Mercury Embrittlement

Monel 400 versus Temperature

Fine Grain Size. Figure 8 shows results of the tensile tests of Monel 400 of 35 μm grain size at the two strain rates of 1.6×10^{-5} s^{-1} and 1.6×10^{-3} s^{-1}. The tensile strength of the Monel declined as temperature was increased for both strain rates. Increasing the strain rate increased the tensile strength. The percent reduction in area versus temperature shows a marked decrease in embrittlement at lower temperature, consistent with the lower end of a "temperature window" at both strain rates. The faster strain rate caused the embrittlement to begin at a higher temperature than the slower strain rate. Figure 9 illustrates a typical load versus displacement curve for a slow strain rate tensile test in air. The more brittle failures in mercury, such as those at the higher temperature end of the curves, broke before the material reached its tensile strength in air; whereas the more ductile failures broke past the tensile strength after necking had begun.

A comparison of the two tensile strength curves in Figure 8a and the reduction in area curves of Figure 8b

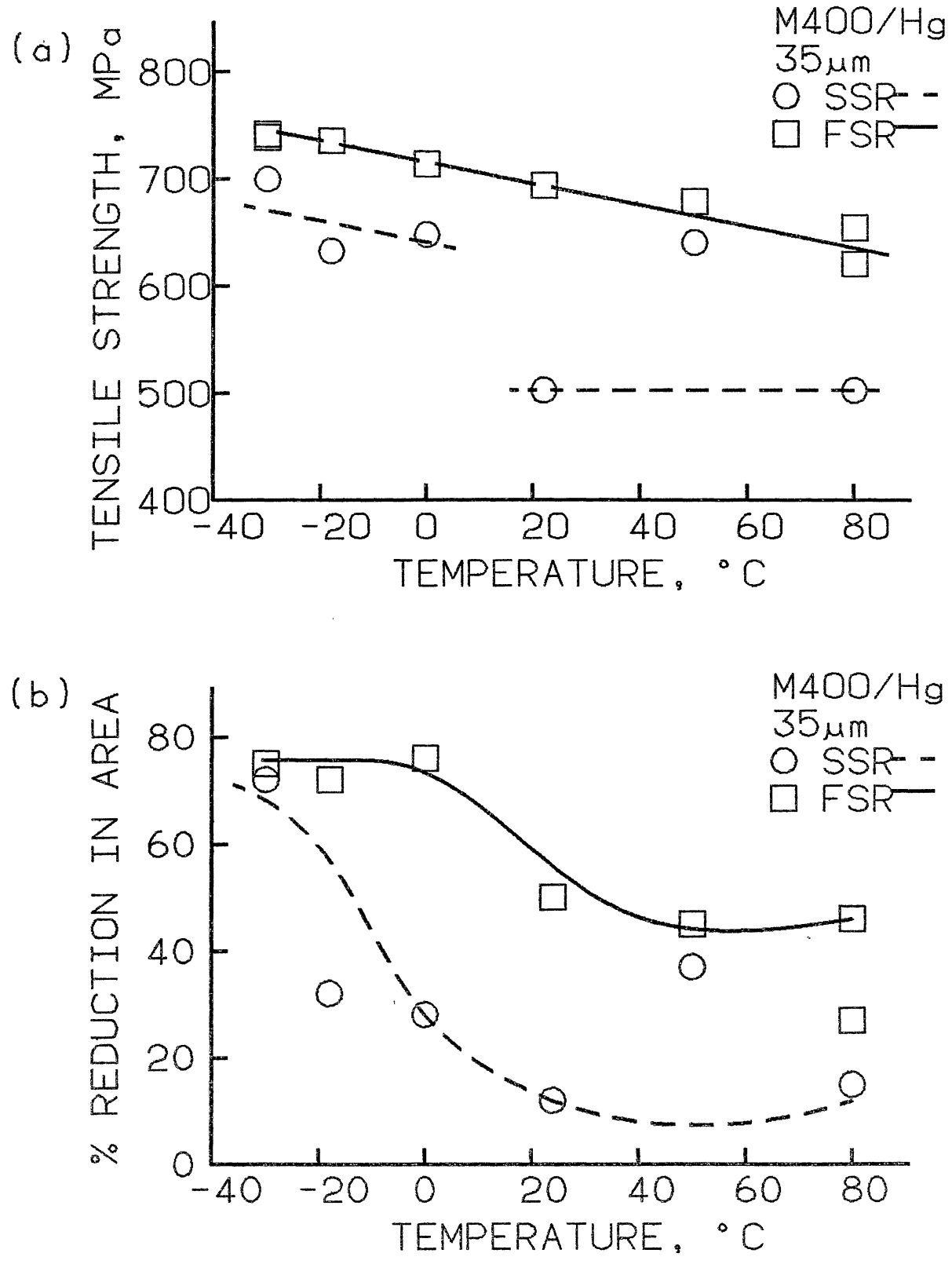

Figure 8. Mechanical properties versus temperature for fine grain Monel 400 in mercury. Tensile test at $1.6 \times 10^{-5} s^{-1}$ (SSR) and $1.6 \times 10^{-3} s^{-1}$ (FSR)

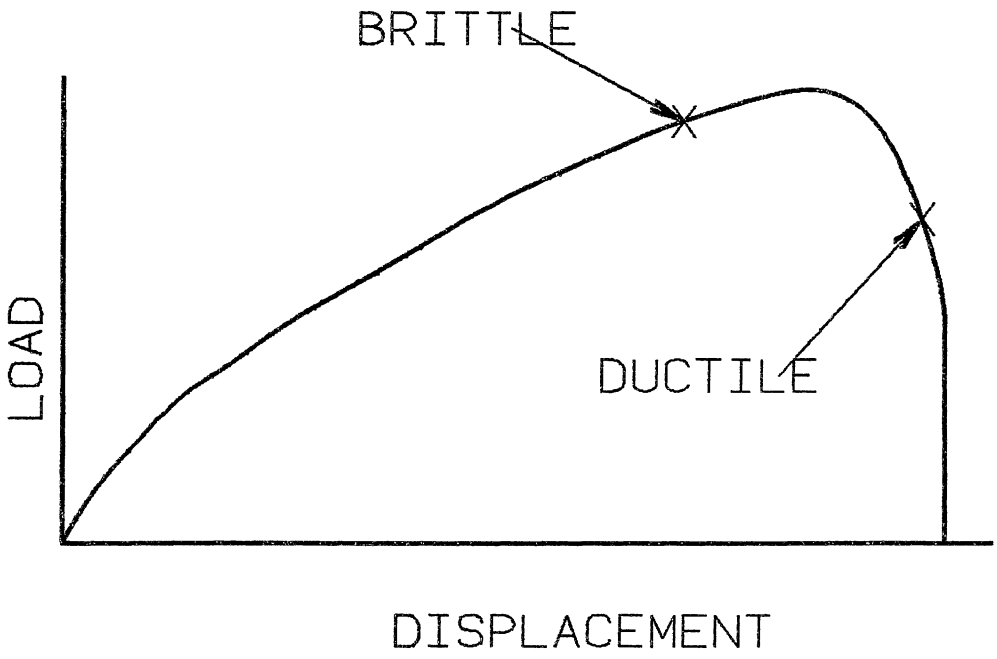

Figure 9. Typical load vs displacement curve for a slow strain rate tensile test under displacement control.

shows that testing at a faster strain rate had an equivalent effect to testing at a lower temperature. Shifting the temperature of one of the tensile strength curves of Figure 8a by 40°C brings tensile strength vs temperature curves for both strain rates into reasonable agreement as illustrated in Figure 10. A 40° temperature shift also results in good agreement between the two reduction in area curves. Thus, increasing the strain rate by two orders of magnitude corresponds to lowering the test temperature by 40°C.

Fractography. The fractography followed a progression as temperature was increased. Figure 11 shows the sequence for both fast and slow strain rates with the diagrams for the slow strain rates offset by 40°C from the fast strain rate diagrams (the same temperature shift used for Figure 10). The sequence begins with ductile cup and cone failures at the fast strain rate at -30°C, -18°C, and at 0°C. The only evidence of embrittlement on the fracture surfaces of these samples was a longitudinal split which extended for approximately 6mm (0.25") from the fracture surface, as shown in Figure 12. They also exhibited a very small amount of 45° side cracking in the necked region. Interestingly, Morris (10) reported similar slight side cracking in air in Monel 400, Inconel 600, and Incoloy 800, yet Incoloy 800 is not significantly embrittled by mercury in tensile tests. As the temperature was increased, the fracture took on the fracture sequence observed in earlier studies (5,8,67):

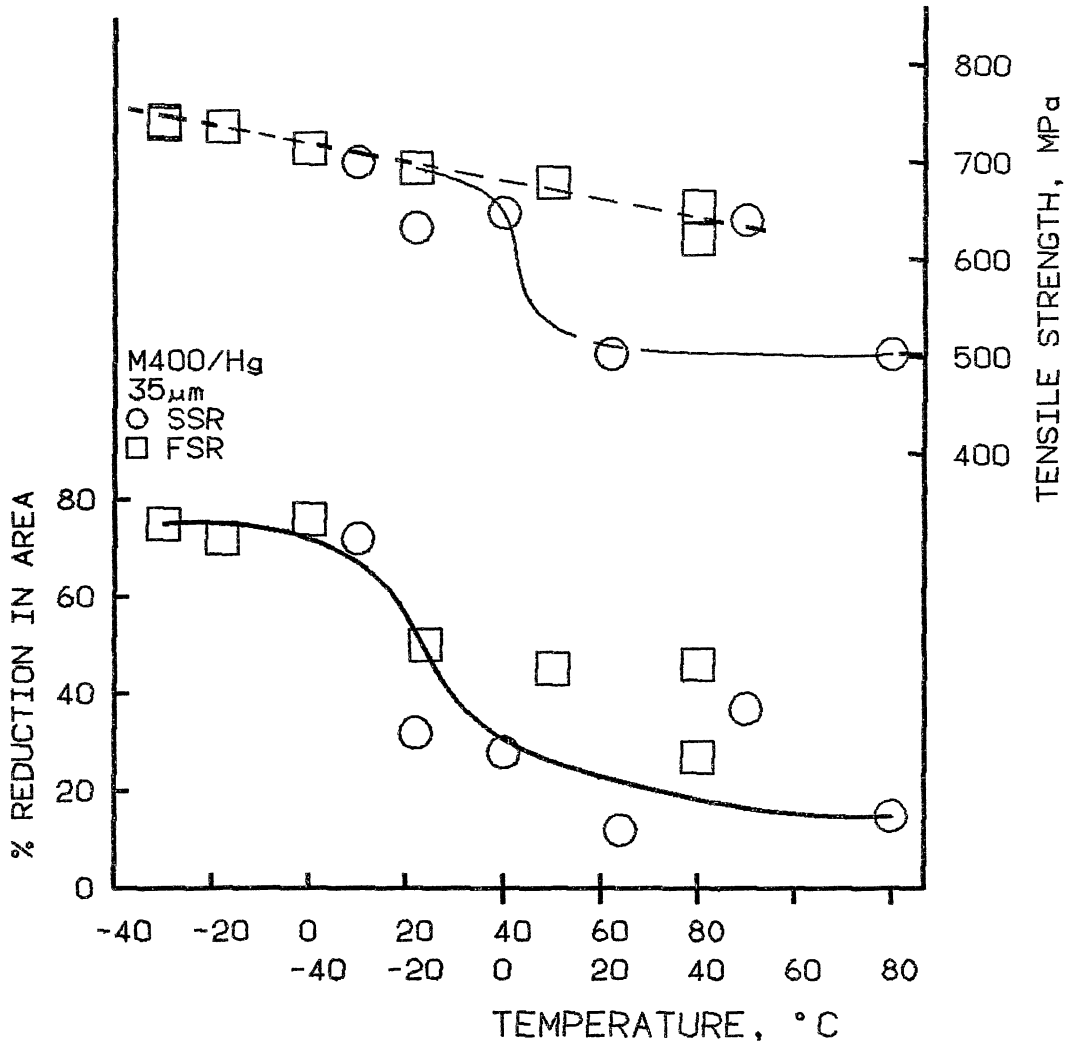

Figure 10. Tensile strength and reduction in area of Monel 400 in mercury vs temperature for both strain rates, plotted with a 40°C temperature shift between slow (SSR) and fast (FSR) strain rates.

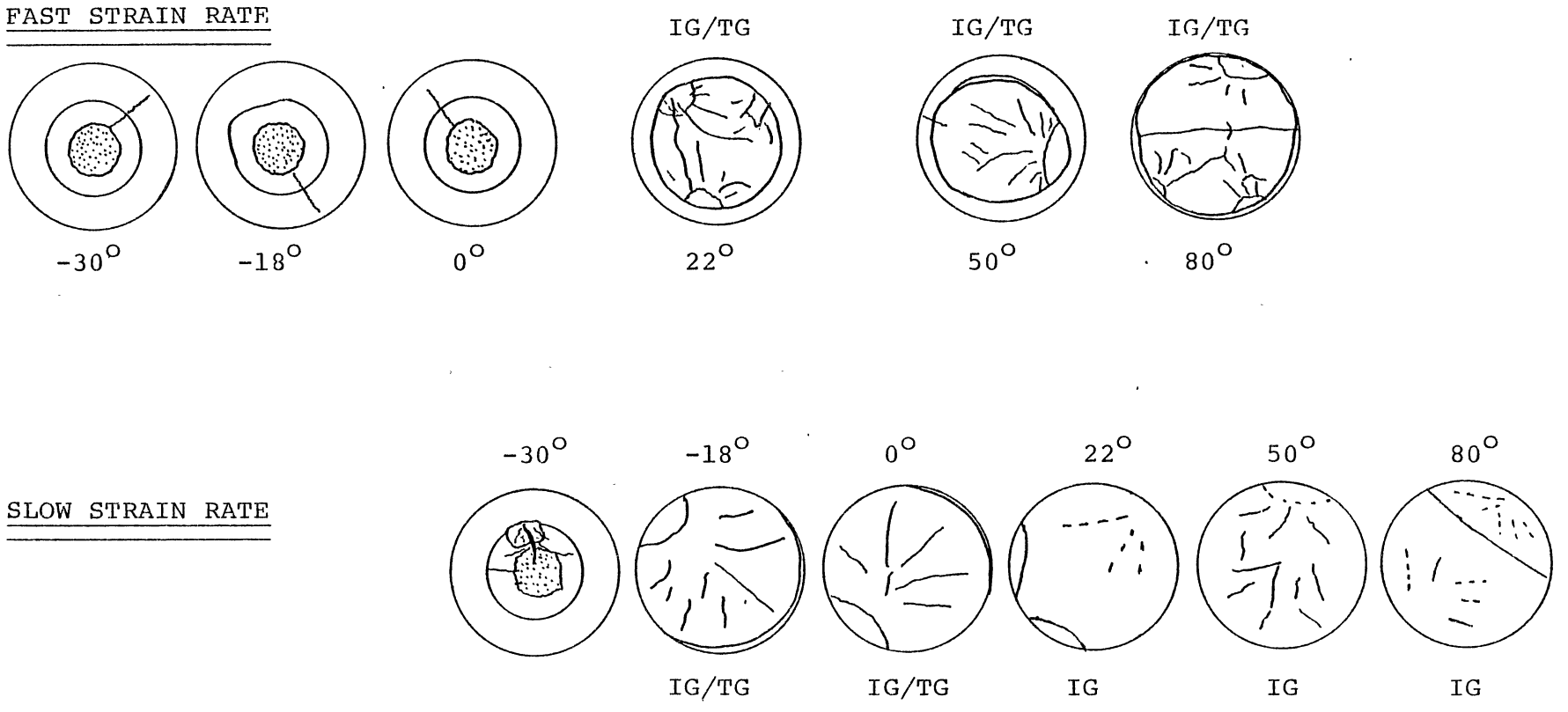

Figure 11. Fractography of 35 μm grain size Monel 400 in mercury versus temperature for the 40°C temperature shift of figure 10

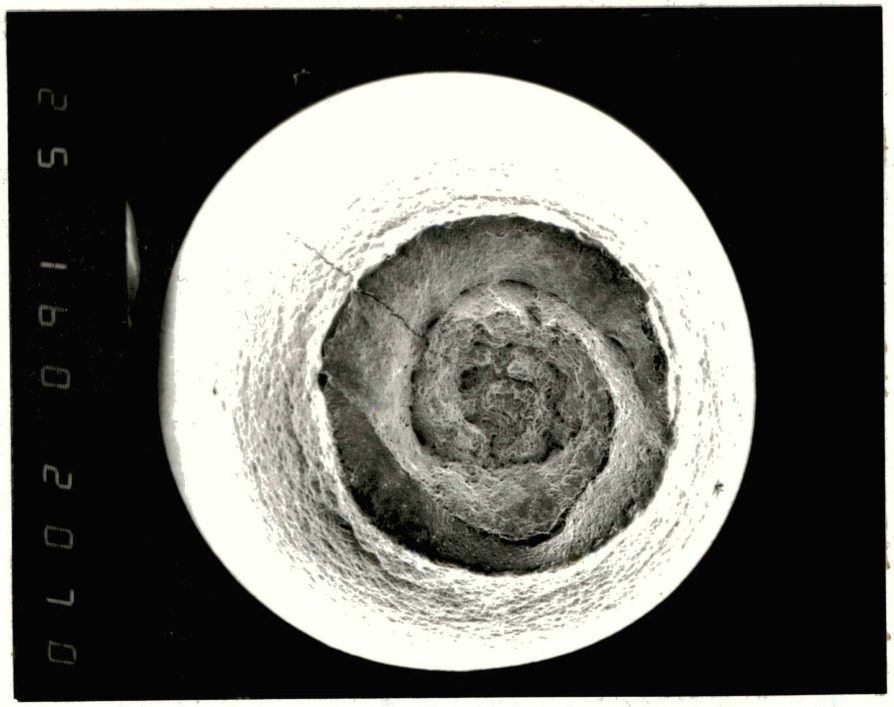

Figure 12. Cup and cone fracture with longitudinal split.
Monel 400/Hg, 35 μm, $1.6 \times 10^{-3} s^{-1}$, 0°C, x 16

Note: In the SEM photographs, the number on the right indicates excitation voltage, magnification, sample number, investigator, and photo number. E.G., for Figure 12:

excitation voltage = 25 MeV
magnification = 16×10^{0} - 16x
sample number = 20
investigator = 7 = KING
photo number = 0 (for sample 20)

that is, intergranular initiation on the surface, followed by transgranular fracture, finally changing to microvoid coalescence fracture, as illustrated by Figure 13. The 35 m fractures exhibited more pronounced radial markings from the origin than was typical in earlier studies, suggesting that they were initiation limited. Longitudinal secondary cracks were common extending radially from the origin. The fracture surfaces of the brittle samples did not have flat intergranular fractography, as in Fredell's study [8], but exhibited slanted fractures on different levels, joined by the radial longitudial cracks. Side cracking was almost completely absent from the fast strain rate failures (except for the slant cracks in the necks), consistent with the view that the fractures are initiation limited. Figure 14 illustrates the 80°C fracture, which exhibited two origins occurring on different levels and linked by shear failure.

The fractography of the slow strain rate failures began with a ductile fracture that was cup and cone except for a small patch of transgranular cracking which originated on the surface after the fracture was almost complete as shown in Figure 15. As temperature was increased, the fractography went to one intergranular origin with substantial longitudinal secondary cracks extending radially from the origin (indicating initiation limited), then to two origins at 80°C. As the temperature was increased the severity of the radial longitudinal cracks was observed to decrease for both strain rates as shown by Figure 16. The

(a)

(b)

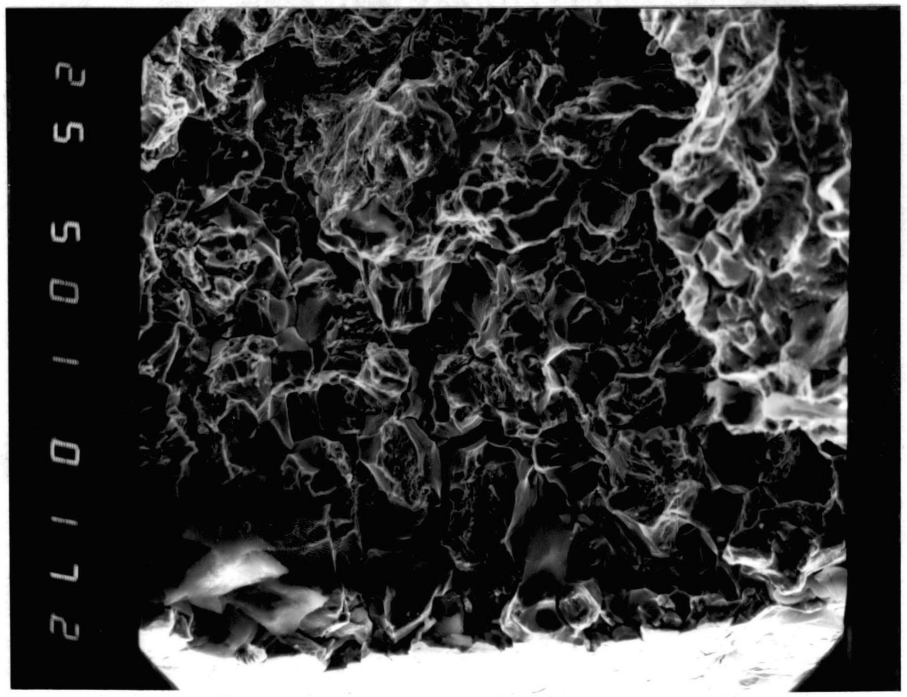

Figure 13. Examples of fracture sequence of intergranular, transgranular, microvoid coalescence in Monel 400. (a) Overall view: Hg, 35 μm, 1.6×10^{-3}, 50°C. (b) Transition from intergranular to transgranular fracture: H, 35 μm, 1.6×10^{-5}, 80°C

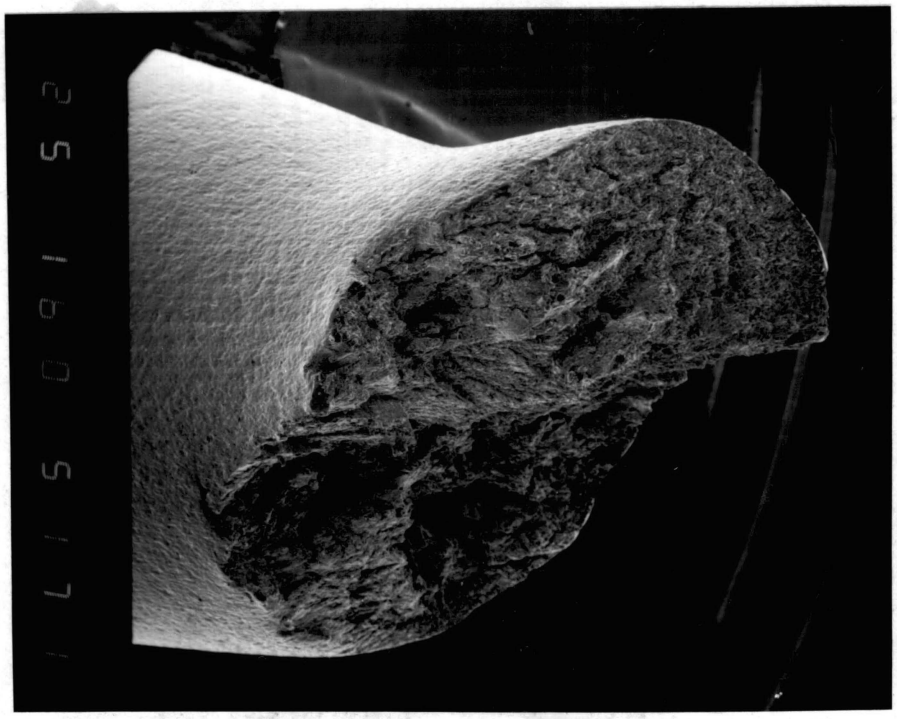

Figure 14. Fast strain rate fracture of fine grain size in mercury at 80°C, exhibiting two origins on different levels. Monel 400/Hg, 35 μm, $1.6 \times 10^{-3} s^{-1}$, 80°C

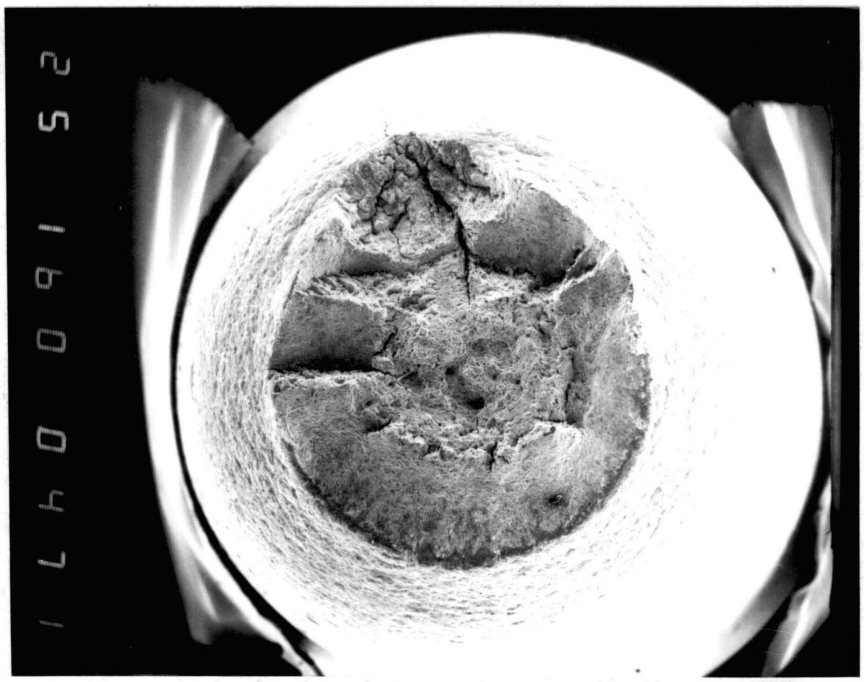

Figure 15. Cup and cone fracture with a patch of transgranular fracture and large secondary cracking. Monel 400/Hg, 35 μm, $1.7 \times 10^{-5} s^{-1}$, -30°C

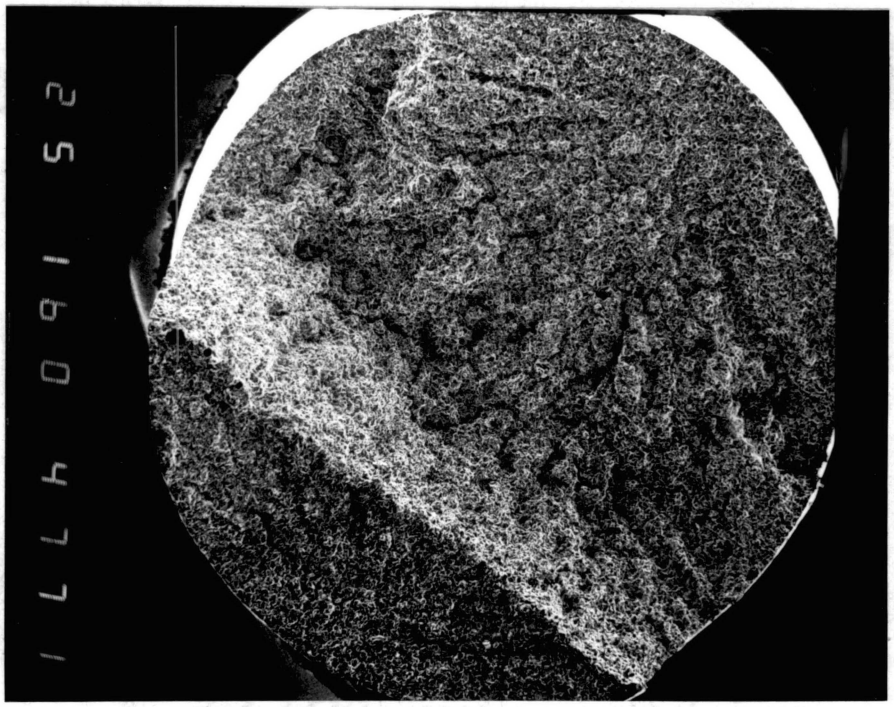

Figure 16. Decreased severity of radial longitudinal markings for mercury fractures as temperature is increased

22°C sample is from Fredell's (8) study, and has a much flatter fracture appearance, with much fewer and smaller radial markings. On the samples with intergranular fracture origins, there was typically a band of transgranular fracture on the surface, extending to a depth of three to five grains.

Thus, the fractography also indicates a temperature shift as strain rate is varied. The apparent temperature shift indicated by the fractography, is in good agreement with the 40°C shift indicated by the mechanical property data of Figure 10. While the general fracture sequence of intergranular/transgranular microvoids is the same as that reported by previous OSU studies, the overall appearance (at low magnification) of the fractures is rather different. Particularly for Fredell's (8) work, the mercury fractures were typically microscopically flat and featureless. Mercury fractures in this study have had much more cracking on different levels and angles linked up by radial longitudinal cracks.

Secondary cracking has been much more common. The large longitudinal splits in otherwise cup and cone fractures were not reported in earlier studies for annealed displacement control tests. Good did however, observe longitudinal splitting under load control and for cold worked material under displacement control. The absence of side cracking is a marked change to Fredell's (8) results. However, at higher magnifications, the more detailed

fractography is much the same as that extensively documented by Good (67), Traylor (5), Fredell (8), and Morris (10). That is, intergranular fractures in this study look like earlier intergranular fractures, etc. Therefore, only a few specific examples of interest of the fractography encountered in this study are presented.

Coarse Grain Size. Figure 17 illustrates tensile strength and reduction in area vs temperature data for the 250 m grain size. Again, increasing the strain rate had an equivalent effect to testing at a lower temperature. For the 250 μm grain size, changing the strain rate by two orders of magnitude is equivalent to approximately a 40° temperature shift as shown by Figure 18. Figure 19 gives yield strength vs temperature data which was obtained from the load vs displacement plots of the tensile tests for the 250 μm grain size. The plots do not have a linear elastic region due to the waisted sample configuration, however a change in slope can be detected at yield on most of the plots. The yield strength data also shows a 40° temperature shift.

Fractography. The fractography for 250 μm grain size shows a sequence similar to that obtained with the 35 μm grain size as temperature is varied. As depicted by Figure 20; the sequence begins at low temperatures and fast strain rates as a transgranular fracture with large secondary cracks and progresses to a completely intergranular fracture surface and finally to an intergranular fracture surface

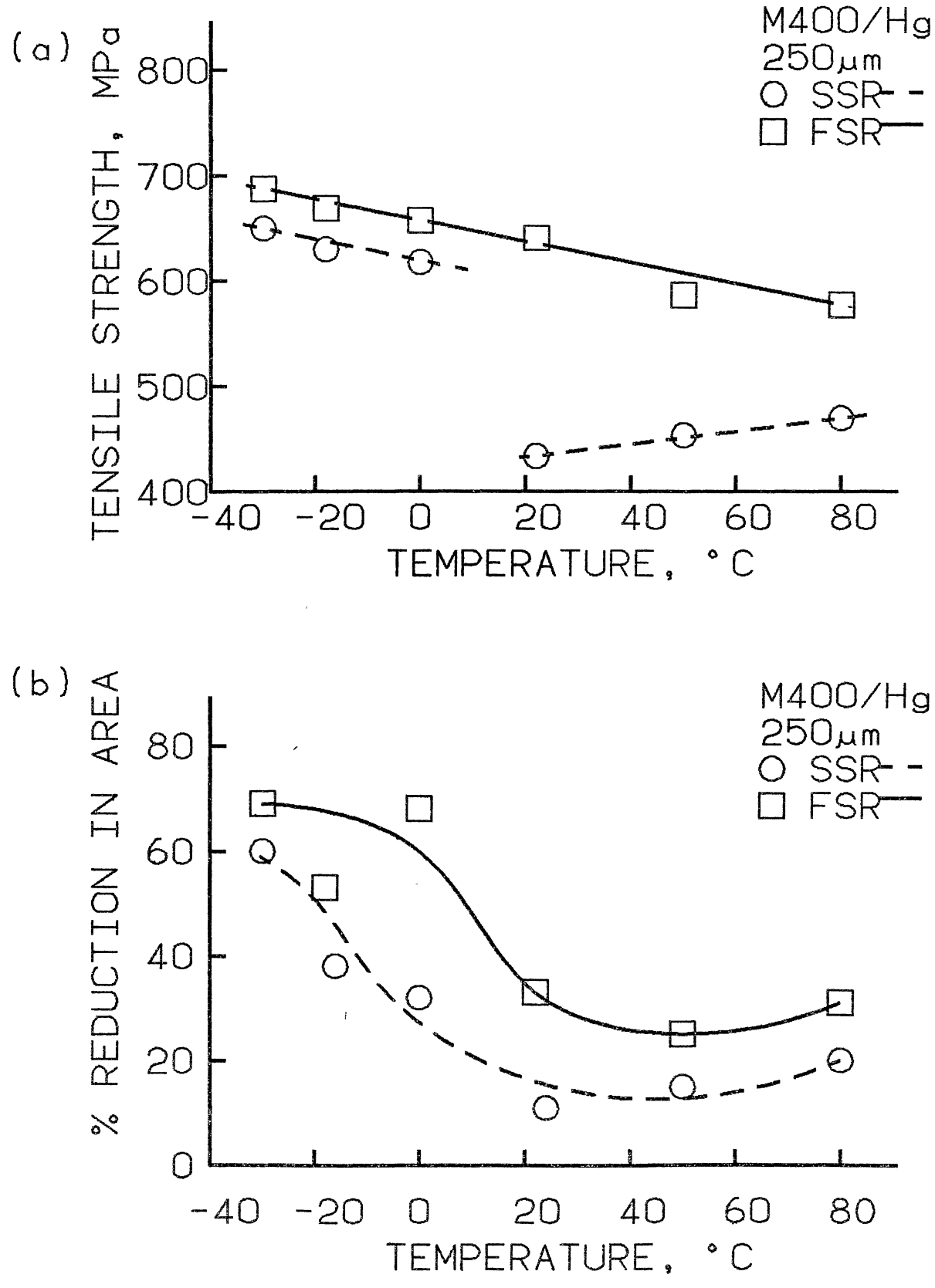

Figure 17. Mechanical properties versus temperature for coarse grain Monel 400 in mercury. Tensile test at $1.6 \times 10^{-5} s^{-1}$ (SSR) and $1.6 \times 10^{-3} s^{-1}$ (FSR)

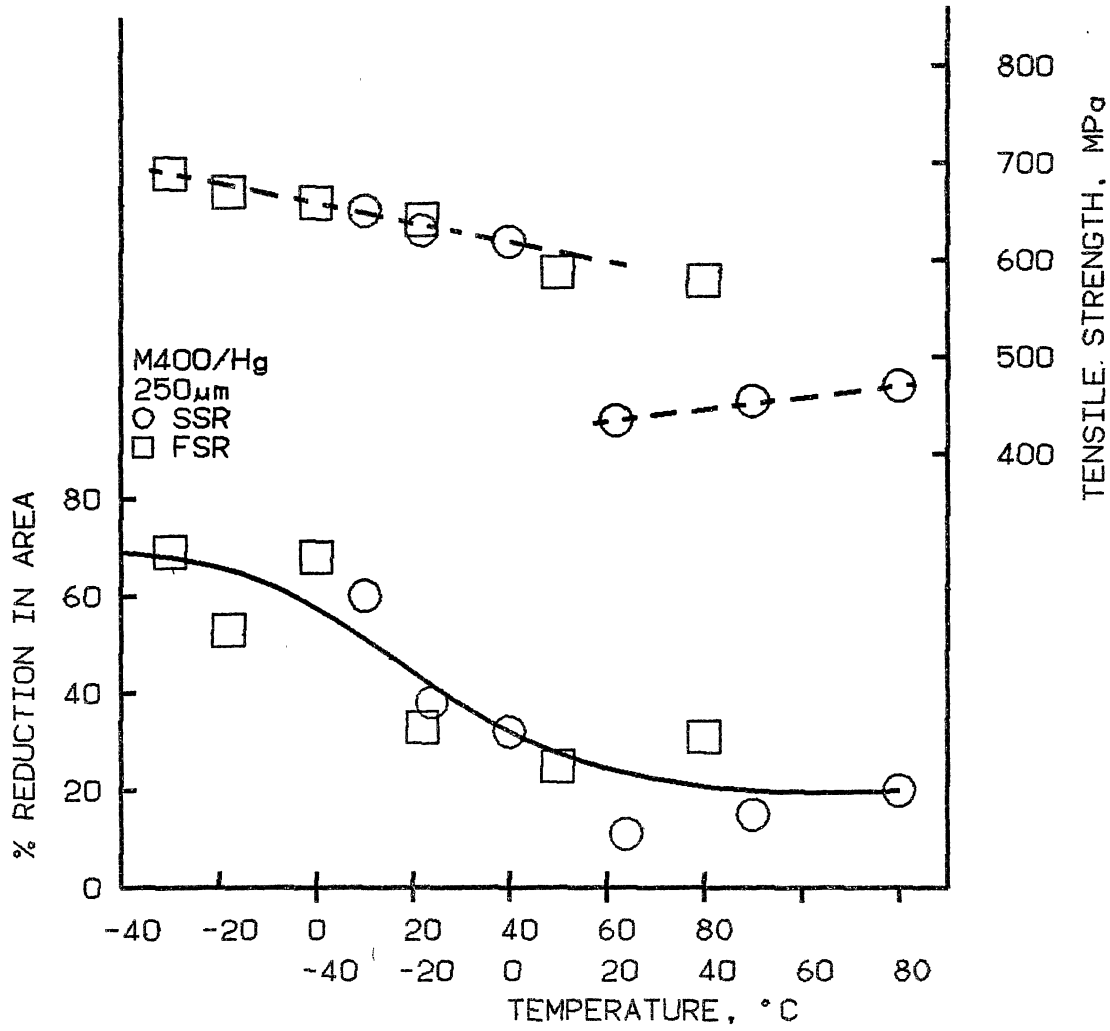

Figure 18. Tensile strength and reduction in area versus temperature of coarse grain Monel 400 in mercury, plotted with a 40°C temperature shift between slow (SSR) and fast (FSR) strain rates

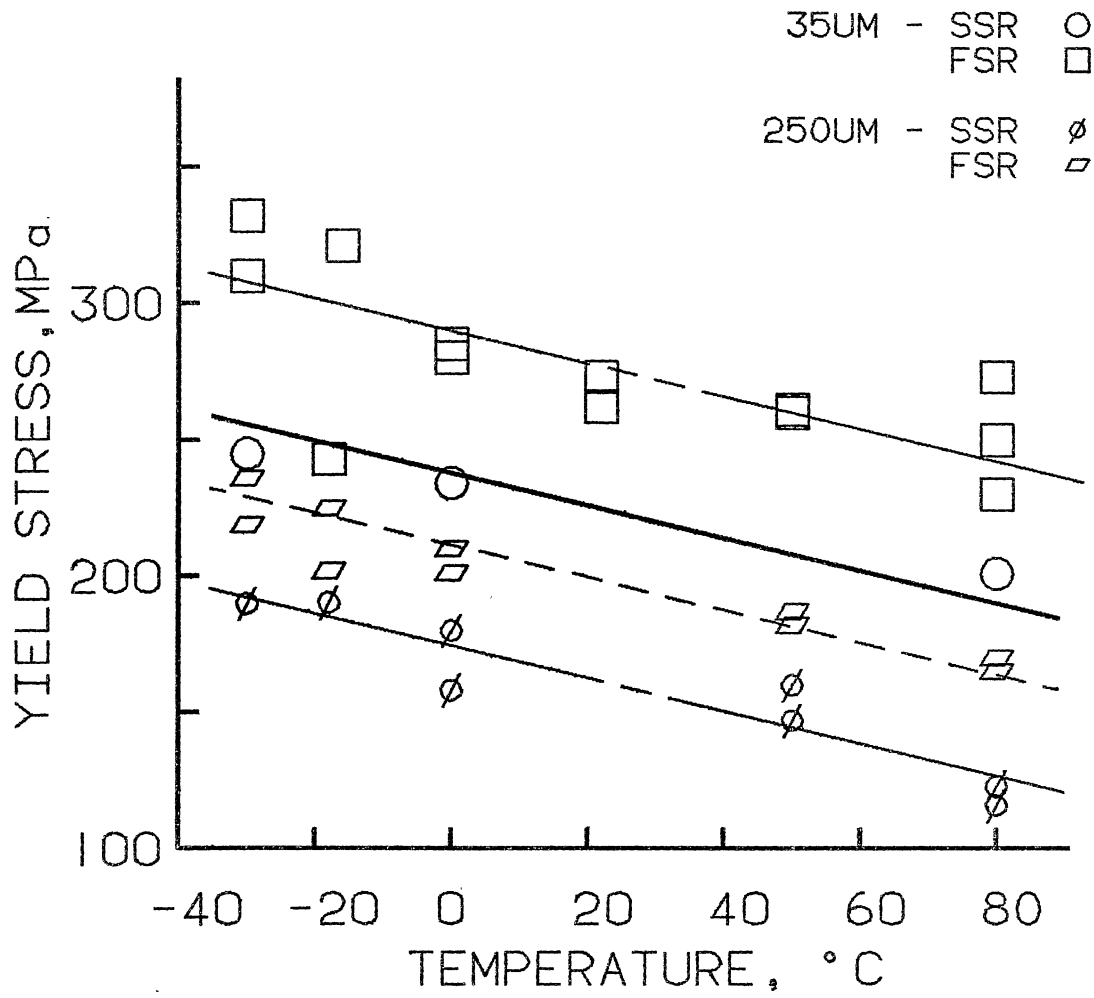

Figure 19. Yield stress versus temperature for Monel 400

with multiple origins. The slow strain rate sequence begins with an intergranular/transgranular mixed fracture surface at low temperatures with large secondary cracks, progressing to a completely intergranular fracture surface at higher temperatures. For both strain rates, the amount of longitudinal secondary cracking decreases as temperature is increased. As in the fine grain sequence, the temperature shift indicated by the fractography is in reasonable agreement with that indicated by the mechanical property data of Figure 18. The coarse grain samples also typically had a transgranular zone on the surface of otherwise intergranular fractures. It typically extended for one or two grains deep. In the slow strain rate samples, the presence and depth of the transgranular zone appeared to be constant with temperature.

None of the Monel 400 samples failed in mercury exhibited appreciable side cracking, as Figure 21 shows. The more ductile samples exhibited a small amount of 45° cracking in the neck region consisting of a few large cracks and no small cracks (see Figure 21). The most brittle samples, such as the coarse grain samples tested at slow strain rates and intermediate temperatures, exhibited an occassional very small amount of shallow intergranular cracking on transverse grain boundaries away from the fracture zone, as shown in Figure 22. This is in contrast to the more extensive side cracking reported by Traylor and Fredell for brittle intergranular fractures of Monel 400 in

FAST STRAIN RATE

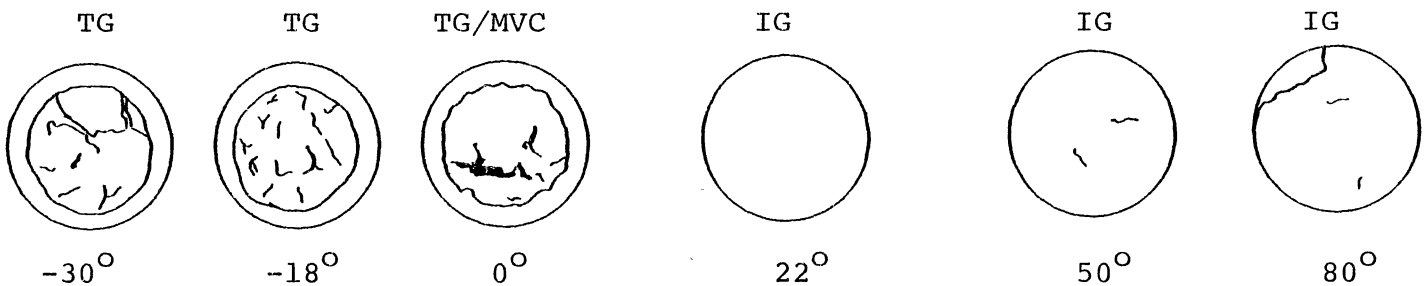

SLOW STRAIN RATE

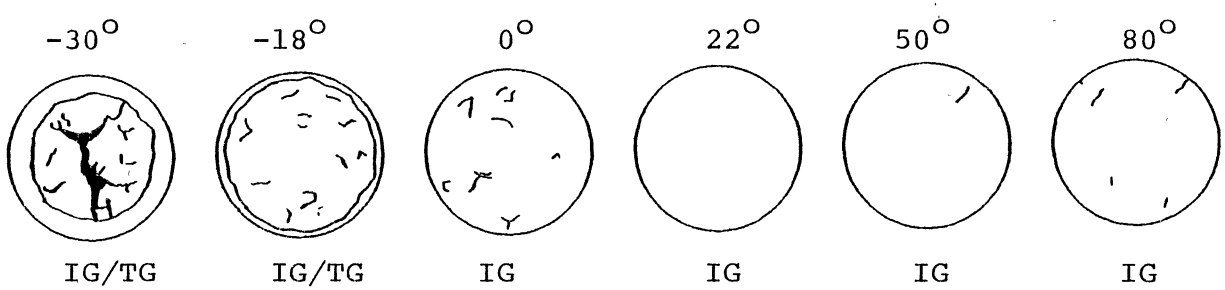

Figure 20. Fractography of 250 μm grain size Monel 400 in mercury versus temperature for the 40°C temperature shift of Figure 18

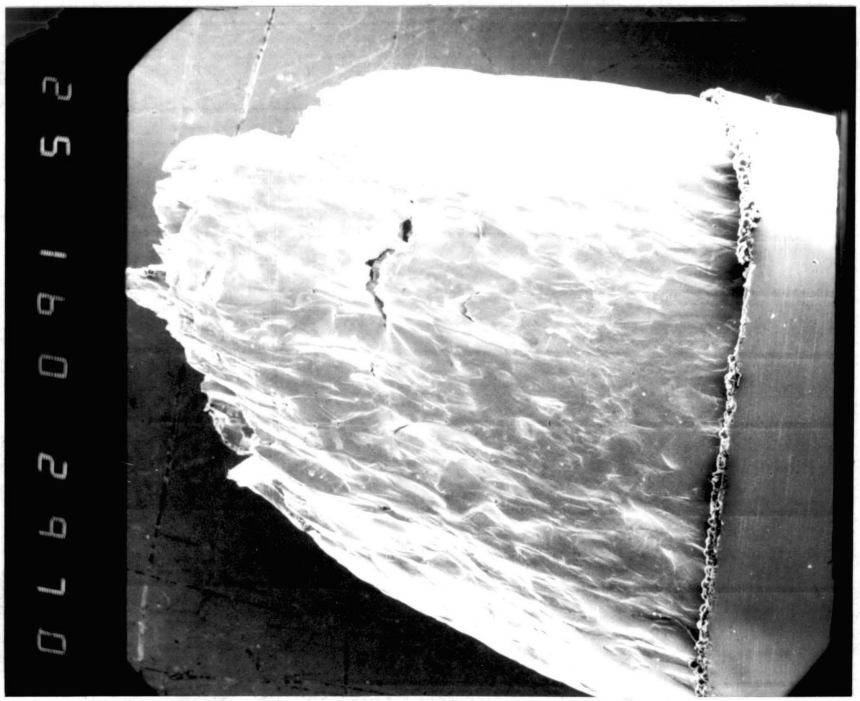

Figure 21. 45° side cracking in the necked region of the more ductile failures in mercury. Monel 400/Hg, 250 μm, $1.6 \times 10^{-5} s^{-1}$, -30°C

mercury (5,8). This suggests that the fractures in this study were more initiation limited, possibly because Fredell used a 600 grit mechanical polish while this study used chemical polished samples (8). Some of Fredell's samples were tested with an as-machined finish, as illustrated by Figure 23. Apparently, the rougher finish allows earlier crack initiation at the brittle test conditions. Here, side cracking occurred on machining marks, and the fracture initiated on machining marks.

Trends: Monel 400 in Mercury

Some trends are evident from this data. At low temperatures or equivalently at fast strain rates, fracture is seen to be initiation controlled. This is evidenced by the fracture occurring past the tensile strength, by the very minimal amount of side cracking, and by the cup and cone fractures beginning from the center of the sample. At low temperatures or fast enough strain rates, a fracture will not initiate from the surface of the sample. Once a fracture does initiate, however, it propagates rapidly. This is evidenced by the single origin at low temperatures, by the longitudinal splits in the cup and cone fractures and by the radial longitudinal secondary cracks. The radial cracks and splits must have propagated rapidly because once they have initiated the stresses to propagate them are very rapidly unloaded. For these initiation limited conditions, cracks do not initiate until the material attains a

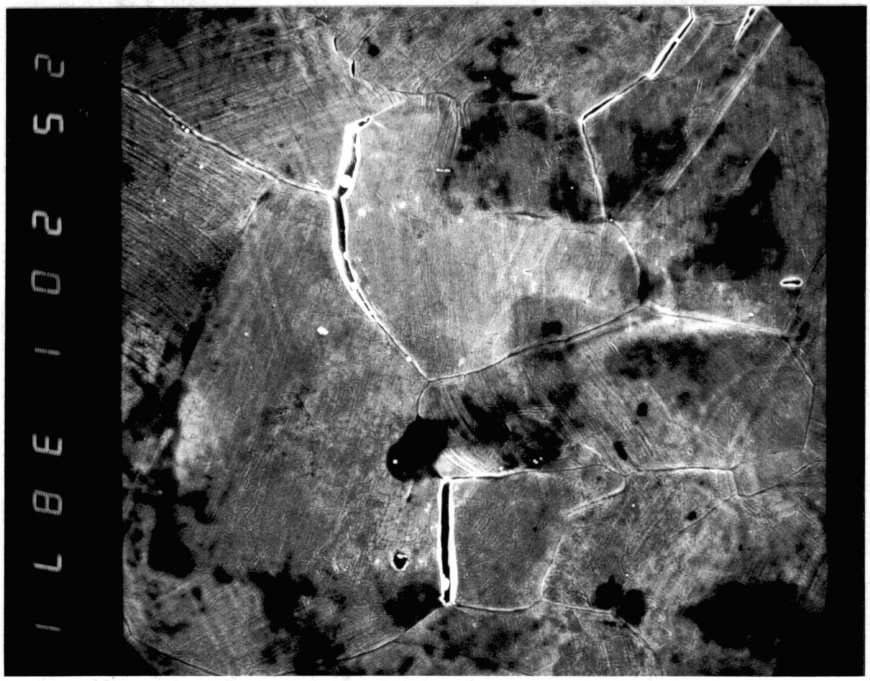

Figure 22. Isolated area of intergranular side cracking on a brittle failure in mercury. Monel 400/Hg, 250μm, $1.6 \times 10^{-5} s^{-1}$, 50°C

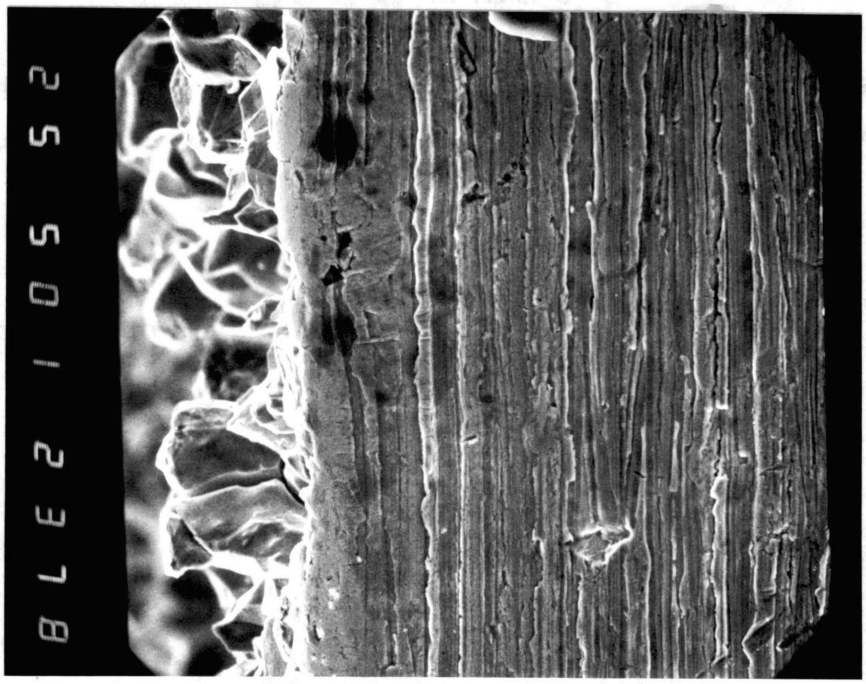

Figure 23. Side cracking of Fredell's sample with as-machined finish. Monel 400/Hg, 35 μm, $1.6 \times 10^{-5} s^{-1}$, 22°C

substantial strain. Using the theory advanced in earlier OSU studies of a threshold strain (at which the fracture mode changes from intergranular to transgranular), the higher strain level favors transgranular fracture (8).

At intermediate temperatures the material is much more brittle in mercury. Fractures can initiate, at lower strains and once they are initiated they propagate easily. This is evidenced by the low values for reduction in area at intermediate temperatures and by the fact that the fractures occur before the tensile strength is reached.

At higher temperatures the fractures are still quite brittle, but give some indications that the sequence is progressing toward becoming more propagation controlled. Fractures can initiate more easily, but once they are initiated they do not seem to propagate as rapidly. Greater ease of initiation is shown by the way that the samples at higher temperatures break before the tensile strength is reached or at the tensile strength. Also, the higher temperature samples exhibit slightly more side cracking. Also, in the higher temperature failures, multiple origins are encountered, and there seems to be a trend progressing from a single origin at lower temperature to multiple origins at higher temperatures. The slower propagation is evidenced by the multiple origins and also by the diminution of the longitudinal splits as the temperature is increased.

Grain size effect. Figure 24 illustrates the effect of

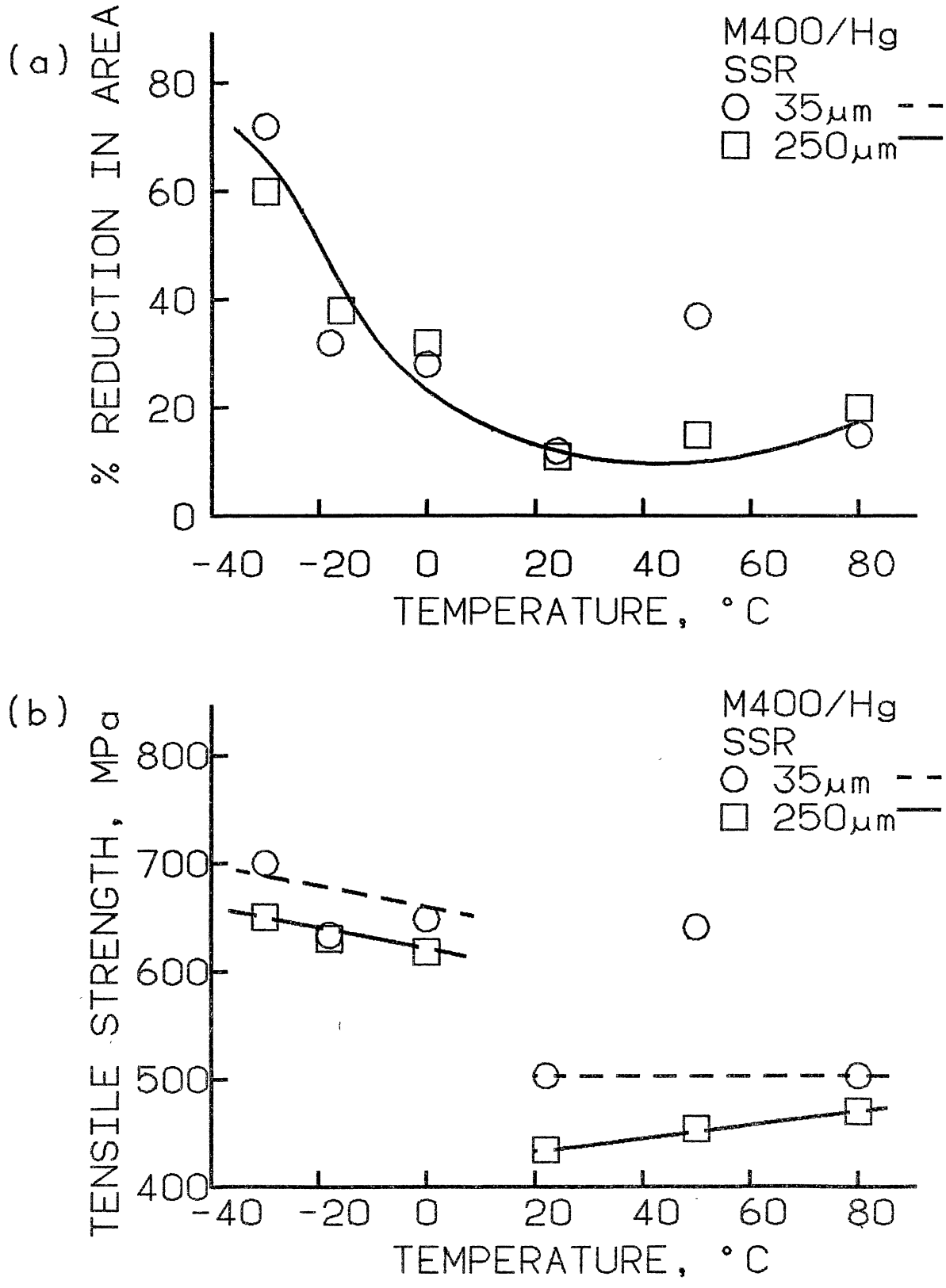

Figure 24. Effect of grain size on mechanical properties of Monel 400 in mercury at the slow strain rate ($1.6 \times 10^{-5} s^{-1}$)

grain size on the percent reduction in area and tensile strength data for the slow strain rate tensile tests on Monel 400. There seems to be no appreciable difference between the reduction in area of the 35 μm and 250 μm grain sizes. Fredell's room temperature tests also exhibited little differences among the reduction in area of 35, 80, 150, and 250 μm grain size Monel 400, with all being quite brittle at 9-12% RA. However, his 500 μm grain size was substantially more ductile. The 35 μm grain size produces a higher tensile strength. The air data superimposed on Figure 24b indicates that this difference is approximately equal to that obtained in an inert environment.

Figure 25 shows percent reduction in area and tensile strength data for the fast strain rates. Again, the fine grain samples show a higher strength than the coarse grain size with the difference seeming to be that experienced in air. Embrittlement begins at lower temperature with the coarse grain size. However, the tensile strength data and reduction in area data are not as readily interpreted in terms of a common temperature shift as was possible when evaluating the effect of strain rate at a constant grain size. The coarse grain size is more brittle at all temperatures investigated. The fine grain size favors cup cone fractures at both strain rates.

One of Kamdar's (12) major points in his analysis of LME according to the decohesion theory is that embrittled materials behave "as a special case of embrittled fracture".

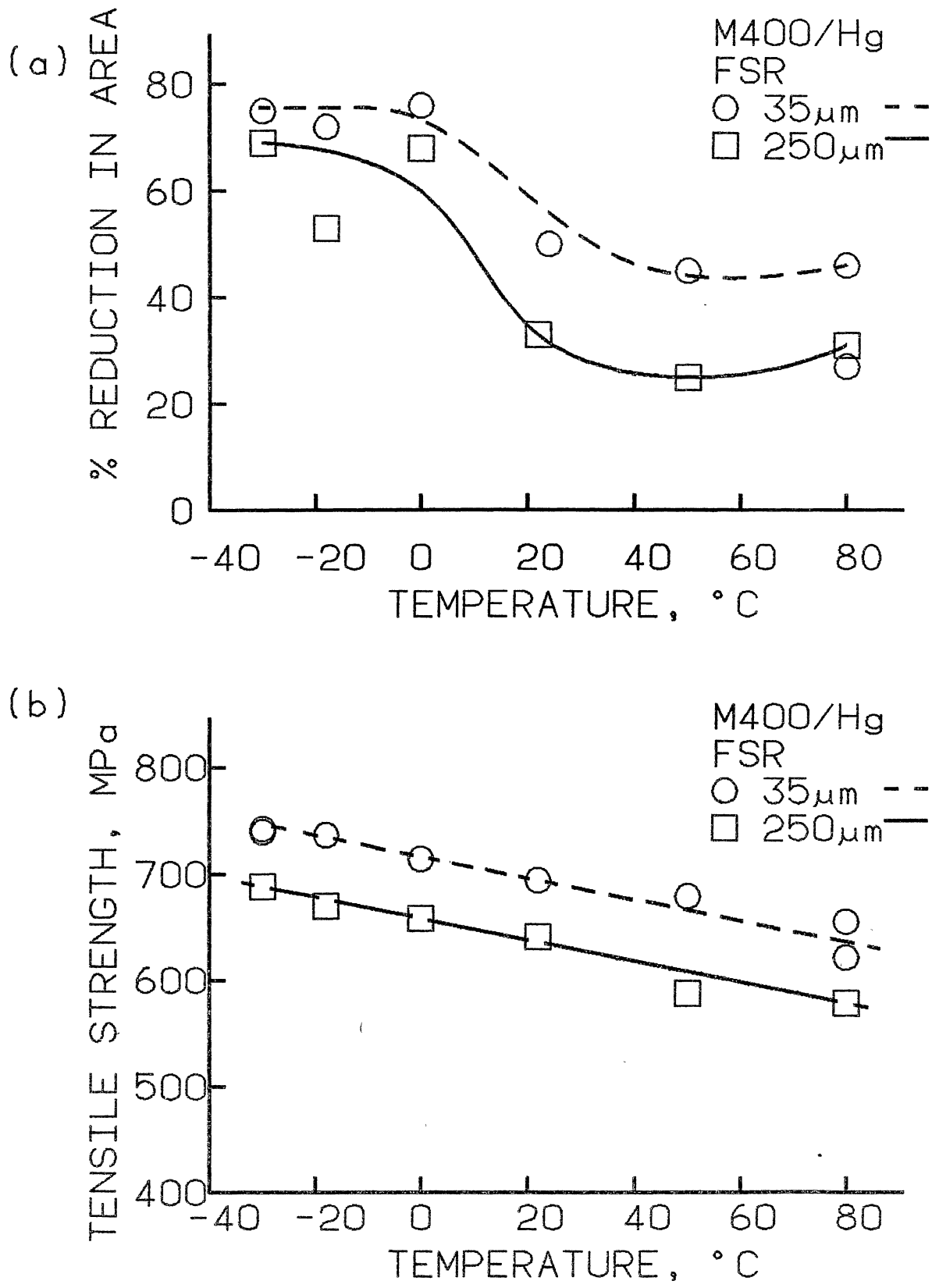

Figure 25. Effect of grain size on mechanical properties of Monel 400 in mercury at the fast strain rate ($1.6 \times 10^{-3} s^{-1}$)

For typical brittle materials, one expects both strength and ductility to decrease with increasing grain size. For this data, the tensile strength exhibited this trend for both strain rates, as did the reduction in area data at the fast strain rate. However, at the slow strain rate, Fredell's very coarse grain size is more ductile than finer grain sizes.

While the lower temperature region seems to indicate the lower end of a temperature window for embrittlement, interpretation of the upper end of the curve is more uncertain. It was reasoned that the reported disappearance of embrittlement at higher temperatures is due to excessive plasticity. Thus, the temperature at which embrittlement goes away was expected to decrease as grain size increases. This trend was observed by Ichinose for aluminum tensile tested in liquid Hg 3% Zn solution (95).

Therefore, samples of larger grain size were tested to see if the reduction in area was increasing at the higher temperatures. Samples were annealed at 1090°C for 4 hours to produce a grain size between 250μm and 500μm (as tested by Fredell). They were slow strain rate tensile tested at 20°C and 80°C. As shown by Table VI, the embrittlement did not decrease with increasing temperature. The apparent increase was deemed to be due to the same type of data scatter observed earlier. Higher data scatter may be expected from more brittle materials or conditions because of the higher sensitivity of brittle failure to such irreg-

TABLE VI

SLOW STRAIN RATE TENSILE TEST OF APPROXIMATELY
350 μm GRAIN SIZE MONEL 400 IN Hg.
STRAIN RATE = $1.5 \times 10^{-5} s^{-1}$

Test Temperature °C	Tensile Strength MPa	(ksi)	% Reduction in Area
20	517	(75)	20
80	421	(61)	13

ularities as surface finish, inclusions, scratches, etc. Thus the upper end of the temperature window for Monel 400 at the slow strain rate is greater than 80°C.

Strain Rate Effect. The effect of varying the strain rate has been discussed in terms of a temperature shift; that is, increasing the strain rate is equivalent to testing at a lower temperature. This trend is the same as that expected from a typical brittle material, such as a ferritic steel at low temperature.

However, for this data and for that of Fredell (8), decreasing the strain rate has produced greater embrittlement in every instance. This is opposite to the behavior expected from a typical brittle material. Therefore, Kamdar's (12) generalization that embrittlement can be treated "as a special case of brittle fracture" does not hold for this case.

Surface Effect. The fractography of the mercury embrittled Monel 400 slow strain rate tensile test specimens indicates that it is harder to get intergranular cracking in the surface zone of the sample than it is beneath the surface. For the 35 μm grain size there seems to be a transgranular zone on the surface of otherwise intergranular fractures that extends to a depth of about 3 to 5 grains. In the 250 μm grain size a similar zone seems to extend for about the first grain or two. This is illustrated by Figure 26 and was also reported by Morris (10). Side views of these samples show that many of the longitudinal splits look

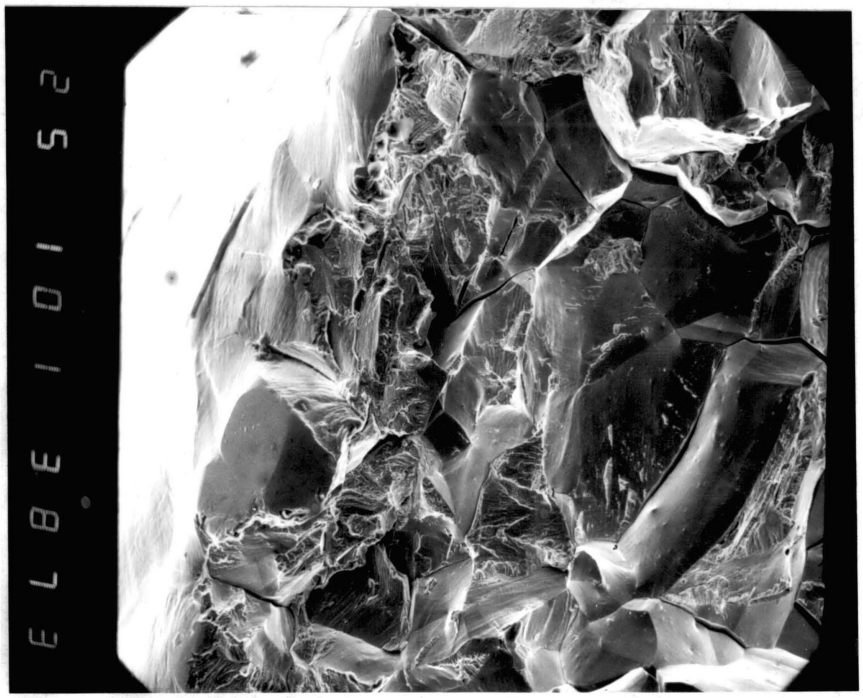

Figure 26. Transgranular fracture zone in the outside few grains of an otherwise intergranular fracture in mercury. Money 400/Hg, 250μm, $1.6 \times 10^{-5} s^{-1}$, 50°C

transgranular on the surface even though they are predominantly intergranular. In addition, many radial longitudinal splits do not propagate all the way to the surface.

Wetting Experiments

One of the requirements for LME is wetting by the embrittler; yet mercury does not wet Monel appreciably. Therefore, wetting must be activated by stress, strain, or the emergence of clean surfaces at slip steps or microcracks. The following experiments were performed to characterize wetting behavior during a tensile test.

Tensile Tests. Tensile tests were performed under displacement control in mercury at the fast strain rate on 250 μm grain size material at room temperature. These conditions were chosen because they produced intermediate embrittlement (33% RA), such that an intergranular fracture occurred after considerable plastic strain.

For the first test, the sample was loaded at the fast strain rate to 530 MPa, (tensile strength for a comparable test was 694 MPa), then held on load while the mercury was removed and the side of the sample observed using the SZM. As the sample strained and pulled out of the mercury, the miniscus, which had been depressed, rose with it on one side. This left the miniscus depressed around part of the circumference, and approximately perpendicular to the sample the rest of the way around the sample. Holding the sample under load and removing the mercury revealed localized

wetting in small patches. The mercury was replaced, and the test was continued to failure. The fracture surface was well wetted. On the side surfaces, the portion of the sample that was under the mercury was wetted, locally in small patches, but the portion which was above the surface had small spherical globules of mercury which did not wet the sample.

As the mercury in the above test had been used in earlier testing, a fresh batch of triple distilled mercury was obtained and the test repeated. The miniscus remained depressed throughout the test. Again, the fracture surface was wetted and the reduction in area was the same. No wetting of the side surfaces could be observed except for internal wetting of a small side crack. Examining the side surfaces with a 400x optical microscope, no distinction could be made between the sample half under the mercury and the half in air.

Thus, with the new mercury, wetting was observable only on the fracture surface and inside of side cracks. With the previously used mercury, some localized strain activated wetting had apparently occurred.

A final tensile test wa done by loading in air at the fast strain rate until the tensile strength was almost reached, then switching to the slow strain rate for five minutes before adding mercury. The intent was to observe wetting under high plastic strain and to confirm that a high enough strain before crack initiation would lead to

transgranular initiation.

The sample fractured in a brittle manner after considerable necking. The transverse fracture was predominately transgranular and was well wetted. The side surface was extremely interesting. No wetting was observed away from the fracture. Within one to two grains of the fracture, very small localized patches of wetting associated with slip bands were observed in the optical microscope at 400X. For example, one grain had six prominent slip bands, each with an associated patach of mercury. Their appearance was very similar to the potographs of gallium wetting zinc and brass presented by Watanabe and coworkers (96,97). Unfortunately, clear photographs could not be obtained due to the limited depth of field in the optical microscope. Apparently, this behavior was not observed in earlier tests because fracture occurred at strains too low for development of adequate slip bands.

Wetting Under Acid. Surface oxide films and adsorbed oxygen can inhibit wetting (98). To observe wetting behavior without oxygen, samples were immersed in concentrated HCl for 2.5 hours, then mercury was added to displace the HCl similar to the technique used by Costas (84) and Funkenbush, Heldt, and Stein (39). This was done for Monel 400, Nickel 200, Inconel 600, and Incoloy 800.

The Monel 400 and Nickel 200 underwent some generalized wetting. The mercury could not be rinsed off or rubbed off the surface with a cloth. Wetting on the Inconel 600 and

Incoloy 800 was very minimal. Thus, the alloys exhibiting the most wetting are those that experience the greatest embrittlement.

Wetting Observations

Some general observations of wetting with LME are:

(i) LME is traditionally limited to couples having limited solubility and wetting.

(ii) Hg embrittles copper much less than Monel (87). Peevy and Willoughby had difficulty in dewetting mercury off the copper.

(iii) Recent Japanese studies of LME of brass and zinc by Gallium show localized patches of wetting associated with slip bands.

(iv) Similar small patches of localized wetting have been observed at OSU on more embrittled copper specimens, and to a slight extent, on Monel.

(v) Side surfaces of Monel are typically unwetted.

(vi) Monel fracture surfaces usually are not wetted. Mercury is present in small globules. Fredell (8) reported that mercury was easily removed by ultrasonic cleaning.

(vii) Morris (10) also reported easy removal of mercury from Nickel 200, Inconel 600, and Incoloy 800.

(viii) Good (67) likewise reported easy removal from the nickel alloys he investigated.

(ix) In this study, sometimes mercury was difficult to

remove. Typically, this occurred on the more ductile fractures.

Hydrogen Embrittlement

Monel 400

Data. Figure 27 gives percent reduction in area vs temperature for both 35 μm and 250 μm grain sizes. For each grain size, embrittlement was quite substantially greater at the slow strain rate. In contrast to the mercury results, changing the strain rate showed no obvious temperature shift in the data. Instead the magnitude of the embrittlement was very much reduced as strain rate was increased. Changing the grain size from 35 μm to 250 μm reduced embrittlement by hydrogen. This was consistent with the room temperature hydrogen embrittlement results obtained by Fredell (8).

The effect of temperature on the tensile strength of Monel 400 in hydrogen is shown in Figure 28 for both grain sizes. For all cases of grain size and strain rate investigated, the tensile strength in hydrogen appears to be somewhat less than in air. During hydrogen tests all of the samples failed after reaching the tensile strength (after necking had begun). This was in contrast to the mercury tests where the more highly embrittled samples failed before reaching the tensile strength. The tensile strength vs temperature curves for the fast strain rates do not have

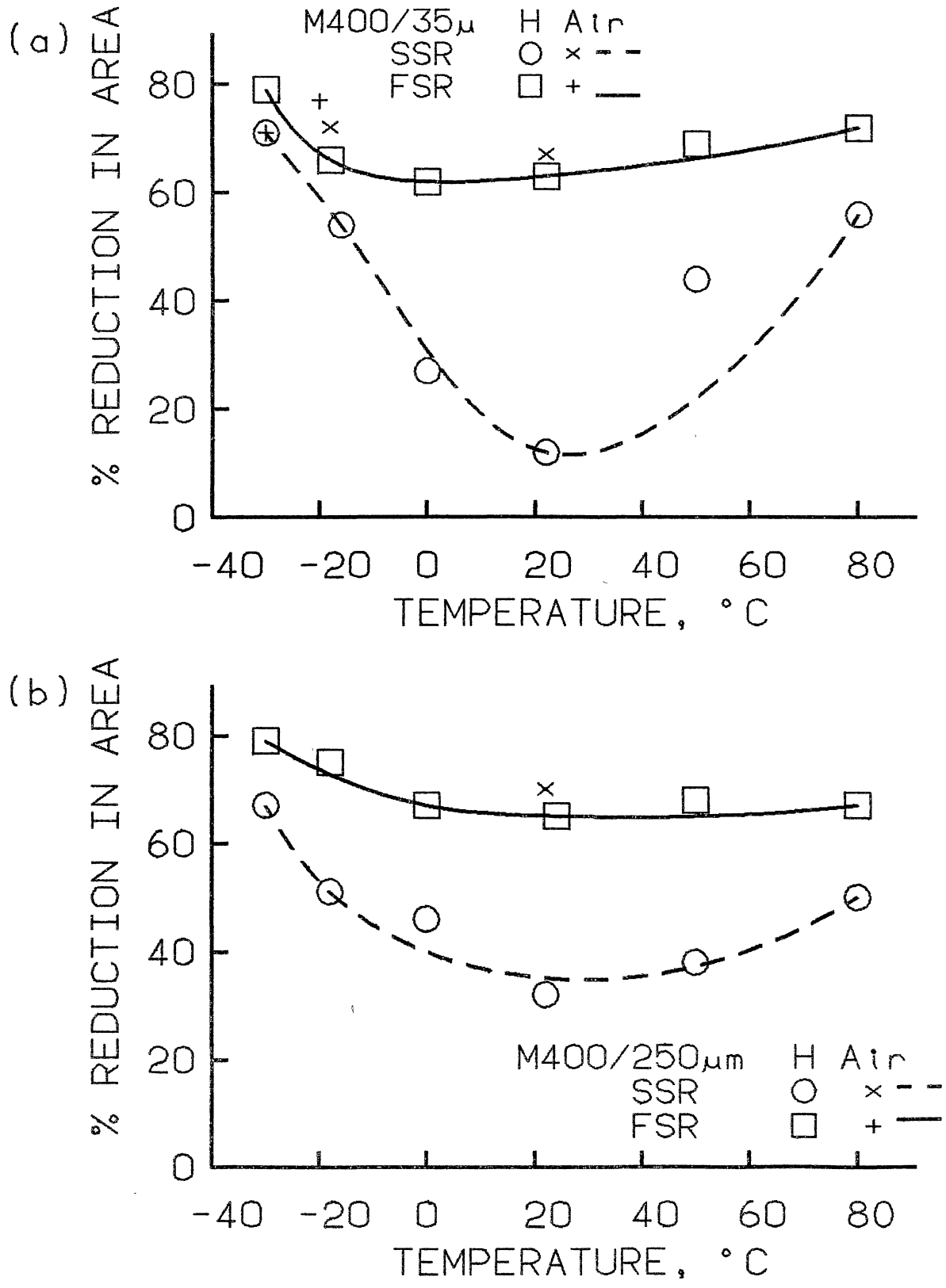

Figure 27. Reduction in area versus temperature in hydrogen for both grain sizes. Air values shown for comparison

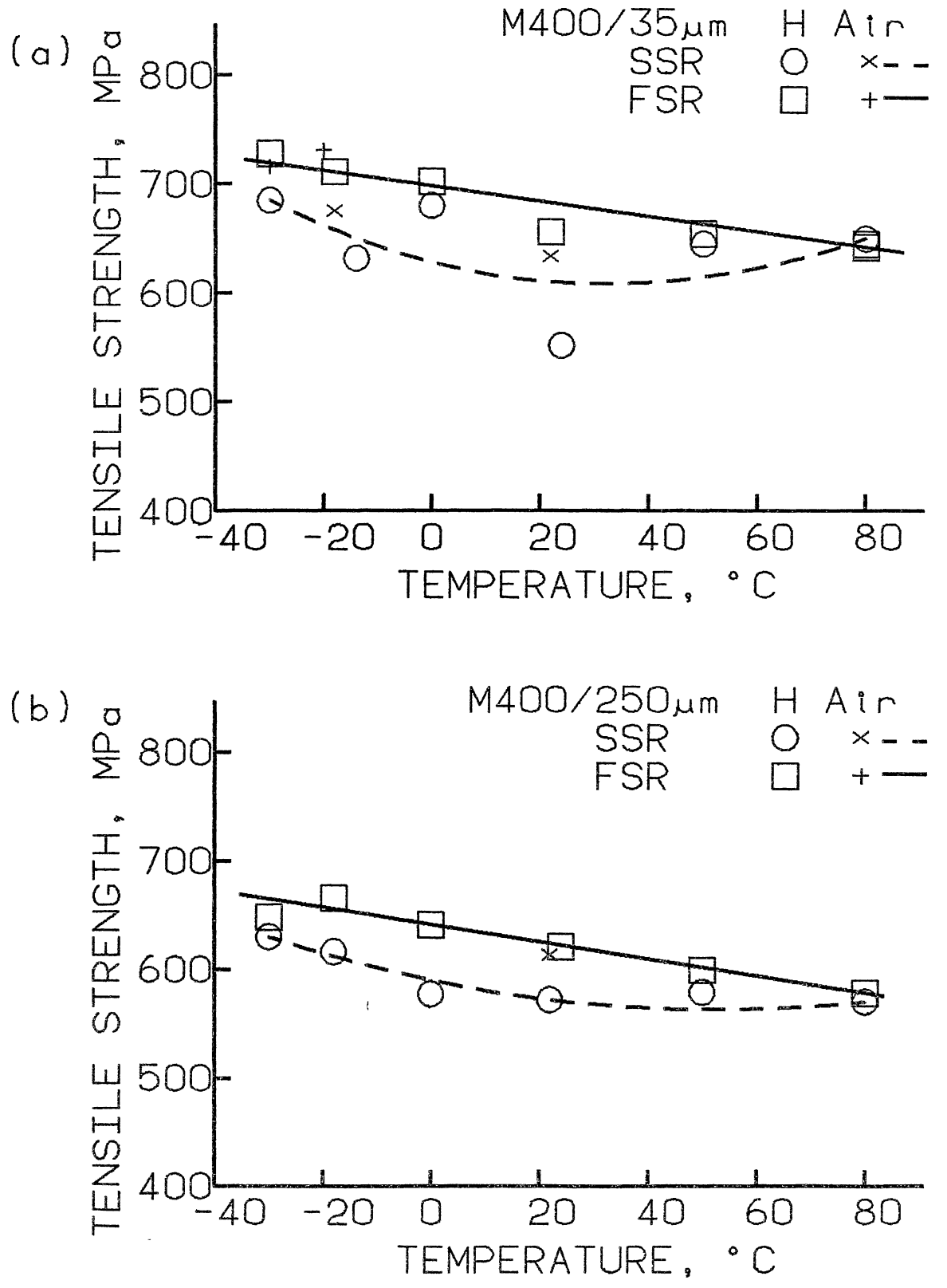

Figure 28. Tensile strength versus temperature in hydrogen for both grain sizes. Air values shown for comparison

much curvature, but lie below the fast strain rate curves in mercury. The curves show lower values in the regions of greatest embrittlement, particularly at the slow strain rates. Thus, since the tensile strength is reduced, even though the sample does not fail until considerable necking has occurred, testing in the hydrogen environment appears to enhance the plasticity of the material.

Fractography

35 μm Grain Size Slow Strain Rate. The most obvious difference between the mercury and hydrogen fractures is that the hydrogen fractures exhibited much, much more side cracking, such that a typical brittle hydrogen fracture is immediately distinguishable from a typical brittle mercury fracture with the naked eye. Side cracking of the hydrogen samples followed an orderly progression with temperature, as shown in Figure 29 for the 35 μm grain size. The fractography of the fine grain size material tested at the slow strain rate exhibited signs of embrittlement at all temperatures. At low temperatures the fractography showed only slight embrittlement. For instance, at -30°C there was only very shallow intergranular cracking about 2 to 6 grains deep. The side surface of the -30°C sample indicates some 45° slant cracks in the necked region, changing to a few flat (90° to the tensile axis) cracks adjacent to the necked region. No intergranular side cracks were observed at -30°C. This very limited degree of embrittlement indicates

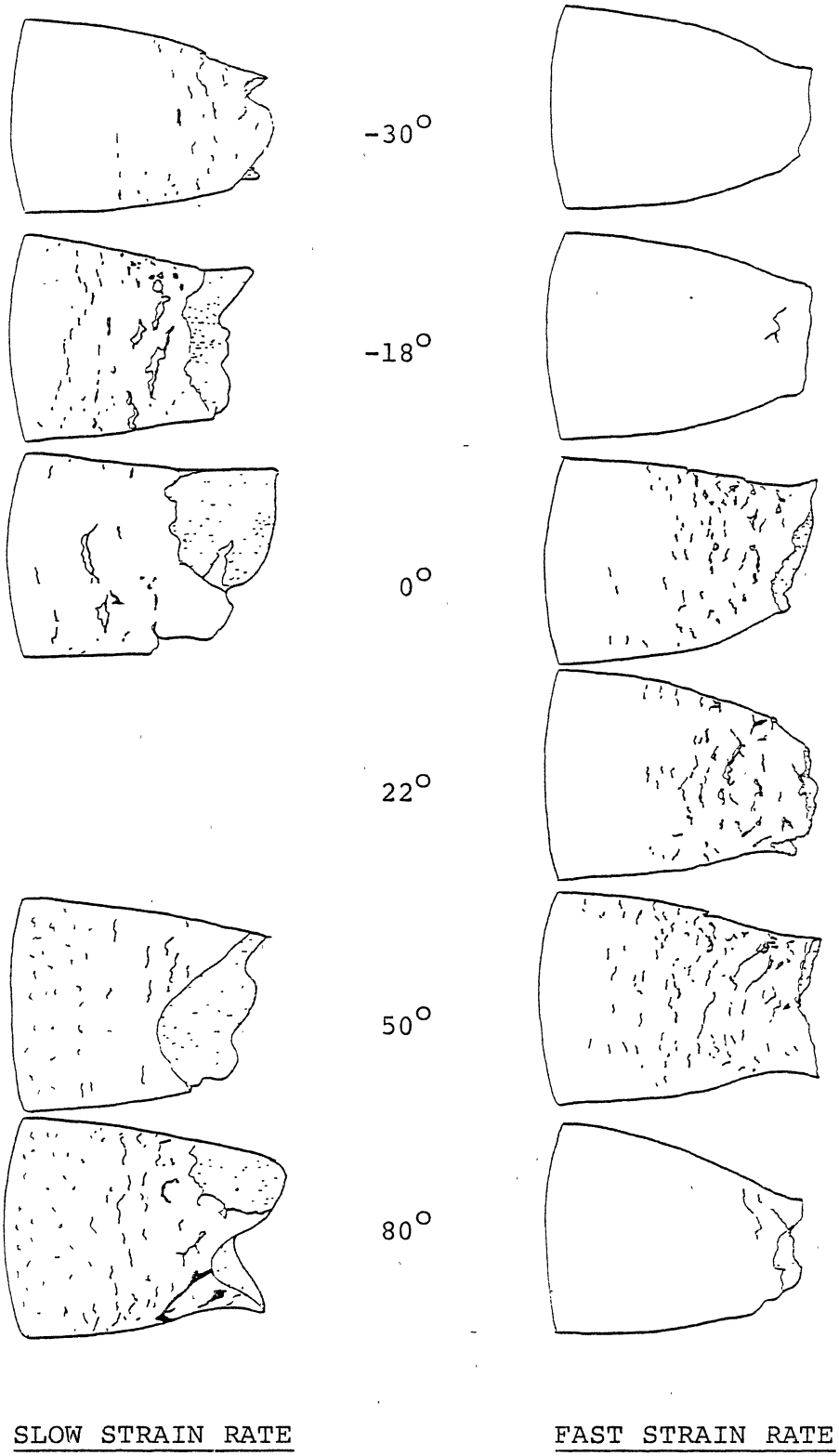

Figure 29. Side cracking of 35 μm grain size Monel 400 in hydrogen versus temperature

that crack initiation probably occurred after the tensile strength was reached. This corresponds with a high reduction in area and tensile strength as shown in Figure 27. As the temperature was increased, crack initiation became easier. The fracture obtained at 0°C has a mixture of clean intergranular cracking and crystallographic transgranular cracking with tearing which propagated to about 1/3 of the sample diameter. The center of the fracture contains microvoids. A side view of the 0°C sample shows large intergranular cracks and the beginnings of general intergranular cracking (fracture along each grain boundary). As the temperature is increased, crack initiation continues to get easier; that is, cracks are initiated earlier, but blunting of cracks gets easier. Figures 30 and 31 are side views of the 80°C test specimen. Every grain boundary in the entire photo of Figure 30 is not only cracked, but the neighboring grains are well separated from each other as shown in Figure 31. There are not as many large intergranular cracks as were observed in the lower temperature fracture, but rather the strain was taken up by the myriad of small grain boundary cracks. The initiation zone of the fracture surface consists of intergranular fracture only a few grains deep. Thus as the temperature is increased, the overall ductility of the sample increases because the increased blunting does not allow the cracks to propagate. Instead the side surfaces of the sample become full of blunt cracks which accommodate

Figure 30. Intergranular side cracking of fine grain sample in hydrogen, tested at 80°C. Monel 400/H, 35μm, $1.6 \times 10^{-5} s^{-1}$, 80°C

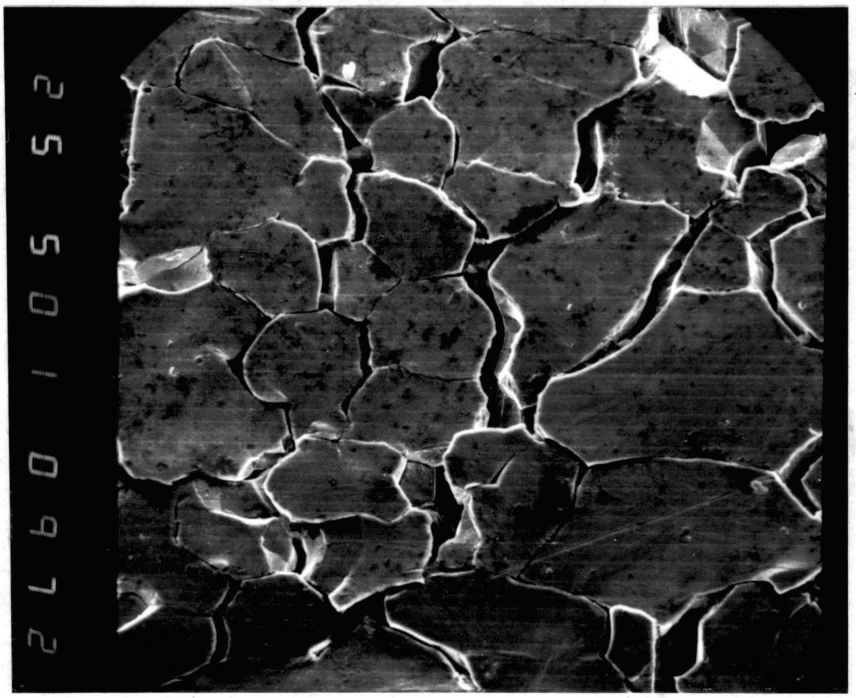

Figure 31. General intergranular cracking in Figure 30. Note the large separation between grains. Monel 400/H, 35 μm, $1.6 \times 10^{-5} s^{-1}$, 80°C

strain by gaping open.

Thus, the material behavior in the hydrogen environment is different than that seen in mercury. Figure 32 illustrates what happens in a slow strain rate hydrogen test. At low temperature, as shown in Figure 32a, crack initiation does not begin until late in the fracture process. The cracks initiate after the tensile strength is reached and after a considerable number of microvoids have been initiated. Fracture occurs before blunting of the cracks can take place. At intermediate temperatures as shown in Figure 32b, crack initiation begins earlier, at or before the tensile strength, and considerable propagation of the cracks occurs before blunting takes place. Ductility is correspondingly low, as shown in Figure 27. At high temperatures, as shown in Figure 32c, crack initiation occurs quite early, but blunting occurs before the cracks can propagate very much. The sample then continues the test full of blunt cracks and necks in the normal ductile manner. Ductility returns to a high level, as seen in Figure 27. Thus, an interesting situation exists where samples that look tremendously brittle from the side (covered with gaping cracks) actually behave macroscopically in a ductile manner.

35 μm Grain Size Fast Strain Rate. From the data shown in Figure 27 and 28, the fractography of the fast strain tests is expected to be much more ductile than that exhibited by the slow strain rate tests. At low temperatures, -30°C and -18°C, the fractures were cup and

(a)

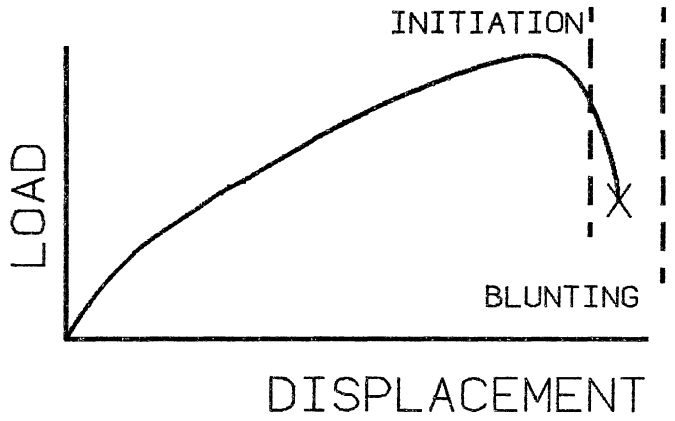

(b)

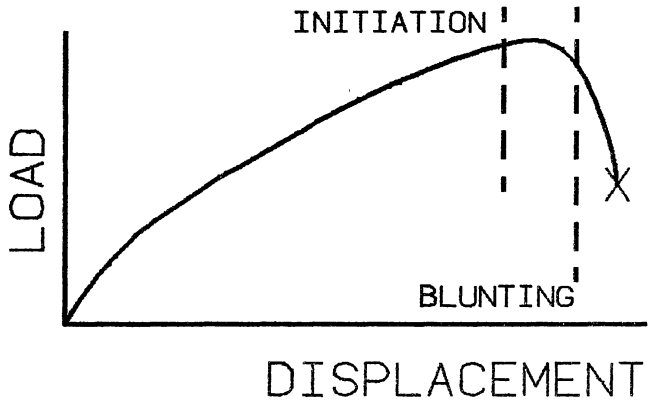

(c)

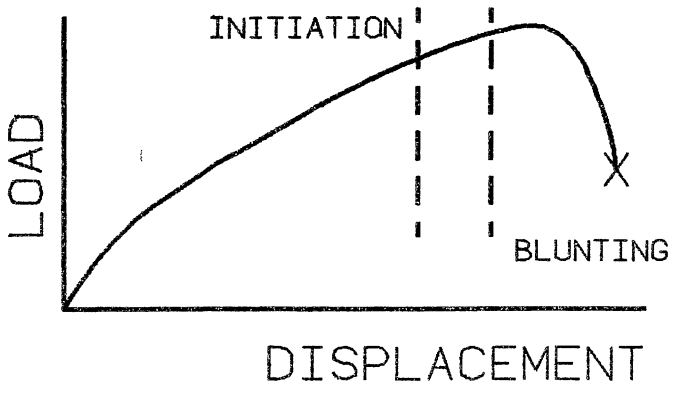

Figure 32. Crack initiation and blunting sequence in hydrogen at: (a) low temperatures, (b) intermediate temperatures, and (c) higher temperatures

cone, and the fracture surfaces were all microvoids. Side views revealed only very minor 45° cracking and very sparse hints of intergranular cracking in the necked region. The fractures exhibited no longitudinal splits as were seen in the cup/cone fractures in mercury. The appearance of the fractures is what might be expected from slow strain rate tests at much lower temperatures. As the temperature was increased to 0°C, intergranular cracks began to be initiated, and were observed throughout the zone exposed to the hydrogen. The fractures were not brittle, however, as the intergranular cracking only propagated a few grains deep. Increasing the temperature to 50°C produced easier initiation and also more crack blunting as was seen in the slow strain tests. This is evidenced by the general homogeneous intergranular side cracking and by the large degree that each crack has gaped open. Thus, the fast strain rate tests show the same trend in fractography as that exhibited by the slow strain rate tests. At 80°C, the intergranular cracking disappeared. The fracture was cup and cone and the only evidence of embrittlement was a small amount of 45° cracking in the neck. As this result was unexpected, the 80°C test was repeated. The results were the same: cup and cone fracture with 45° cracking in the neck.

Up to 80°C, the side cracking exhibits the same trend as observed in the slow strain rate tests. Increasing the temperature results in earlier crack initiation and

blunting. The 80°C test does not fit this trend in that significant initiation of cracks at the surface did not occur. The fast strain rate tests were all more ductile than those at slow strain rate, as evidenced both by the numerical data and by the fracture surfaces. Cracks were not allowed to propagate in a brittle manner for a significant distance in any test performed at the fast strain rate.

250 μm Grain Size, Slow Strain Rate. Side cracking of the coarse grain test samples is shown in Figure 33. The larger grain size material yields earlier than the 35 m grain size and exhibits much, much more plastic deformation, as is evident by the extensive rumpling of the side surfaces. The major difference between the fine and coarse grain fractography on the fracture surfaces is that the coarse grain size exhibits a much greater amount of transgranular fracture. At low temperatures little embrittlement was experienced. The fracture surface at -30°C exhibited a few grains of transgranular fracture at the origin followed by microvoids, and the sample had only a very small amount of side cracking. Increasing the temperature to -18°C gives rise to transgranular side cracks progressing to intergranular side cracks at 22°C. Interestingly, the side cracking at -18°C was all transgranular except for a small region about 0.8 cm (0.3") from the fracture surface which contained intergranular cracks coexisting with the transgranular cracks. Since this

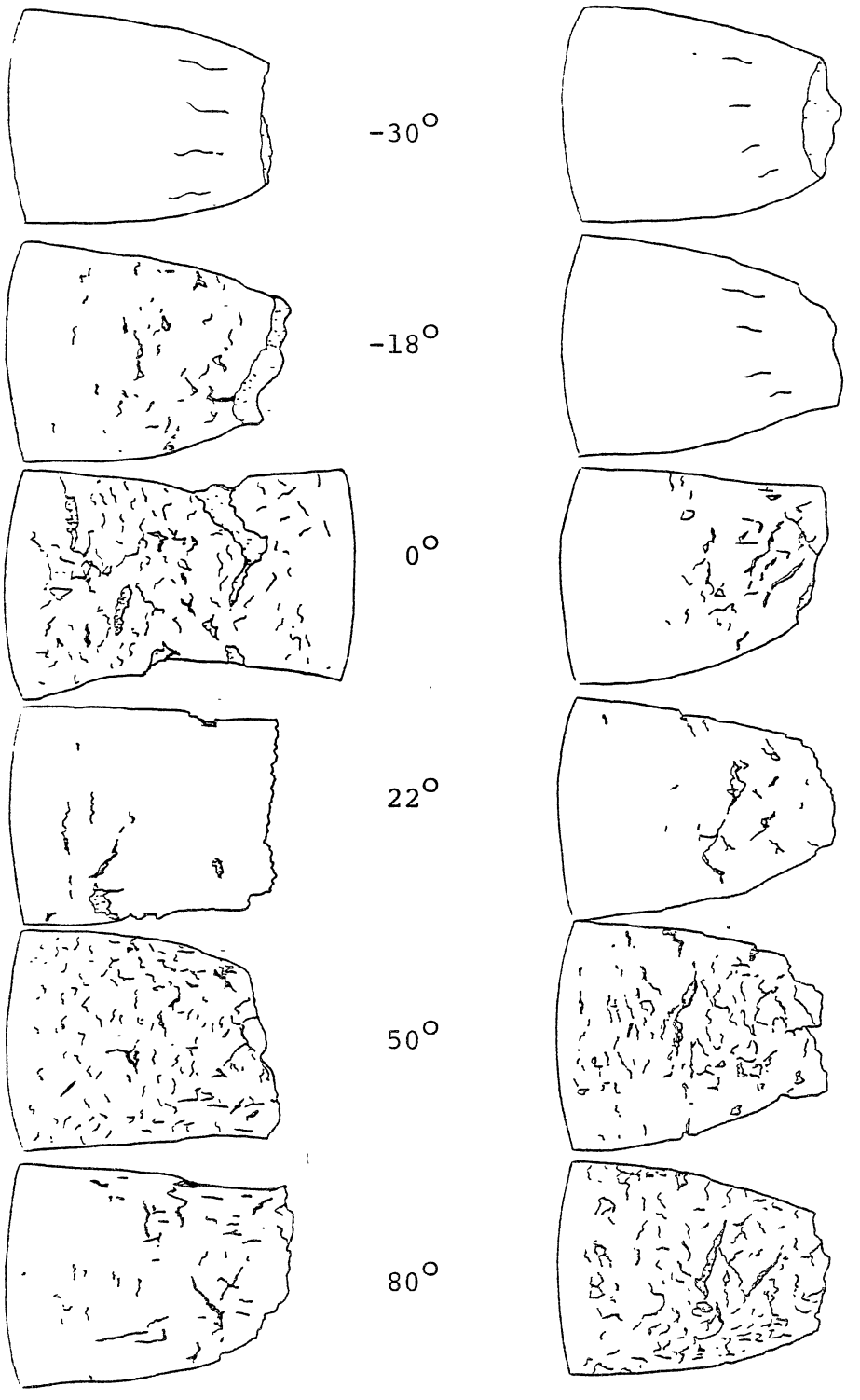

Figure 33. Side cracking of 250 μm grain size Monel 400 in hydrogen versus temperature

portion of the waisted sample has a much larger diameter than the point of fracture, the rates of increase of load and strain were slower at this point. This was equivalent to testing at a slower strain rate. The occurrence of intergranular cracks at this point suggests that fracture may have been more intergranular had testing been performed at a slower strain rate. The fractures at 0°C and 22°C had the most brittle fracture surfaces, each containing a large mixed intergranular/transgranular zone. As temperature was increased to 50°C there were fewer large side cracks, but the specimen became full of small cracks. These cracks were both intergranular and transgranular slip band cracks as shown in Figure 34. The transgranular cracks generally were opened wider than the intergranular cracks. Similar to the fractography seen in the 35 μm samples, the existence of this multitude of cracks did not produce extremely brittle behavior in the sample, but rather the cracks blunted and accommodated strain by gaping open. As the temperature was increased to 80°C, the sample behaved in a much more ductile manner. The percent reduction in area increased, the area of the transgranular zone on the fracture surface decreased, and most of the side cracking was gone. Side cracking was limited to some 45° cracks in the necked region and a few occasional intergranular cracks. Interestingly, the slow strain rate 250 μm sample at 80° looks similar to the fast strain rate 35 μm sample at 80°C.

250 μm Grain Size, Fast Strain Rate. At low

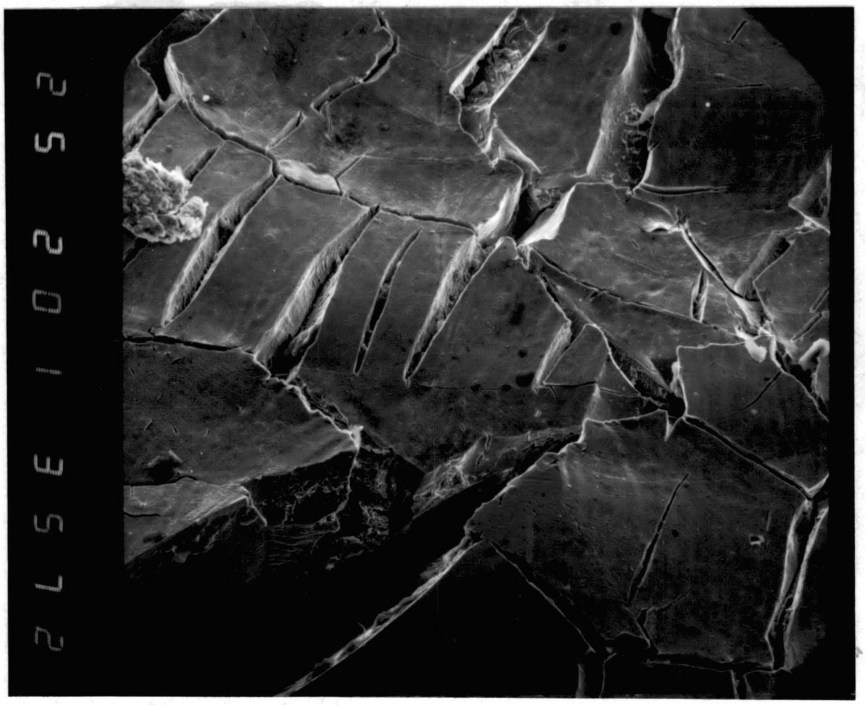

Figure 34. Side cracking of coarse grained sample in hydrogen at 50°C at the slow strain rate. Transgranular slip band bracks are coexisting with the general intergranular cracking. Monel 400/H, 250 μm, SSR, 50°C

temperatures of -30 and -18°C the fast strain rate test produced cup and cone fractures much as might be expected if the slow strain rate tests were performed at lower temperatures. There were no longitudinal splits as were observed in the mercury cup cone fractures. There was little evidence of side cracking at these temperatures, however, in the -30° test there were the beginnings of grain boundary cracks in some places. As the temperature was increased to 0°C and 24°C, more side cracks occurred. These cracks typically had a mix of transgranular and intergranular (with tearing) fractography. The fracture surfaces of these two samples consisted mostly of voids with transgranular-/intergranular origins. Increasing the temperature to 50°C produced a very large increase in the number of side cracks. The side cracks were predominantly intergranular, coexisting with small transgranular cracks which seem to be on slip bands. The intergranular cracks had opened considerably in many places but the transgranular cracks displayed limited opening. The 80° sample was also full of side cracks as shown in Figure 35, but the cracks were almost completely intergranular. These cracks had gaped open considerably and there was only a hint of transgranular cracking.

The two higher temperature fast strain rate tests displayed the same type of fractography as seen in the fine grain samples, that is, the ductility remained quite high

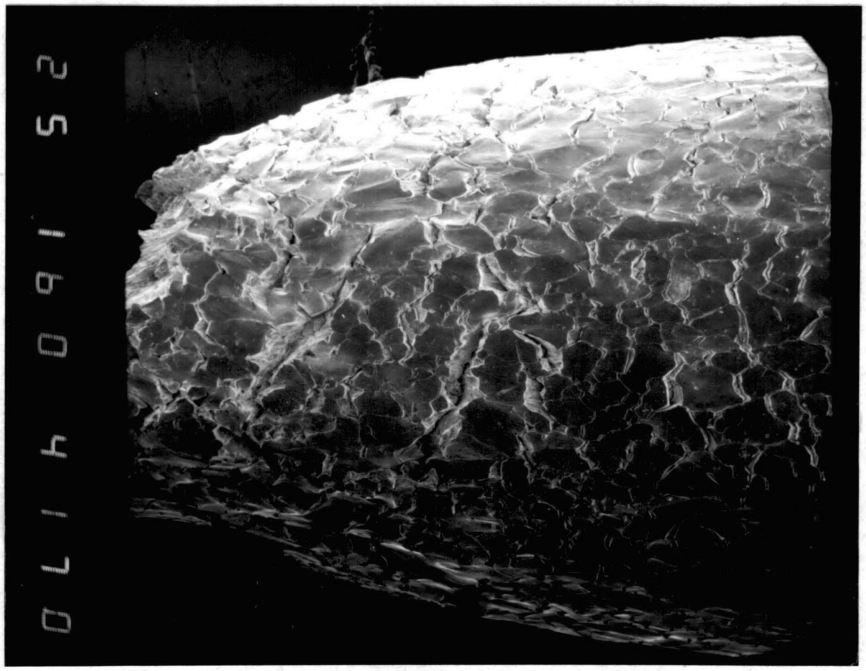

Figure 35. 80°C test of coarse grain size at the slow strain rate in hydrogen. Many large intergranular cracks with only a hint of transgranular fracture. Monel 400/H, 250 μm, SSR, 80°C

even though the side surfaces of the samples were completely full of cracks. The samples accommodated high strain at the side surfaces by the gaping open of a large number of small cracks which became quite blunt. The fracture surfaces in both cases consisted of mainly microvoids with origins of a few grains of transgranular or dirty intergranular fracture.

Monel 400: Fatigue Tests

The widely separated general intergranular cracking observed at higher temperatures (35 μm slow strain rate, Figure 28, and 250 μm fast strain rate, Figure 30) is very similar to that observed by Price and Morris (99) in Inconel 600 at room temperature. They reasoned that the hydrogen promoted plastic deformation, resulting in early blunting of cracks. This hypothesis was supported by the enhancement of the fatigue life of Inconel 600 in hydrogen relative to air. They proposed that other alloys would display the same effect, if tested under appropriate conditions.

To test this hypothesis, sample fatigue tests were run on Monel 400 at the conditions which gave the maximum amount of intergranular side cracking. If the myriad of blunt intergranular cracks at these conditions is a result of blunting due to enhanced slip, then fatigue life should be enhanced by this same crack blunting process. Two 250 μm grain size samples were fatigued in alternating tension in the hydrogen environmental chamber at 80°C; one with no charging, and one at the customary charging rate of 200A/m^2.

The uncharged test was considered to be equivalent to a test in air, as was demonstrated by Traylor (5) for Nickel 200 at room temperature. The cycle frequency was 30 Hz. The maximum stress was 407 MPa (59.1 ksi) and minimum stress zero.

The test results are given in Table VII. The hydrogen sample lasted over 2.3 times longer than the uncharged sample, supporting the hypothesis that the hydrogen promotes slip, resulting in blunting of cracks.

Trends: Monel 400 in Hydrogen

The behavior of the hydrogen embrittled Monel 400 was similar in some respects to that produced by mercury embrittlement. The major difference was that the samples failed in the mercury environment fractured after very little side cracking, whereas the most of the hydrogen samples initiated a myriad of cracks which quickly blunted; resulting in less overall embrittlement. The same trend was reported by Funkenbush, Heldt, and Stein (39) for Monel 400. For the hydrogen embrittled samples, increasing the temperature generally led to easier (earlier) crack initiation but also to earlier blunting of the cracks. However, if the temperature is increased far enough, crack initiation becomes more difficult.

Grain Size Effect. The finer grain size was generally more brittle, particularly at the slow strain rate This agrees with Fredell's results at room temperature, but is

TABLE VII

FATIGUE TESTS OF MONEL 400 AT 80°C IN HYDROGEN AND INERT ENVIRONMENTS. GRAIN SIZE, 250 μm; 30Hz

Samples	Environment	Maximum Stress MPA	Maximum Stress ksi	Cycles to Failure
77	Hydrogen	407	59.1	217,400
78	Inert	407	59.1	93,800

opposite to the behavior expected of brittle materials.

The large grained samples exhibited much more plastic deformation, more surface rumpling, and more slip band cracking.

Strain Rate Effect. The hydrogen embrittlement numerical data for Monel 400 (Figure 27 & 28) does not exhibit an obvious temperature shift due to changing the strain rate, as did the mercury data. However, the fractography of some of the fast strain rate tests is what would be expected from slow strain rate tests at lower temperatures. Particularly (for both grain sizes), the fast strain rate tests produced cup and cone fractures at the lower temperatures which were not obtained in any slow strain rate tests. When the temperatures were raised, significant embrittlement did not occur at the fast strain rate, except for a profusion of surface cracking at some conditions. At the fast strain rate, transgranular and intergranular surface cracks can readily initiate, just as at the slow strain rate, but they fail to propagate more than a few grains deep. Significant crack propagation seems to be limited by not enough time available. Thus the HE seems to have a time effect, either in the kinetics of hydrogen transport to the fracture process zone, or in the embrittlement mechanism itself. This behavior is opposite to that expected from a typical brittle material, where high strain rates reduce ductility.

Discussion

Comparison of Environments

Similar fractographies were obtained in hydrogen and mercury environments, in accord with previous work (6-10,67-85). There is therefore no necessity to invoke differing mechanisms for LME and HE. Similarly to earlier studies, as the strain at which fracture initiates increases, crack initiation becomes transgranular rather than intergranular. Intergranular cracking was observed in samples less than about 40% reduction in area. Mercury is the more injurious environment for Monel 400, as Fredell's (8) room temperature results had suggested. Embrittlement begins at approximately same temperature, around -20°C, for both environments. Ductility is recovered by 80°C in hydrogen, but not in mercury. In hydrogen, embrittlement is initiation limited at low temperatures, but becomes propagation limited as temperature is increased. Mercury induced fractures are primarily initiation limited, but progress toward becoming propagation controlled at higher temperatures in the coarse grain size.

Hydrogen promotes plasticity, as evidenced by the decreased tensile strength in the presence of necking and by the enhanced fatigue life. This promotes crack blunting, resulting in the multiplicity of side cracks. As

temperature is increased, excessive plasticity occurs so early that cracks never initiate.

Onset of Embrittlement

An important consideration is, "why does embrittlement in two so diverse environments begin at approximately the same temperature?" It is suggested that crack initiation is limited at lower temperatures by similar processes: adsorption of hydrogen, and wettability of mercury. Wedler (100) describes results of 14 methods of investigating adsorption of hydrogen onto nickel, including: enthalpy and entropy of adsorption, isotope exchange measurements, field emission microscopy, and low energy electron diffraction. A fairly extensive picture emerges, revealing that the adsorption is a complex phenomenon. A number of different adsorption states are reported, including one physiadsorption and at least two chemisorption states, with results depending on the crystallographic plane under observation. Particularly interesting is that the chemisorbed hydrogen is immobile at low temperatures and mobil at high temperatures, with the transition occurring around 195-240°K. The existence of this mobility is proposed as being a prerequisite for HE.

Wedler (100) also presents a summary of adsorption systems, listing combinations of adsorbents and adsorbates which have been reported as being adsorbing and nonadsorbing. While hydrogen adsorbs quite strongly on

nickel, it does not adsorb onto copper. This explains why Peevy (53) and Willoughby (101) were unable to observe HE of copper, even though it was embrittled by mercury.

For LME, many authors have drawn attention to a "temperature window" for embrittlement without advancing a clear explanation for such an effect. Stoloff (88) has stated that the upper temperature limit of the window is often subject to metallurgical and test variables, while the lower limit is not (as typified by Figure 1). The lower limit for LME has traditionally been associated with the melting point of the embrittler, and it has sometimes been tacitly assumed that embrittlement starts as soon as the embrittler melts (1). The recent awareness of solid metal embrittlement at temperatures as low as .75 T_m, along with the fact that embrittlement in many instances begins well above the embrittler melting point, requires a better explanation (88).

In the present study mercury embrittlement did not begin until 20 to 40°C above the melting point of mercury.

A possible reason may be that embrittlement at lower temperatures may be limited by adsorption. For both LME and HE (of unprecharged metal), adsorption of the embrittler is a primary step. For LME, this is associated with wetting, and wetting is a prerequisite for embrittlement (98). The mercury/Monel 400 system exhibits poor wetting, as do the other nickel alloys tested in previous OSU studies (6-10,67,87). Typically, the mercury on the fracture

surfaces exists as globules, as Lynch reported for mercury on zinc and D6AC steel (102). The globules indicate that "dewetting' has occurred after fracture, leading Lynch (102) to suggest that adsorption at the crack tip may be promoted by strain. This idea of "strain activated chemisorption" was advanced in 1963 by Westwood & Kamdar (103). They suggested that the role of elastic strain in the vicinity of the crack tip might be either (i) to supply an activation energy necessary for chemisorption (a chemical effect) or (ii) to produce the appropriate atomic spacing for the electronic interaction needed for chemisorption (a geometrical effect). The observation of very small patches of localized wetting on side surfaces associated with slip bands leads support to this approach.

If their proposed geometrical effect is valid, then increasing the temperature would have the same effect of increasing the lattice spacing, allowing increased chemisorption. The author is unaware of data specifically documenting the effect of temperature on chemisorption of mercury on Monel 400 or nickel. However, chemisorption typically increases with increasing temperature (104). Also, the surface tension of liquid metals typically decreases with increasing temperature, indicating better wetting as the temperature increases (see (105) & (106) for examples).

If such a "strain activated chemisorption" process is in effect, then a stress versus temperature relationship for

wetting such as that shown in Figure 36 exists. As illustrated in Figure 36, such a relationship would give rise to regions of different material behavior. In region A, the specimen fractures in the normal ductile manner before the strain can get high enough to allow wetting anywhere on the surface. In region B, wetting occurs locally after substantial strain. Therefore, wetting first becomes possible at locally active sites, such as grain boundaries or slip bands. Such a localized effect would give impetus to embrittlement, as brittle behavior is necessarily a localized phenomenon. In region C, general wetting occurs without the need for plastic deformation. General wetting provides no localized effect, and thus no embrittlement would be expected. Liquid/solid metal couples with high solubility and thus good wetting do not typically undergo LME (12). For example, Breyer and Johnson (107) reported that LME of 4145 steel was more severe for lead with antimony added which did not wet the steel, than for lead with tin added which wetted well.

Recovery of Ductility

At the other end of the "window," why does embrittlement almost disappear at high temperature (as observed in hydrogen)? It has been shown that hydrogen promotes plasticity, and that HE cracks are blunted by plastic deformation. Plasticity increases with temperature, until excess plasticity does not allow the formation of the stress

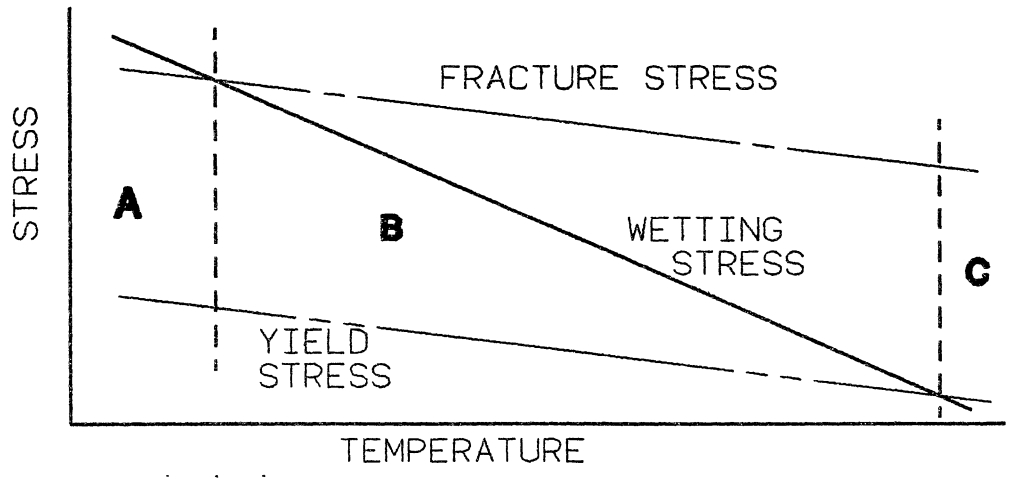

Figure 36. Effect of proposed strain activated chemisorption process.

concentrations required for crack initiation. While failures in mercury are brittle to 80°C, the same process is expected to occur at higher temperatures. The upper limit for HE is lower than for LME because hydrogen is so effective at enhancing the plasticity.

The same considerations also describe the grain size effect. In hydrogen, the fine grain size is most embrittled at the slow strain rate, with neither grain size undergoing much reduction in mechanical properties at the fast strain rate. Embrittled fracture by hydrogen is typically propagation limited. The coarse grain size allows more plasticity, limiting crack propagation. Thus, in hydrogen, the fine grain size is more brittle.

In mercury, both grain sizes are quite brittle at the slow strain rate, no significant difference in embrittlement between the two grain sizes. At the fast strain rate, the coarse grained samples exhibit greater embrittlement over the observed temperature range. The fine grained material is typically initiation limited; thus, the deceased embrittlement at the fast strain rate must be due to retarded crack initiation. Cracks in LME are generally regarded to begin at stress concentrations, such as dislocation pile-ups, as evidenced by the requirement for plastic deformation prior to crack initiation (87,108). The coarse grained material's lower yield strength allows earlier plasticity and crack initiation. The slow strain rate allows more plasticity, permitting early crack initiation for both grain sizes.

Time Effect

Embrittlement in both environments is subject to a time effect as seen by comparing data at the two strain rates. Embrittlement was reduced at fast strain rates in both environments, drastically so in hydrogen. This reduction for LME is not a result of exceeding the available crack propagation rate, for LME crack propagation has been reported at many mms^{-1} (4). Apparently, therefore the decreased embrittlement results from either time dependent plasticity or an incubation time. Crack initiation requires plastic deformation to provide the necessary stress concentrations. The higher yield stress at the fast strain rate (see figure 19) won't allow cracks to initiate as early as the slow strain rate, allowing less embrittlement before the process is truncated by ductile failure. This rationale would apply to the LME results, as they were typically initiation limited, but not the HE results which were typically propagation limited.

Estimated yield stresses were typically about 40 MPa higher at the fast strain rate, from Figure 19. It is questionable that this difference would produce a pronounced decrease in embrittlement when the tensile strength in air also increases by about the same amount at the fast strain rate.

The inference is that an incubation time is needed for cracks to develop. It is known that an incubation time for

mercury LME of Monel must be accompanied by a continually increasing stress, as Fredell was unsuccessful in producing embrittlement with long hold times above the fracture stress from tensile tests. An incubation time could result from: (i) a penetration time, (ii) slow crack growth to critical depth, or (iii) time dependent adsorption.

For LME and SME, Gordon and An (70) have proposed an incubation time during which grain boundary penetration by the embrittler occurs. They were able to develop static fatigue curves for 4140 steel in indium, where the incubation time decreased at increased stress. However, such a mechanism is not envisioned for the Monel/mercury system because embrittlement does not result from hold times with a static load.

For HE, the idea of a penetration time is more attractive. The apparent reason for hydrogen to enhance slip so greatly, while mercury doesn't, is that the hydrogen can diffuse into the metal, to be in direct contact with slip bands. Vehoff & Rothe (37) estimated from their tests of nickel single crystals in gaseous hydrogen that embrittlement is controlled by the hydrogen concentration in the fracture process zone, less than 100 nm ahead of the crack tip. If penetration into the metal matrix is required, then for unprecharged material, a crack can only propagate as fast as the hydrogen can diffuse ahead of it. If the crack outruns the hydrogen, blunting results.

For both HE and LME, the fast strain rate favors TG

cracking over the IG cracking favored at the slow strain rate. Thus, TG cracking would be expected at the fast strain rate in hydrogen. The rate of diffusion of hydrogen through the metal can be readily calculated. However, it is generally acknowledged that hydrogen diffusion can be greatly enhanced locally in stressed regions as hydrogen is swept along slip planes in dislocation cores (109). Vehoff & Rothe reported TG fracture in nickel single crystals on the [110] plane (37). Slip in nickel occurs on the [111] planes, which are bisected by the fracture plane. Thus, in crystallographic TG crack growth, the hydrogen being swept from the crack tip along slip planes does not intersect the fracture process zone directly ahead of the crack. Thus, most of the entry of hydrogen into the fracture process zone should occur by diffusion through the bulk material. According to Vehoff & Rothe (37), the fracture process zone is about 100 nm ahead of the crack tip. Appendix A calculates the time required for the hydrogen to diffuse 100 nm is 0.05 s, allowing an average crack propagation rate of 2 m/s. The fast strain rate tests last about three minutes, of which a maximum of about one minute is after crack initiation. Thus a transgranular crack would only be expected to propagate 120 m during the test, not enough to cause a large reduction in mechanical properties of the sample.

However, the surface of the sample can precharge slightly during the initial part of the test and during any

delays occurring due to problems with the grips, temperature control, etc., promoting surface cracking.

Vehoff & Rothe (37) have advanced a similar explanation for their tests in gaseous hydrogen. At temperatures of 20-100°C, they found that embrittlement was not dependent on crack growth rate. At temperatures less than 20°C, embrittlement decreased with increasing crack growth rate, which they attributed to cracking being limited by hydrogen transport to the fracture process zone. At temperatures above 100°C, embrittlement increases with increasing crack rate, which they attribute to embrittlement being limited by excess plasticity.

A second proposed incubation time is time required for slow crack growth to a critical depth. From fracture mechanics, if a given stress intensity, K, is required to propagate a crack, and

$$K = Y\sigma\sqrt{a} \qquad (4.1)$$

where: K = stress intensity factor

σ = nominal stress

a = crack depth

Y = geometrical constant

then as crack length approaches zero, nominal stress must go to infinity. Therefore, a crack must have a certain length before it "knows it's a crack" and fracture mechanics principles may be applied. Lynch (110) has invoked this explanation to account for observed LME incubation times in conjunction with his enhanced shear model. Similarly, the

surface of the sample is in a state of pure plane stress. Constraints are absent and plasticity occurs more readily than below the surface. The crack must get through this region before it can build up significant stress concentrations.

A third approach to incubation times is time dependent adsorption. The idea of time dependent adsorption is attractive, particularly since adsorption concepts can be used to explain observed temperature effects. The concept of stress aided adsorption discussed above accounts for the requirement for continually increasing stress to obtain embrittlement. This is particularly applicable because oxide films and adsorbed oxygen on the surface can prevent adsorption of the embrittler, requiring the production of clean surfaces in the presence of the embrittling species (98). In this regard, recent work at Tahoku University contains interesting photographs of intergranular fracture surfaces in zinc and beta brass embrittled by gallium (96,97). The gallium wetted the fracture surface in small localized patches associated with slip bands much as was observed in the present study (see results). This provides evidence for strain activated wetting. The concept of time dependent adsorption is promising and needs further study.

Longitudinal Splits

Long longitudinal splits were noted on the surface of the cup-cone LME fractures at low temperatures. LME

failures having one origin typically contained deep radial cracks on the fracture surface. The radial cracking diminished at higher temperatures where conditions were beginning to get more ductile. A requirement for LME cracking is the existence of a tensile stress normal to the crack plane. The tensile stress for the longitudinal cracking resulted from plastic constraint as the primary fracture propagated. None of the longitudinal cracks originated at the surface of an uncracked sample. They initiated on the fracture surface either (i) as the primary fracture propagated from the surface in for brittle conditions; or (ii) as the primary fracture propagated from the center out for the cup and cone fractures. Note that both of these conditions are roughly equivalent to a notched tensile test, where triaxial stresses result from plastic constraint.

The longitudinal cracks must propagate very rapidly because the stress to open them unloads quickly once they initiate. The combination of stress and exposure to mercury for the longitudinal cracks must be a transient effect, and no incubation time is possible. Thus it is difficult to imagine any sort of diffusion or penetration process being associated with this cracking. In this vein, it may be noted that no significant longitudinal cracking occurred in the hydrogen. If a time dependent adsorption model is considered, perhaps the fresh surface exposed by the advancing primary crack, coupled with the triaxial state of stress

imposed by the plastic constraint, avoids the need for the incubation time required for adsorption on the surface.

Correlation with Other Alloys

In Monel 400, by varying the temperature and strain rate, the complete range of affects seen in nickel alloys in previous OSU studies can be obtained. These include: cup and cone fractures with no embrittlement; brittle fractures breaking on the first crack initiated; samples with ductile mechanical properties but replete with blunt side cracks, reductions in area of less than 10% and greater than 70%; and fractures anywhere in the general sequence of intergranular/transgranular/microvoid coalescence fracture. No effect is observable at room temperature in other alloys that is not found in Monel 400 at some temperature, strain rate, or grain size. Therefore, the other alloys differ from Monel 400 only in degree, and not in basic behavior.

For nickel 200, the behavior at low temperature (particularly in hydrogen) is initiation limited, and it is propagation limited at higher temperatures, just as in Monel 400. However, it does not have the brittle region at intermediate temperature that was noted in the Monel. Rather the two other regions overlap, so that as soon as cracks are able to initiate, they immediately become propagation limited. Fractures in mercury had trouble initiating over the entire temperature range.

In Inconel 600, the hydrogen fractures at room tempera-

ture behaved like those in Monel 400 at higher temperatures. Fractures initiated and blunted very early, and the sample was covered with blunt side cracks. Fatigue lives were also enhanced in hydrogen. In mercury at room temperature, cracks would not initiate, similar to Monel 400 at lower temperatures.

In Incoloy 800 at room temperature, fractures do not initiate in hydrogen or in mercury. This behavior is similar to that observed in Monel 400 at lower temperatures, except that no longitudinal splits were observed in mercury. Initiating cracks by fatigue produced intergranular origin in mercury. This gives the expectation that longitudinal splits and more brittle fractures may result at higher temperatures, if they do not become limited by excess plasticity.

Morris (10) examined several possible correlations of material properties with embrittlement for these alloys, without a positive result. An alternative approach would be to investigate the nature of wetting and adsorption in the alloys. Apparently no embrittlement occurs if no wetting occurs, or if the wetting is too general. It may be noted that while Good (67) & Traylor (5) reported that the nickel alloys containing iron were the least embrittled, Costas (84) reported that the Ni-Cu alloys which contained iron were the hardest to wet. The preliminary wetting tests described in the results section support this hypothesis. The alloys exhibiting the most embrittlement, Monel 400 and

Nickel 200, wetted more than Inconel 600 and Incoloy 800 which were less embrittled.

Mechanisms

As discussed in the literature review, a variety of mechanisms have been proposed for LME and HE, but recent work largely advances three: (a) a reduction in cohesive strength, (b) enhanced dislocation nucleation, and (c) time dependent grain boundary penetration. Theories involving surface energy reduction are not normally mechanisms, but prerequisites or necessary conditions for embrittlement.

Reduction in cohesive strength provides a viable mechanism for the intergranular failures encountered in this study. There is much evidence to support such a view. For many embrittled intergranular fractures, no evidence of plasticity or shear can be found on the fracture surfaces (37). Segregation of impurities to grain boundaries can greatly increase or reduce embrittlement, and plausible explanations have been advanced based on a decohesion argument. The longitudinal splits observed in this work have clean intergranular fractures. Here, triaxial stresses with little shear favor decohesive fracture. Also, to apply his enhanced dislocation nucleation model to intergranular fracture, Lynch (110) discussed his enhanced shear model in terms of slip directly adjacent to grain boundaries. This application of his model seems forced, and he has offered no evidence in support of it. It is interesting that Lynch

(102) has recently stated that both the reduction in cohesive strength and enhanced dislocation nucleation models may be applicable under the right conditions.

While the reduction in cohesive strength model can also explain transgranular cracking, it offers no explanation of why the fracture mode should change from intergranular to transgranular fracture (nor does any other proposed mechanism). A more attractive explanation is that transgranular cracking results from a competing fracture mode. Lynch (102) and Stoloff (88) have also stated that embrittled fracture occurs by more than one mechanism.

Lynch's (4) enhanced dislocation nucleation model is attractive for transgranular fracture. This model was originally presented after studying nickel single which, of necessity, undergo transgranular fracture. He has presented good evidence for intense shear along the required planes (110). Also, in this study, the grains immediately on and beneath the surface tended toward transgranular fracture. Here, in the plane stress zone, shear stresses are higher than in the interior of the sample.

The grain boundary diffusion model of Gordon & An (70) cannot explain the extremely rapid crack initiation and propagation occurring with the longitudinal splits in mercury. Also, it does not correlate with the Monel's failure to break after hold periods at static load in mercury. As discussed above, diffusion of hydrogen into the fracture process zone is required, and can limit embrittlement at high stress rates.

CHAPTER V

CONCLUSIONS

1. Intergranular, transgranular, and microvoid coalescence fractures can be obtained in both hydrogen and mercury environments. The fracture mode is governed by the strain at fracture, regardless of the environment.

2. Embrittlement ceases below approximately -20°C in both environments. This is believed to be due to the lack of mobility of the adsorbed hydrogen and lack of wetting by the mercury.

3. Embrittlement of Monel 400 is generally more severe in mercury than in hydrogen because the hydrogen very effectively blunts cracks. Hydrogen promotes plasticity, evidenced by decreased tensile strength and enhanced fatigue life.

4. In hydrogen, embrittlement ceases at about 80°C because excess plasticity promotes crack blunting. In the limit excess plasticity prevents crack initiation.

5. Fractures in mercury remain brittle to 80°C, but evidence of increasing plasticity gives the expectation that embrittlement will cease at high temperatures.

6. An incubation period is normally needed. This is required either for adsorption of the embrittler or for penetration of the crack through the plane stress surface zone.

7. Otherwise ductile failures in mercury often exhibit longitudinal splitting. Under high triaxial tension, rapid crack initiation and propagation can occur without an incubation period. This is believed to be due to the combination of high normal stresses, low shear stress, and a clean surface. This is inconsistent with embrittlement models requiring diffusion.

8. The plane stress surface region promoted transgranular fracture, while the plane strain region associated with the longitudinal splits encouraged intergranular cracking.

9. The existance of a temperature "window" for LME can be explained on the basis of strain-activated localized wetting.

10. Results of this study are consistent with a reduction in cohesive strength mechanism producing intergranular fracture; competing with an enhanced dislocation nucleation mechanism producing transgranular fracture.

11. Monel 400 exhibited almost the complete range of features observed heretofore for other nickel base alloys when tested under appropriate conditions of temperature, strain rate, and grain size.

SELECTED BIBLIOGRAPHY

1. Stoloff, N. S., "Recent Developments in Liquid Metal Embrittlement." In Environment Sensitive Fracture of Engineering Materials, Z. A. Foroulis, Ed., pp. 486-520, TMS-AIME, Warrendale, PA (1979).

2. Atomistics of Fracture, (Proceedings of a NATO Advanced Research Institute on Atomistics of Fracture, May 22, 1981, Corsica, France), R. M. Latanision & J. R. Pickens, Eds., Plenum Press, N.Y. (1983).

3. Johnson, W. H., R. Soc. Lond. Proc. 23, p. 168, (1874-5).

4. Lynch, S. P., "Hydrogen Embrittlement & Liquid Metal Embrittlement in Nickel Single Crystals." Scripta Met., 13, 1051-1056 (1979).

5. Traylor, L. B., "A Comparison of Hydrogen & Mercury Embrittlement of Nickel Based Alloys." (Unpub. M. S. Thesis, Oklahoma State University, 1983.)

6. Price, C. E. & L. B. Traylor, "A Study of Hydrogen Embrittlement in Nickel 200 (UNS N02200) at Room Temperature, with Some Comparisons to Mercury Embrittlement." Submitted to Corrosion, Apr., 1984.

7. Traylor, L. B., & C. E. Price, "A Comparison of Hydrogen and Mercury Embrittlement in Monel Alloys at Room Temperature." (Unpublished research, Oklahoma State University, 1984).

8. Fredell, R. F., "A Detailed Comparison of Hydrogen and Mercury Embrittlement in Monel 400." (Unpub. M.S. thesis, Oklahoma State University, 1983.)

9. Price, C. E. & R. S. Fredell, "A Study of the Comparative Embrittlement of Monel 400 at Room Temperature in Hydrogen and in Mercury, as Function of Strain Rate, Grain Size, and Cold Work." (Unpublished research, Oklahoma State University, 1984).

10. Morris, J. A., "Hydrogen & Mercury Embrittlement of Selected Nickel-based Alloys." (Unpub. M.S. thesis, Oklahoma State University, 1984.)

11. Lynch, S. P., "Mechanisms of Hydrogen-Assisted Cracking." Metals Forum, 2, 189-200 (1979).

12. Kamdar, M. H., "Embrittlement by Liquid Metals." Prog. Mat. Sci., 15, 289-371 (1973).

13. Gilman, J. J., "Stress-Corrosion Cracking in Plastic Solids Including the Role of Hydrogen." Phil. Mag., 26, 801-812 (1972).

14. Speidel, M. O., "Stress Corrosion Cracking of Aluminum Alloys." Met. Trans. A, 6A, 631-651 (1975).

15. Petch, N. J., and P. Stables, "Delayed Fracture of Metals Under Static Load." Nature, 169, 842-843 (1952).

16. Uhlig, H. H., "Stress Corrosion Cracking", in Fracture, III, 645-677, H. Liebowitz, Ed., Academic Press, New York (1971).

17. Nichols, H., & W. Rostoker, "On the Mechanism of Crack Initiation in Embrittlement by Liquid Metals." Acta Met., 9, 504-509 (1961).

18. Seah, M. P., & E. D. Hondros, "Atomistic Mechanisms of Intergranular Embrittlement." In Atomistics of Fracture, pp. 855-887, Plenum Press, N.Y. (1983).

19. Jokl, M. L., J. Kameda, C. J. McMahon, Jr., & V. Vitek, "Solute Segregation & Intergranular Fracture in Steels." Met. Sci., 14, 375-384 (1980).

20. Jones, R. H., S. M. Bruemmer, M. T. Thomas, & D. R. Baer, "Relative Effects of S, Sb, & P on the Intergranular Fracture of Iron & Nickel Tested at Cathodic Potentials." In Atomistics of Fracture, pp. 895-900, Plenum Press, N.Y. (1983).

21. Dinda, S., & W. R. Warke, "The Effect of Grain Boundary Segregation on Liquid Metal Induced Embrittlement." Mat'ls. Sci. Engr., 24, 199-208 (1976).

22. Briant, C. L., & R. P. Messmer, Electronic Effects of Sulphur in Nickel, A Model for Grain Boundary Embrittlement." Phil. Mag., 42, 569-576 (1980).

23. Gray, H. R., "Testing for Hydrogen Environment Embrittlement: Experimental Variables," ASTM STP543, Am. Soc. Testing & Mat'ls, 1974.

24. Stoloff, N. S., "Liquid & Solid Metal Embrittlement." In Atomistics of Fracture, pp. 921-953, Plenum Press, N.Y. (1983).

25. Volkl, J., & G. Alefield, "Diffusion of Hydrogen in Metals." From Hydrogen in Metals 1, Topics in Applied Physics, G. Alefield & J. Volkl, Eds., Springer-Verlag, N.Y. (1978).

26. Hirth, J. P., "Effects of Hydrogen on the Properties of Iron & Steel." Met. Trans. A, 11A, 861-890 (1980).

27. Birnbaum, H. K., "Hydrogen Related Fracture of Metals." in Atomistics of Fracture, 733-769, Plenum Press, N.Y. (1983).

28. Boniszewski, T., & G. C. Smith, "A Note on Nickel Hydride." J. Physics & Chem. Solids. 21, 115-118 (1961).

29. Zapffe, C. A., & C. E. Sims, "Hydrogen Embrittlement, Internal Stress, and Defects in Steel." Trans. AIME, 145, 225-271 (1941).

30. Tien, J. K., in Effect of Hydrogen on the Behavior of Materials. TMS-AIME, Warrendale, Pa. (1975).

31. Troiano, A. R., "The Role of Hydrogen & Other Interstitials in the Mechanical Behavior of Metals." Trans. ASM., 52, 54-80, 1960.

32. Oriani, R. A., & P. H. Josephic, "Testing of the Decohesion Theory of Hydrogen-Induced Crack Propagation." Scripta Met., 6, 681-688 (1972).

33. Kelly, A., M. R. Tyson, & A. H. Cottrell, "Ductile & Brittle Crystals." Phil. Mag., 15, 567-586 (1967).

34. Rice, J. R., & R. Thompson, "Ductile versus Brittle Behavior of Crystals." Phil. Mag., 29, 73-97 (1974).

35. Beachem, C. D., "A New Model for Hydrogen-Assisted Cracking (Hydrogen 'Embrittlement')." Met. Trans., 3, 437-451 (1972).

36. Lynch, S. P. "Nucleation & Egress of Dislocations at Crack Tips." in Atomistics of Fracture, 955-963, Plenum Press, N.Y. (1983).

37. Vehoff, H., & W. Rothe, "Gaseous Hydrogen Embrittlement in FeSi & Ni Single Crystals." Acta Met., 31, pp.1781-1793 (1983).

38. Griffith, A. A., "The Phenomena of Rupture & Flow in Solids." Phil. Trans., Royal Soc. London, A221, p. 163 (1920). (This article has been republished with additional commentary in Trans. ASM, 61, 871-906 (1968).

39. Funkenbusch, A. W., L. A. Heldt, & D. F. Stein, "The Influence of Grain Boundary Phosphorous Concentration on Liquid Metal & Hydrogen Embrittlement of Monel 400." Met. Trans. A, 13A, 611-618 (1982).

40. Williams, P., C. A. Evans, Jr., M. L. Grossbeck, & H. K. Birnbaum, "Ion Microprobe Analysis for Niobium Hydride in Hydrogen Embrittled Niobium." Anal. Chem., 48, 964-968 (1976).

41. Clark, E. A., R. Yeske, & H. K. Birnbaum, Met. Trans. A., 11A, 1903 (1980).

42. Beachem, C. D., In Stress Corrosion Cracking and Hydrogen Embrittlement of Iron Base Alloys. Staehle, R. W., J. Hochmann, R. D. McCright, & J. E. Slater, Eds., p. 375, NACE, Houston, (1977).

43. Kimura, H., & H. Matsui, "Softening & Hardening in High Purity Iron & Its Alloys." in Hydrogen in Metals, I. M. Bernstein, & A. W. Thompson, Eds., 191-208, TMS-AIME (1981).

44. Eastman, J., F. Heubaum, T. Matsumoto, H. K. Birnbaum, "The Effect of Hydrogen on the Solid Solution Strengthening & Softening of Nickel." Acta Met., 30, 1579-1586 (1982).

45. Eastman, J., T. Matsumoto, N. Narita, F. Heubaum, & H. K. Birnbaum, "Hydrogen Effects in Nickel--Embrittlement or Enhanced Ductility?" In Hydrogen in Metals, Bernstein, I. M., and A. W., Thompson, Eds., 397-409, TMS-AIME (1981).

46. Oriani, R. A. & P. H. Josephic, "Aspects of Hydrogen-Induced Cracking of Steels." Acta Met., 22, 1065-1074 (1974).

47. Oriani, R. A. & P. H. Josephic, "Equilibrium & Kinetic Studies of the Hydrogen-Assisted Cracking of Steel." Acta Met., 25, 979-988 (1977).

48. Lynch, S. P., "A Comparative Study of Stress-Corrosion Cracking, Hydrogen Assisted Cracking, and Liquid Metal Embrittlement in Al, Ni, & Ti Alloys," Hydrogen Effects in Metals, I.M. Bernstein & A. W. Thompson, Eds., The Metall. Soc., AIME, Warrendale, PA (1981).

49. Lynch, S. P., "A Fractographic Study of Gaseous Hydrogen Embrittlement in a Tempered Martensitic Steel," Acta Met., 32, 79-90 (1984).

50. McClintock, F. A., Int. J. Fract. Mech., 4, 101 (1968).

51. Culp, A. W., Principles of Energy Conversion. McGraw Hill, N.Y. (1979).

51. Culp, A. W., Principles of Energy Conversion. McGraw Hill, N.Y. (1979).

52. Friehe, W., "Strain-Induced Stress Corrosion Cracking in Steels in Liquid Metals." Werkstoffe und Korrosion, 29, 747-753 (1978), Translation, C. E. Trans. 7685.

53. Breyer, N. N., "Embrittlement of Steels by Low Melting Point Metals." Corrosion 1982 Symposium Proceedings, NACE, Houston, 1982.

54. Mellor, B. G., K. Tabeshfar, & G. A. Chadwick, "Liquid Metal Embrittlement in Monel 400." The Metall. and Mat. Tech., Sept., 1982, 385-386.

55. Atkinson, J. T., and N. H. van Droffelaar, Corrosion & Its Control. p. 180, NACE, Houston (1982).

56. Shchukin, E. D., L. S. Bryukhanova, Z. M. Polukarova, & N. D. Peutsov, Sov. Mat. Sci. 12, p. 40 (1976).

57. Shchukin, E. D. Y. V. Goryunov, N. V. Pertsov, & L. S. Bryukhanova, Sov. Mat. Sci., 14, p 341 (1978).

58. Nicholas, M. G., & C. F. Old, "Review, Liquid Metal Embrittlement." J. Mat. Sci., 14, 1-18 (1979).

59. Kamdar, H., ed., Embrittlement by Liquid & Solid Metals, Conference Proceedings, The Metal Soc., AIME (1983).

60. Rostoker, W., J. M. McCaughey, & M. Markins, Embrittlement by Liquid Metals, (Reinhold, New York, 1960).

61. Stoloff, N. S., Surface & Interfaces 14, Sagamore Army Mat. Res. Conf., 1968, p. 159, Ed. by J. Burke, N. Reed, & W. Weiss.

62. Kelly, M. J., & N. S. Stoloff, "Analysis of Liquid Metal Embrittlement from a Bond Energy Viewpoint." Met. Trans. A., 6A, 159-166 (1975).

63. Roth, M. C., G. C. Weatherly, W. A. Miller, "The Temperature Dependence of the Mechanical Properties of Aluminum Alloys Containing Low-Melting-Point Inclusions." Acta Met., 28, 841-853 (1980).

64. Old, C. F., & P. Travena, "Liquid Metal Embrittlement of Aluminum Single Crystals by Gallium." Met. Sci., 13, 591-596 (1979).

65. Toropovskaya, N., "Applications of Thermodynamic Criteria for Estimating the Strength of Metals Deformed in Melts." Sov. Mat. Sci., (Trans. of Fiziko-Khimcheskeya Mekhanika Materialov.), 1, 324-327 (1970).

66. Shunk, Francis, A. & W. R. Warke, "Specificity as an Aspect of Liquid Metal Embrittlement." Scripta Met., 8, 519-526 (1974).

67. Price, C. E., & J. K. Good, "The Tensile Fracture Characteristics of Nickel, Monel, and Selected Superalloys Broken in Liquid Mercury." ASME J. Engr. Mat. Tech., 106, 184-191 (1984).

68. Stoloff, N. S. & T. L. Johnson, "Crack Propagation in a Liquid Metal Environment," Acta Met., 11, pp. 251-256, 1963.

69. Westwood, A. R. C. & M.H. Kamdar, Phil. Mag., 8, 787 (1963).

70. Gordon, Paul, & H. H. An, "The Mechanisms of Crack Initiation & Crack Propagation in Metal Inducted Embrittlement of Metals." Met. Trans. A, 13A, 457-472 (1982).

71. Rinnovatore, J. V., J. D. Corrie, & H. Marcus, "The Effect of Grain Boundary Penetration on the Delayed Failure of Cu-2%Be." Trans. ASM, 59, 665-671 (1966).

72. Clum, J. A., Scripta Met., 9, 51-58 (1975).

73. Robertson, W. M., "Propagation of a Crack Filled with Liquid Metal." Trans. TMS-AIME, 236, 1478-1482 (1966).

74. Krishtal, M. A., "The Formation of Dislocations in Metals on Diffusion of Surface-Active Substances in Connection with the Effect of Adsorption Embrittlement." Sov. Phys. Doklady, 15, 614-617 (1970).

75. Marya, S. K., G. Wyon, "Temporary Embrittlement Followed by Increase in Ductility After Gallium Penetration in Cold Rolled Aluminum." Scripta Met., 9, 1009-1016 (1975).

76. Boniszewski, T., & G. C. Smith, "The Influence of Hydrogen on the Plastic Deformation, Ductility, and Fracture of Nickel in Tension." Acta Met., 11, 165-178 (1963).

77. Wilcox, B. A., & G. C. Smith, "The Portevin-LeChatelier Effect in Hydrogen Charged Nickel." Acta Met., 12, 371-376 (1964).

78. Wilcox, B. A., & G. C. Smith, "Intercrystalline Fracture in Hydrogen-Charged Nickel." Acta. Met., 13, 331-343 (1965).

79. Windle, A. H., & G. C. Smith, "The Effect of Hydrogen on the Plastic Deformation of Nickel Single Crystals." Met. Sci. J., 2, 187-191 (1968).

80. Windle, A. H., & G. C. Smith, "The Effect of Hydrogen on the Deformation & Fracture of Polycrystalline Nickel." Met. Sci. J., 4, 136-144 (1970).

81. Wayman, M. L., & G. C. Smith, "The Hydrogen Embrittlement of Fe-Ni Martensites." Met. Trans., 1, 1189-1193 (1970).

82. Wayman, M. L., G. C. Smith, "The Effects of Hydrogen on the Deformation & Fracture of Nickel-Iron Alloy." Acta Met., 19, 227-231 (1971).

83. Latanision, R. M., & H. Opperhauser, Jr., "The Intergranular Embrittlement of Nickel by Hydrogen: The Effect of Boundary Segregation." Met. Trans., 5, 483-492 (1974).

84. Costas, L. P., "Effect of Phosphorus on the Embrittlement of Copper-Nickel Alloys by Mercury." Corrosion, 31, 91-96 (1975).

85. Price, C. E., & J. K. Good, "The Fatigue Behavior of Nickel, Monel & Selected Superalloys Tested in Liquid Mercury and Air; A Comparison." ASME J. Engr. Mat. Tech., 106, 178-183 (1984).

86. Kane, R. D., & B. J. Berkowitz, "Effect of Heat Treatment & Impurities on the Hydrogen Embrittlement of a Nickel-Cobolt Base Alloy," Corrosion, 36, 29-36 (1980).

87. Peevy, G. R., "The Embrittlement of Cold Worked Copper, Monel, and Nickel by Mercury, With Some Comparisons to Hydrogen Embrittlement." (Unpub. M.S. report, Oklahoma State University, 1984.)

88. Stoloff, N. S., "Metal Induced Embrittlement - A Historical Perspective," in Embrittlement by Liquid & Solid Metals, pp. 3-26, TMS-AIME, Warrendale, Pa. (1984).

89. Pickens, J. R., & A. R. C. Westwood, "Recent Soviet Contributions to the Understanding and Application of Liquid Metal Embrittlement Phenomena," in Embrittlement by Liquid & Solid Metals, pp. 3-26, TMS-AIME, Warrendale, Pa. (1984).

90. Shchukin, E. D., and Yuschenko, J. Mater. Sci., 16, p. 313 (1981).

91. Popovich, V. V., and I. G. Dmukhovskaya, Sov. Mater. Sci., 12, 394-399 (1976).

92. Metal Progress Databook, Mid-June, 1980.

93. Fontana, M. G., & N. D. Greene, Corrosion Engineering, Second Ed., McGraw-Hill, (1978).

94. Johnson, C. A., Metallography Principles and Procedures, LECO Corporation, St. Joseph, Mo (1977).

95. Ichinose, H., Trans. Japan Inst. Metals, 9, 35 (1968).

96. Watanabe, T., S. Shima, and S. Karashima, "Misorientation Dependence of Liquid Metal - Induced Intergranular Fracture of Zinc Bicrystals," Embrittlement by Liquid and Solid Metals, pp 27-50, TMS-AIME, Warrendale, Pa. (1984).

97. Watanabe, T., M. Tanaka, and S. Karashima, "Intergranular Fracture Caused by Liquid Gallium in Polycrystalline Beta Brass with BCC Structure," Embrittlement by Liquid and Solid Metals, pp 27-50, TMS-AIME, Warrendale, Pa. (1984).

98. Nicholas, M. G., "A Survey of Literature on Liquid Metal Embrittlement of Metals and Alloys," Embrittlement by Liquid and Solid Metals, pp 27-50, TMS-AIME, Warrendale, Pa. (1984).

99. Price, C. E., & J. A. Morris, "The Comparative Embrittlement of Example Nickel Alloys by Hydrogen & Mercury," ASM International Conference on Corrosion of Nickel-Base Alloys, Cincinnati, OH, Oct., 1984.

100. Wedler, G., Chemisorption: An Experiment Approach, Butterworths, Boston (1976).

101. Willoughby, J. K., "The Susceptibility of Copper to Embrittlement by Mercury & by Hydrogen, A Comparison." (Unpub. M.S. report, Oklahoma State University, 1984.)

102. Lynch, S. P., "Mechanisms of Fracture in Liquid-Metal Environments," in Embrittlement by Liquid & Solid Metals, pp. 3-26, TMS-AIME, Warrendale, Pa. (1984).

103. Westwood, A. R. C., & M. H. Kamdar, "Concerning Liquid Metal Embrittlement, Particularly of Zinc Monocrystals by Mercury," Phil. Mag., 8, 787-804. (1963).

104. Castellan, G. W., Physical Chemistry, Second Ed. p. 437, Addison-Wesley, Reading, Mass. (1971).

105. Libman, E. E., "The Surface Tension of Molten Metals with a Determination of the Capillary Constant of Copper," U. of Ill. Engineering Experiment Bulletin No. 173, U. of Ill., Urbana, Ill. (Jan. 31, 1928).

106. Rideal, E. K., "The Surface Phase in Metals," in Surface Phenomena of Metals, 3-10, Soc. Chem. Ind., London (1968).

107. Breyer, N. N., and K. L. Johnson, "Liquid Metal Embrittlement of 4145 Steel by Lead-Tin and Lead-Antimony Alloys," J. Testing and Evaluation, ASTM, 2. 471-477 (1974).

108. Hancock, P. C., & M. B. Ives, "The Role of Plastic Deformation in Liquid Metal Embrittlement," Can. Met. Quart., 10, 207-211 (1971).

109. Kurkela, M., & R. M. Latanision, Scripta Met., 13, 927-32, (1979).

110. Lynch, S. P., "Liquid-Metal Embrittlement in an AP-6% Zn - 3% Mg Alloy," Acta Met., 29, 325-340 (1981).

111. Van Vlack, L. H., Materials Science for Engineers, Reading, Mass., Addison-Wesley, 1970, p. 172.

112. Abramowitz, M., and I. A. Stegun, Eds., Handbook of Mathematical Functions, National Bureau of Standards, Washington, D.C. (1970).

APPENDIX A

HYDROGEN DIFFUSION VELOCITY ESTIMATION

Assume that hydrogen is diffusing from the crack tip into the bulk of the material. The amount of hydrogen being generated electrolytically on the surface can be calculated directly from the charging current. However, much of it bubbles off as gaseous hydrogen, rather than diffusing into the metal.

Traylor's work gives insight into the effect of hydrogen. He determined that HE of Nickel 200 in slow strain tensile tests increased with hydrogen charging current density, up to about $200mAm^{-2}$, where it saturated. This suggests that at $200mAm^{-2}$ and above, the hydrogen concentration in the fracture process zone is practically equal to that at the surface (crack tip). He observed very little embrittlement at and below about $70mAm^{-2}$. Assuming that the concentration of hydrogen in the fracture process zone is directly proportional to the charging current density, the concentration required for embrittlement to occur is 70/200 = 0.175 times the concentration at the crack tip. Since this study used a current density high enough to produce saturation, it is assumed that a hydrogen concentration of 0.35 times the surface concentration is needed to cause embrittlement.

Modeling as an infinite source of hydrogen diffusing into a semi-infinite slab, the concentration at distance x into the slab is given by (111).

$$\frac{C_s - C_x}{C_s - C_o} = \text{erf} \quad \frac{x}{2\sqrt{Dt}} \qquad \text{(A-1)}$$

Where C_s is the concentration at the surface, C_o is the original or base concentration, C_x is the concentration at x, D is the diffusion coefficient, t is time, and erf denotes the Gaussian error function (tabulated in (112)).

Assuming that $C_o = 0$ and $D = 5.5\text{x}10^{-10}\text{cm}^2\text{s}^{-1}$ for nickel at 25°C, how much time is required for the concentration at x = 100nm to reach 0.35 C_s [25]?

$$\frac{C_s - 0.35\ C_s}{C_s - 0} = \text{erf} \quad \frac{10^{-5}\text{cm}}{2\sqrt{5.5\text{x}10^{-10}t}} \qquad \text{(A-2)}$$

$$0.65 = \text{erf} \quad \frac{.2132}{\sqrt{t}} \qquad \text{(A-3)}$$

$$t = 0.10\ \text{s} \qquad \text{(A-4)}$$

Thus 0.15s is required for diffusion to 100nm. Assuming that the crack cannot propagate faster than this without "out running" the hydrogen, it can travel at

$$\frac{100\text{nm}}{0.15} = 1.0\mu\text{m/s} \qquad \text{(A-5)}$$

APPENDIX B

TEST DATA

1. Monel 400/Inert

No.	Ref.	Date	R_B	T (°C)	TS (MPa)	TS (ksi)	% RA	Remarks
2	-	840224	61	-18	675	98	72	35μm, 0.5 SSR, (1)
15	-	840622	68	-30	716	104	71	35μm, FSR, (1)
16	-	840622	68	-20	731	106	77	35μm, FSR, (1), (2)
-	5	-	-	22	581	-	67	SSR, (3)
-	8	-	70	22	634	92	67	35μm, SSR
-	8	-	57	22	613	89	70	250μm, SSR
-	8	-	-	22	648	94	74	250μm, (4)
-	10	-	66	22	634	92	77	SSR, (5), (6)

(1) Electrolyte - no charging.
(2) Short anneal cycle (2.75 hour) due to power failure.
(3) Annealed 1 hr. at 750°C.
(4) Very fast strain rate $1.6 \times 10^{-2} s^{-1}$.
(5) Annealed 2 hr. at 750°C.
(6) 255 MPa (37 ksi) yield strength.

2. Monel 400/Hg

(a) 35μm grain size - slow strain rate ($1.6 \times 10^{-5} s^{-1}$)

No.	Ref.	Date	R_B	T (°C)	TS (MPa)	TS (ksi)	% RA	Remarks
4	-	840306	67	-30	700	102	72	
3	-	840303	66	-18	633	92	32	(7)
46	-	840714	65	0	648	94	28	(8)
14	-	840620	68	0	679	98	47	(9)
23	8	-	-	22	503	73	12	
10	0	840615	67	50	641	93	37	(9)
47	-	840716	65	80	503	73	15	(8)
12	-	840618	68	80	632	92	28	(9)

(7) Strain rate: $8 \times 10^{-6} s^{-1}$.
(8) 750°C anneal (others are 700°C).
(9) Mercury suspected of being contaminated with Pb and Sn from thermocouple.

(b) 35μm grain size - fast strain rate ($1.6 \times 10^{-3} s^{-1}$)

No.	Ref.	Date	R_B	T (°C)	TS (MPa)	TS (ksi)	% RA	Remarks
18	-	840621	68	-30	739	107	75	(9)
52	-	840721	66	-30	742	108	75	
19	-	840621	69	-18	736	107	73	(9)
20	-	840621	68	0	714	104	76	(9)
58	-	840823	69	22	694	101	50	
21	-	840621	65	50	679	99	45	(9)
45	-	840707	66	80	621	90	27	(8)
51	-	840721	67	80	655	95	46	

2. Monel 400/Hg continued

(c) 250μm grain size - slow strain rate ($1.6 \times 10^{-5} s^{-1}$)

No.	Ref.	Date	R_B	T (°C)	TS (MPa)	TS (ksi)	% RA	Remarks
42	-	840714	51	-30	650	94	60	
27	-	840705	51	-30	625	91	31	(9)
28	-	840705	50	-18	630	91	38	
29	-	840706	51	0	618	90	32	
28	8	-	-	22	434	63	11	
38	-	840706	52	50	454	66	15	
30	-	840706	52	50	618	90	56	(10)
40	-	840707	51	80	470	68	19	

(10) Anneal time between two and three hours due to power failure.

(d) 250μm grain size - fast strain rate ($1.6 \times 10^{-3} s^{-1}$)

No.	Ref.	Date	R_B	T (°C)	TS (MPa)	TS (ksi)	% RA	Remarks
49	-	840723	51	-30	688	100	69	
26	-	840702	51	-30	666	97	42	(9), (11)
36	-	840706	52	-18	669	97	53	
37	-	840506	51	0	658	95	68	
32	8	-	-	22	641	93	33	
53	-	840722	50	50	587	85	25	
44	-	840707	51	80	578	84	31	

2. Monel 400/Hg continued

(e) Additional Tests

No.	Date	E (s^{-1})	G.S. (m)	R_B	T (°C)	TS (MPa)	TS (ksi)	% RA	Remarks
54	840723	SSR	250	53	22	652	66	15	Air Cooled
55	840723	FSR	250	50	50	613	89	39	Air Cooled
75	841123	FSR	500	51	19	614	89	43	
79	841124	SSR	350	52	20	515	75	20	
80	841124	SSR	350	51	80	420	61	13	

(11) Anneal time 10.75 hr.

3. Monel 400/H

(a) 35µm grain size - slow strain rate ($1.6 \times 10^{-5} s^{-1}$)

No.	Ref.	Date	R_B	T (°C)	TS (MPa)	TS (ksi)	% RA	Remarks
5	-	840707	68	-30	685	99	71	
1	-	840221	61	-14	632	92	54	1/2 SSR
13	-	840618	68	0	680	99	27	
89	8	-	-	22	552	80	12	
6	-	840606	65	50	645	94	44	
9	-	840608	65	80	650	94	56	

3. Monel 400/H continued

(b) 35μm grain size - fast strain rate ($1.6 \times 10^{-3} s^{-1}$)

No.	Ref.	Date	R_B	T (°C)	TS (MPa)	TS (ksi)	% RA	Remarks
22	-	840625	70	-30	728	106	79	
23	-	840626	68	-18	711	103	66	
17	-	840623	70	0	702	102	62	
48	-	840718	66	22	656	94	63	(8)
11	-	840619	69	50	654	95	69	
43	-	840703	65	80	642	93	72	(8)
76	-	841125	68	80	645	94	75	

(c) 250μm grain size - slow strain rate ($1.6 \times 10^{-5} s^{-1}$)

No.	Ref.	Date	R_B	T (°C)	TS (MPa)	TS (ksi)	% PA	Remarks
8	-	840625	50	-30	630	91	67	
24	-	840627	51	-18	616	89	51	
25	-	840628	52	0	577	84	46	
29	8	-	-	22	572	83	32	
35	-	840629	51	50	579	84	38	
39	-	840702	51	80	570	83	50	

3. Monel 400/H continued

(d) 250μm grain size - fast strain rate ($1.6 \times 10^{-3} s^{-1}$)

No.	Ref.	Date	R_B	T (°C)	TS (MPa)	TS (ksi)	% RA	Remarks
33	-	840628	51	-30	648	94	79	
31	-	840627	52	-18	665	96	75	
32	-	840627	53	0	641	93	67	
57	-	840811	51	24	621	90	65	
34	-	840627	51	50	599	87	68	
41	-	840702	52	80	578	84	67	

(e) Fatigue, 30 Hz.

No.	Date	G.S.	R_B	T	Stress MPa	Stress ksi	Env.	N_f
77	841123	250	54	80	407	59	H	217 K
78	841123	250	51	80	407	59	Irt.	93 K

VITA 2

Randall Kent King

Candidate for the Degree of

Doctor of Philosophy

Thesis: ENVIRONMENTALLY INDUCED FRACTURE OF NICKEL ALLOYS: A COMPARISON OF HYDROGEN AND MERCURY EMBRITTLEMENT WITH RESPECT TO TEMPERATURE

Major Field: Mechanical Engineering

Biographical:

Personal Data: Born in Kansas City, Missouri, February 7, 1950, the son of Mr. and Mrs. Joe King. Married to Deborah D. Salmon on July 27, 1974.

Education: Graduated from Guymon High School, Guymon, Oklahoma, in May, 1968; received Bachelor of Science Degree in Mechanical Engineering from Oklahoma State University in December, 1972; received Master of Engineering Degree from Oklahoma State University in May, 1974; completed requirements for Doctor of Philosophy Degree at Oklahoma State University in May, 1985.

Professional Experience: Research Engineer, Boeing - Wichita, 1974-1975; Research Engineer, Fluid Power Research Center, Oklahoma State University, 1975-1980; Teaching Assistant, School of Mechanical and Aerospace Engineering, Oklahoma State University, 1983-1984; Senior Engineer, Halliburton Services, 1984 to present.